Nonlinear finite element analysis of space frames

Reijo Kouhia

Teknillinen korkeakoulu
Rakennetekniikan laitos

Helsinki University of Technology
Department of Structural Engineering

Espoo 1990

Julkaisu/Report 109

Kouhia, R., NONLINEAR FINITE ELEMENT ANALYSIS OF SPACE FRAMES. Helsinki University of Technology, Department of Structural Engineering, Report 109, 118 p.

ABSTRACT

In this study a finite element method for geometrically and materially nonlinear analyses of space frames is developed. The element stiffness matrices and internal force vectors for beams with either solid or thin-walled open cross-section are derived. Both Timoshenko and Euler-Bernoulli beam theories are considered.

The equilibrium equations are formulated using an updated incremental Lagrangian description, where the reference configuration is the previous known equilibrium state. The elements can undergo large displacements and large rotations but the strains are assumed to be small. The linearized incremental displacement assumptions are used and the incremental rotations are also assumed to be small.

In the case of a beam with a thin-walled open cross-section the torsional behaviour is modelled by Vlasov's theory or by a two parametric deplanation model, where the angle of twist and it's derivative have independent approximations. Also a penalty formulation to impose the Vlasov's contraint in the two parametric deplanation model is presented.

Material behaviour is described by elasto-plastic, viscoplastic and temperature dependent elasto-plastic models. Besides, the conventional layered model is applied likewise the simple approximate yield surfaces, expressed in terms of stress resultants.

The discretized equilibrium equations are solved using the orthogonal trajectory method which allows the determination of the post-buckling regime. Special attention is paid to the detection of singular points and branching onto the secondary equilibrium path. In dynamic cases the time integration methods of Newmark family are used.

The presented numerical examples have been compared to analytical experimental and other numerical solutions found in literature.

CONTENTS

Abstract

Notations

1 Introduction 1

2 Equations of equilibrium 4

3 Beams with solid cross-section 8
3.1 Kinematics of beam 8
3.2 Beam elements 12
3.2.1 Elements based on Timoshenko beam theory 12
3.2.2 Elements based on Euler-Bernoulli beam theory 21

4 Thin-walled beams with open cross-section 25
4.1 Kinematical relations 25
4.2 Thin-walled beam elements 27
4.2.1 Elements based on Timoshenko beam theory 27
4.2.2 Elements based on Euler-Bernoulli beam theory 34

5 Transformation between local and global coordinate systems 36

6 Constitutive models 39
6.1 Elasto-plastic material model 39
6.2 Viscoplastic material model 41
6.3 Thermo-elasto-plastic material model 41
6.4 Yield surfaces expressed in terms of stress resultants 42

7 On the penalty method 43

8 Solution procedures of nonlinear equilibrium equations 46
8.1 Continuation methods 46
8.1.1 Basic procedure 46
8.1.2 Detection of singular points 49
8.1.3 Branching onto the secondary path 53
8.1.4 Some computational aspects 55
8.1.4.1 Determination of arc-lenght and weighting factors 55
8.1.4.2 Convergence estimation of corrector iterations 56
8.1.4.3 Solution of nearly singular equation systems 57
8.2 Time integration methods 58
8.2.1 Central difference method 58
8.2.2 Newmark family 59

8.2.3 Energy balance 60

9 Numerical examples 61
9.1 Torsional behaviour of elasto-plastic beams 61
9.2 Large deflection analysis of a circular bend 66
9.3 Instability analysis of shallow hexagonal frame 66
9.4 Instability analysis of a framed dome 68
9.5 Tezcan's frame 71
9.6 Lateral buckling analysis of cantilever beams 72
9.7 Elastic Lateral buckling analysis of a simply supported beam 77
9.8 Lateral buckling analysis of redundant beams 80
9.9 Lateral buckling of a space truss 82
9.10 Elasto-plastic lateral buckling analysis of simply supported I-beams 83
9.11 Elasto-plastic lateral buckling analysis of continuous I-beams 84
9.12 Post-buckling analysis of hybrid beams 89
9.13 Thermo-elasto-plastic analysis of steel frames 90
9.14 Dynamic plastic bifurcation of a pin-ended beam 97
9.15 Dynamic analysis of an elasto-plastic cantilever beam 100
9.16 Dynamic elasto-plastic behaviour of a portal frame 102
9.17 An I-beam impacted by a mass 107

10 Discussion and conclusions 108

References 109

Appendix 1 Differential equations for a torsion bar 117
Appendix 2 Grading functions 118

NOTATIONS

A	cross-sectional area
B	bimoment
$\mathbf{B}$	linearized strain-displacement matrix
$\mathbf{D}$	rate of deformation tensor
C	configuration
$\mathbf{C}$	tensor or matrix containing material parameters
E	modulus of elasticity
E_p	plastic hardening modulus
E_t	tangent modulus
$\mathbf{e}$	vector of generalized strains
$\mathbf{E}$	Green-Lagrange strain tensor
f	yield function
$\mathbf{f}$	external body forces
$\mathbf{F}$	deformation gradient, vector of unbalanced forces
G	shear modulus
$\mathbf{H}$	displacement gradient
$\mathbf{I}$	unit tensor, unit matrix
I_p	polar moment of inertia
I_s	shear constant in warping torsion
I_t	torsion constant
I_ω	warping constant
I_y, I_z	moments of inertia
$\mathbf{K}$	stiffness matrix
$\mathbf{K}_G$	geometric stiffness matrix
$\mathbf{K}_L$	load stiffness matrix
$\mathbf{L}$	velocity gradient tensor
M_ω	warping torque
M_{xf}	St. Venant torque
M_x, M_y, M_z	moments about x,y and z axes
M_{xp}, M_{yp}, M_{zp}	full plastic moments
M_{xy}	yield moment of M_x
$\mathbf{M}$	mass matrix
$\mathbf{N}$	row vector containing interpolation functions
N	axial force
$\mathbf{P}$	first Piola-Kirchhoff stress tensor

$\mathbf{q}$	nodal point displacement vector
Q_y, Q_z	shear forces
$\mathbf{Q}$	rigid body rotation, external load vector
	vector of stress resultants
$\mathbf{R}$	rotation tensor, vector of internal forces
s	path parameter
$\mathbf{S}$	second Piola-Kirchhoff stress tensor
t	time
$\mathbf{t}$	surface traction vector
T	kinetic energy
$\mathbf{T}$	Cauchy stress tensor, transformation matrix
$\mathbf{u}$	displacement vector
U	internal energy
u, v, w	displacement components
W	external energy
W_x, W_y, W_z	elastic section modulae
W_{xp}, W_{yp}, W_{zp}	plastic section modulae
$\mathbf{W}$	rate of rotation tensor, weighting matrix
$\mathbf{x}$	material point coordinate vector
x, y, z	orthogonal coordinate system

α	penalty parameter
α, β, γ	Euler angles
δ_{ij}	Kronecker delta
ε	axial strain
ϕ	eigenvector
γ_{xy}, γ_{xz}	shear strains
λ	load parameter
κ	hardening parameter
κ_x	twist per unit length
κ_y, κ_z	bending curvatures
ν	Poisson's ratio
ϕ, ψ, θ	rotations about x,y and z axes
θ	temperature
ρ	material density
σ_x	axial stress
σ_y	yield stress
τ_{xy}, τ_{xz}	shear stresses
ω	warping function, eigenvalue

Sub- and superscripts

$[\cdot]^T$	transpose of a matrix
$\bar{(\cdot)}$	prescribed value
	quantity measured in local coordinate system
$\dot{(\cdot)}$	time derivative
$\overset{*}{(\cdot)}$	corotational Zaremba-Jaumann rate
$\hat{(\cdot)}$	unit vector
$(\cdot)_c$	centroidal
$(\cdot)_{cr}$	critical value
$(\cdot)_r$	reference value
$(\cdot)_{,x}$	derivative with respect to x-coordinate
$(\cdot)'$	deviator
$(\cdot)^e$	elastic
$(\cdot)^{ep}$	elasto-plastic
$(\cdot)^p$	plastic
$(\cdot)^{vp}$	viscoplastic

Special symbols

$\hat{\delta}$	variation
$\delta, \boldsymbol{\delta}$	iterative change
$\Delta, \boldsymbol{\Delta}$	increment
$\cdot$	dot product
:	double dot product, i.e. $\mathbf{A} : \mathbf{B} = A_{ij} B_{ij}$
da, dv	area and volume elements with respect
	to the deformed configuration
dA, dV	area and volume elements w.r.t. the reference configuration
det	determinant
dim	dimension
div	divergence operator w.r.t. the deformed configuration
Div	divergence operator w.r.t. the reference configuration
grad	gradient operator w.r.t. the deformed configuration
ker	nullspace
tr	trace

1 INTRODUCTION

Frames are common load carrying systems in engineering constructions. Effective use of high strength materials and the tendency to optimazed constructions result in thin and slender structures. Due to the slenderness and increased imperfection sensitivity the stability problems become more significant. The character of the load deformation path in the post-buckling range is important in assessing the safety of the structure. Coupled geometrical and material nonlinearities complicate the structural analysis, and only numerical solutions are feasible in practical cases.

In this study a finite element method for both geometrically and materially nonlinear analyses of space frames is developed. Beams with both solid and thin-walled open cross-sections have been considered. The equations of equilibrium have been formulated using an updated incremental Lagrangian description. The elements developed can undergo large displacements and rotations, but the incremental rotations are assumed to be small. The material models adopted are elasto-plastic, temperature dependent elastic-plastic and visco-plastic models with special reference to metals. Additionally some computationally more economical formulations based on the relationship between stress resultants and generalized strain quantities have been presented. In the case of thin-walled beams the torsional behaviour is modelled using a two parametric deplanation model, where the angle of twist and it's derivative have independent approximations. This approach yields the average warping shear strains directly from the displacement assumptions and no discrepancy between stress and strain fields exist. Special emphasis has also been given to the solution algorithms of the discretized nonlinear equilibrium equations and the handling of critical points along the equilibrium path.

The earliest numerical analysing procedures for the nonlinear response of space frames were mainly based on the beam-column theory, where the effect of axial forces to the behaviour of the frame is taken into account, e.g. Renton (1962), Connor et al. (1968), Chu and Rampetsreiter (1973), Papandrakakis (1981) and Virtanen and Mikkola (1985). In those approaches the tangent stiffness matrix is formulated using the exact solution of the differential equation for a beam-column. It gives good accuracy in cases where the moments of inertia in the principal directions of the cross section are of same magnitude. In cases where the axial forces are small or the cross-section moments of inertia differ greatly, i.e. in lateral buckling problems, the analyses of space structures with the beam-column elements do not give satisfactory results.

The noncommutative nature of finite rotations in three dimensional space complicates the formulation of incremental equilibrium equations, capable for handling large rotation increments. Several studies for handling the large rotation

effects can be found in References, e.g. Argyris et al. (1978), Argyris (1982), Simo (1985), Cardona and Geradin (1988), Dvorkin et al. (1988), Friberg (1988a, b). Argyris et al. (1978) have introduced the semitangential rotation concept. In contrast to rotation about fixed axes these semitangential rotations which correspond to the semitangential torque of Ziegler (1968) possess the most important property of being commutative. Simo and Vu-Quoc (1986) have developed the configuration update procedure which is the algorithmic counterpart of the exponential map and the computational implementation relies on the formula for the exponential of a skew-symmetric matrix. In this Eulerian approach the tangent operator is non-symmetric in non-equilibrium configuration but the symmetry is shown to be recovered at equilibrium provided that the loading is conservative. Cardona and Geradin (1988) have used the rotational vector to parametrize rotations. They have treated Eulerian, total- and updated Lagrangian formulations. As pointed out by Cardona and Geradin (1988) an Eulerian approach allows, on one hand, a relatively simple derivation of fully linearized operators but, on the other hand these opeators are non-symmetric in a general case. Full symmetry of operators is obtained in the Lagrangian approach. Large deflection finite element formulations have been presented by e.g. Belytschko et al. (1977), Bathe and Bolourchi (1979), Remseth (1979). In these studies the nonlinear equations of motion have been formulated by the total Lagrangian or by the updated Lagrangian approach. In large deflection problems of beams the updated formulation has been found to be more economical and convenient than the total Lagrangian formulation, Bathe and Bolourchi (1979). A total Lagrangian formulation does not allow an easy manipulation of rotations exceeding the value of π, Cardona and Geradin (1988). Recently Sandhu et al. (1990) have used a co-rotational formulation in deriving the equations of equilibrium for a curved and twisted beam element. In the co-rotational formulation the rigid body motion is eliminated from the total displacements.

In all of the above mentioned studies the warping torsion has not been taken into account. The stiffness matrix of a thin-walled beam seems to have been first presented by Krahula (1967). The effects of initial bending moments and axial forces have been considered by Krajcinovic (1969), Barsoum and Gallagher (1970), Friberg (1985) and many others. Mottershead (1988a,b) has extended the semiloof beam element to include warping torsion of beams with thin-walled open cross-section. All the above mentioned studies have considered linear stability problems. The effect of pre-buckling deflections to the critical loads have been studied by, e.g. Attard (1986a) and van Erp (1989). Computational tools for nonlinear post-buckling analyses have been presented by Rajasekaran and Murray (1973), Besseling (1977), Hasegawa et al. (1987b), van Erp et al. (1988). Bažant and El Nimeiri (1973) have formulated the finite element equilibrium equations of a thin-

walled beam element for large deflection analysis, taking into account also initial bimoments. The study of Rajasekaran and Murray (1973) includes also elasto-plastic material properties. The above mentioned studies for thin-walled beams have utilized the Vlasov's theory of torsion and the Euler-Bernoulli theory for bending of thin beams. Seculović (1986) has proposed an alternative formulation which takes into account also the shear deformation in the middle line of the cross-section. In this formulation the warping of the cross-section is described by a set of axial displacement parameters, the number of which depends on the shape of the cross-section. It is also applicable for both closed and open cross-sections. Both Epstein and Murray (1976) and Chen and Blandford (1989) have suggested a formulation which takes into account the average shear strains due to warping torsion. Chen and Blandford presented a C^0 beam element for linear analysis while Epstein and Murray formulated an element capable for nonlinear problems.

Wunderlich et al. (1986) have used an incremental updated Lagrangian description in the derivation of the basic beam equations from a generalized variational principle. They have explored the influence of loading configuration, material parameters, geometric nonlinearities and warping constraints on the load-carrying behaviour and on the bifurcation and ultimate loads of thin-walled beam structures. The influence of material parameters have been investigated with both J_2 flow and deformation theories of plasticity. In their study the tangential stiffness matrices are obtained by direct numerical integration of the governing incremental differential equations and no a priori assumptions on the distribution of the field quantities have been made as in conventional finite element analyses.

A nonlinear theory of elastic beams with thin-walled open cross-sections has been derived by Møllmann (1981). In this theory the beam is regarded as a thin shell, and the appropriate geometrical constraints are introduced which constitute a generalization of those employed in Vlasov's linear theory. The rotations of the beam are described by means of a finite rotation vector. Computational results based on this theory have been presented by Pedersen (1982a,b) in which Koiter's general theory of elastic stability is used to carry out a perturbation analysis of the buckling and post buckling behaviour.

Attard (1986b) has developed a nonlinear theory for the non-uniform torsional response of straight prismatic beams with open cross-sections under conservative loads. Some computational results of nonlinear finite element analyses based on this theory are presented by Attard (1987).

2 EQUATIONS OF EQUILIBRIUM

The Euler's laws of motion state, Malvern (1969), Mikkola and Tuomala (1989), that the total force acting on the body $\mathcal{B}$ is equal to the rate of change of the linear momentum

$$\mathcal{P} = \int_v \rho \dot{\mathbf{x}} dv \tag{2.1}$$

of the body and that the total torque is equal to the rate of change of the angular momentum

$$\mathcal{L} = \int_v \mathbf{x} \times \rho \dot{\mathbf{x}} dv, \tag{2.2}$$

i.e.

$$\int_s \bar{\mathbf{t}}_n \cdot \hat{\mathbf{n}} ds + \int_v \rho \bar{\mathbf{f}} dv = \frac{d}{dt} \mathcal{P}, \tag{2.3}$$

$$\int_s \mathbf{x} \times \bar{\mathbf{t}}_n ds + \int_v \mathbf{x} \times \rho \bar{\mathbf{f}} dv = \frac{d}{dt} \mathcal{L}. \tag{2.4}$$

In these formulas $\bar{\mathbf{t}}_n, \bar{\mathbf{f}}$ denote the surface traction and the body force vectors, respectively. The exterior unit normal vector $\hat{\mathbf{n}}$ the surface area and the volume elements ds, dv, the material density ρ and the material point coordinate vector $\mathbf{x}$ are measured in the deformed configuration C_t at time t.

Making use of the Cauchy's stress principle

$$\bar{\mathbf{t}}_n = \mathbf{T} \cdot \hat{\mathbf{n}}, \tag{2.5}$$

where $\mathbf{T}$ is the Cauchy (Euler) stress tensor, and the divergence theorem, the Cauchy's laws of motion are obtained

$$\mathrm{div}\mathbf{T} + \rho \bar{\mathbf{f}} = \rho \ddot{\mathbf{x}}, \tag{2.6}$$

$$\mathbf{T} = \mathbf{T}^T. \tag{2.7}$$

The Cauchy's laws of motion (2.6) and (2.7) are related to the deformed configuration C_t. In solid mechanics it is more convenient to express the equations of motion in terms of quantities related to the known reference configuration C_o. Using the first Piola-Kirchhoff stress tensor $\mathbf{P}$, the local equations of motion can be expressed as

$$\mathrm{Div}\mathbf{P} + \rho_o \bar{\mathbf{f}} = \rho_o \ddot{\mathbf{x}}, \tag{2.8}$$

$$\mathbf{P} \cdot \mathbf{F}^T = \mathbf{F} \cdot \mathbf{P}^T, \tag{2.9}$$

in which Div denotes the divergence operator with respect to the reference configuration, $\mathbf{F}$ is the deformation gradient tensor and ρ_o is the material density

at the reference state. The first Piola-Kirchhoff stress tensor is related to the true Cauchy stress by the equation

$$\mathbf{P} = J\mathbf{T} \cdot \mathbf{F}^{-T}, \tag{2.10}$$

where J is the determinant of the deformation gradient and the superscript $-T$ means the transpose of the inverse tensor. If the symmetric second Piola-Kirchhoff stress tensor

$$\mathbf{S} = \mathbf{F}^{-1} \cdot \mathbf{P} = J\mathbf{F}^{-1} \cdot \mathbf{T} \cdot \mathbf{F}^{-T} \tag{2.11}$$

is used, then the first law of motion (2.8) can be written in the form

$$\mathrm{Div}(\mathbf{F} \cdot \mathbf{S}) + \rho_o \bar{\mathbf{f}} = \rho_o \ddot{\mathbf{x}}. \tag{2.12}$$

The sum of internal and external virtual works has to be zero for a body in an equilibrium state. Expressed in terms of Eulerian quantities the equation of virtual work has the form

$$\int_v \mathbf{T} : \hat{\delta}\mathbf{D} dt dv = \int_{\partial v} \bar{\mathbf{t}}_n \cdot \hat{\delta}\mathbf{u} ds + \int_v \rho(\bar{\mathbf{f}} - \ddot{\mathbf{x}}) \cdot \hat{\delta}\mathbf{u} dv, \tag{2.13}$$

where $\hat{\delta}$ means the variation and $\mathbf{D}$ is the rate of deformation tensor, i.e. the symmetric part of the velocity gradient tensor $\mathbf{L} = \mathrm{grad}\dot{\mathbf{x}}$. Equation (2.13) can be formulated in the reference configuration using the first or second Piola-Kirchhoff stress and the corresponding deformation measure, i.e.

$$\int_V \mathbf{P} : \hat{\delta}\mathbf{H} dV = \int_{\partial V} \bar{\mathbf{t}}_N \cdot \hat{\delta}\mathbf{u} dS + \int_V \rho_o(\bar{\mathbf{f}} - \ddot{\mathbf{x}}) \cdot \hat{\delta}\mathbf{u} dV, \tag{2.14}$$

$$\int_V \mathbf{S} : \hat{\delta}\mathbf{E} dV = \int_{\partial V} \bar{\mathbf{t}}_N \cdot \hat{\delta}\mathbf{u} dS + \int_V \rho_o(\bar{\mathbf{f}} - \ddot{\mathbf{x}}) \cdot \hat{\delta}\mathbf{u} dV, \tag{2.15}$$

in which $\mathbf{H} = \mathbf{F} - \mathbf{I}$ is the displacement gradient, $\mathbf{E} = (\mathbf{F}^T \cdot \mathbf{F} - \mathbf{I})/2$ the Green-Lagrange strain tensor and $\bar{\mathbf{t}}_N$ the traction vector per unit reference area

$$\bar{\mathbf{t}}_N dS = \mathbf{P} \cdot \hat{\mathbf{N}} dS = J\mathbf{T} \cdot \mathbf{F}^{-T} \cdot \hat{\mathbf{N}} dS = \mathbf{T} \cdot \hat{\mathbf{n}} ds = \bar{\mathbf{t}}_n ds.$$

The virtual work expression (2.15) is commonly used as a basis in the numerical computations.

The solution of the nonlinear equation (2.15) is obtained step by step. Therefore the incremental form of equation (2.15) is required. It is now assumed, that the solution has achieved configuration C_1, and the solution for an adjacent configuration C_2 is looked for. The incremental decompositions of stress and strain are

$$\begin{aligned} {}^2\mathbf{S} &= {}^1\mathbf{S} + \boldsymbol{\Delta}\mathbf{S}, \\ {}^2\mathbf{E} &= {}^1\mathbf{E} + \boldsymbol{\Delta}\mathbf{E}, \end{aligned} \tag{2.16}$$

and the variation of the Green-Lagrange strain at configuration C_2 is

$$\begin{aligned}\hat{\delta}({}^2\mathbf{E}) &= \frac{1}{2}({}^2\mathbf{F}^T \cdot \hat{\delta}\mathbf{F} + \hat{\delta}\mathbf{F}^T \cdot {}^2\mathbf{F}), \\ &= \hat{\delta}({}^1\mathbf{E}) + \frac{1}{2}(\boldsymbol{\Delta}\mathbf{H}^T \cdot \hat{\delta}\mathbf{H} + \hat{\delta}\mathbf{H}^T \cdot \boldsymbol{\Delta}\mathbf{H}).\end{aligned} \tag{2.17}$$

Substituting equations (2.17) and (2.16) into the virtual work expression (2.15) yields

$$\begin{aligned}&\int_V [\boldsymbol{\Delta}\mathbf{S} : \hat{\delta}({}^2\mathbf{E}) + (\boldsymbol{\Delta}\mathbf{H} \cdot {}^1\mathbf{S}) : \hat{\delta}\mathbf{H}]dV = \\ &\int_S {}^2\bar{\mathbf{t}}_N \cdot \hat{\delta}\mathbf{u}dS + \int_V \rho_o({}^2\bar{\mathbf{f}} - \ddot{\mathbf{x}}) \cdot \hat{\delta}\mathbf{u}dV - \int_V {}^1\mathbf{S} : \hat{\delta}({}^1\mathbf{E})dV.\end{aligned} \tag{2.18}$$

Two commonly used alternatives for the reference configuration are the undeformed state C_o or the last known equilibrium configuration C_1. These incremental strategies are known as total and updated Lagrangian formulations, respectively.

In the finite element method the displacement field $\mathbf{u}$ is approximated using shape functions $\mathbf{N}$ and nodal point displacement variables $\mathbf{q}$

$$\mathbf{u} = \mathbf{N}\mathbf{q}. \tag{2.19}$$

Substituting the approximation (2.19) into the virtual work equation, and expressing the stress increment in the form

$$\boldsymbol{\Delta}\mathbf{S} = \mathbf{C} : \boldsymbol{\Delta}\mathbf{E}, \tag{2.20}$$

where $\mathbf{C}$ is a fourth order tensor containing material parameters, yield the discretized incremental equations of motion, linearized with respect to $\boldsymbol{\Delta}\mathbf{q}$

$${}^1(\mathbf{K}_1 + \mathbf{K}_G)\boldsymbol{\Delta}\mathbf{q} = {}^2\mathbf{Q} - \mathbf{M}{}^2\ddot{\mathbf{q}} - {}^1\mathbf{R}, \tag{2.21}$$

where $\mathbf{K}_G$ is the initial stress or geometric stiffness matrix, $\mathbf{Q}$ the external load vector, $\mathbf{R}$ the internal force vector, $\mathbf{M}$ the consistent mass matrix and $\boldsymbol{\Delta}\mathbf{q}$ the incremental nodal point displacement vector. In the total Lagrangian formulation matrix $\mathbf{K}_1$ contains the linear stiffness and initial rotation matrices. In the updated Lagrangian formulation matrix $\mathbf{K}_1$ is dependent on the incremental displacement between configurations C_1 and C_2.

If the surface tractions depend on displacement configuration, an additional difficulty is encountered. It is assumed that the surface traction vector can be expressed as a function of a single parameter λ, i.e.

$${}^2\bar{\mathbf{t}} = {}^2\lambda\,{}^2\bar{\mathbf{t}}_r, \qquad {}^2\bar{\mathbf{t}}_r = \bar{\mathbf{t}}_r({}^2\mathbf{u}), \tag{2.22}$$

where $\bar{\mathbf{t}}_r$ is a reference traction vector, dependent on the deformations. However, the displacements ${}^2\mathbf{u}$ are unknown quantities and the traction vector ${}^2\bar{\mathbf{t}}$ has to be approximated by the equation

$$ {}^2\bar{\mathbf{t}} \approx {}^2\lambda\,{}^1\bar{\mathbf{t}}_r + \frac{\partial {}^1\bar{\mathbf{t}}}{\partial \mathbf{u}} \Delta\mathbf{u}. \tag{2.23} $$

For further details on displacement dependent loadings see Hibbit (1979), Argyris et al. (1982), and Schweizerhof and Ramm (1984). The last term in Equation (2.23) contributes to the tangent stiffness matrix, and the discretized equations of motion take the form

$$ {}^1(\mathbf{K}_1 + \mathbf{K}_G - \mathbf{K}_L)\Delta\mathbf{q} = {}^2\mathbf{Q} - \mathbf{M}\,{}^2\ddot{\mathbf{q}} - {}^1\mathbf{R}, \tag{2.24} $$

in which

$$ \mathbf{K}_L = \frac{\partial \mathbf{Q}}{\partial \mathbf{q}} \tag{2.25} $$

is the load stiffness matrix. In nonconservative loading cases the load stiffness matrix is unsymmetric.

The equations of motion can be solved also from the equation

$$ \mathbf{M}\,{}^2\ddot{\mathbf{q}} = {}^2\mathbf{Q} - {}^1\mathbf{R} \tag{2.26} $$

if an explicit integrator is used. The solution algorithms of the systems (2.24) and (2.26) are discussed in Chapter 8.

3 BEAMS WITH SOLID CROSS-SECTION

3.1 Kinematics of a beam

The deformation of an initially straight beam with undeformable cross-section is studied. With reference to Figure 3.1, let C be the centroidal axis of the cross-section and $(\hat{\mathbf{e}}_1, \hat{\mathbf{e}}_2, \hat{\mathbf{e}}_3)$ the unit orthonormal vector system in the reference configuration, with $\hat{\mathbf{e}}_1$ along the beam axis (x-axis), and $\hat{\mathbf{e}}_2, \hat{\mathbf{e}}_3$ principal axes of the cross-section (y- and z-axes). A deformed configuration of the beam is then defined by the vector function $\mathbf{r}(x)$, which characterizes the position of the beam axis, and by the function $\mathbf{Q}(x)$; an orthogonal tensor defining the rigid rotation of the cross-section at x, Ascione and Grimaldi (1983),

$$\mathbf{Q} \cdot \hat{\mathbf{e}}_i = \hat{\mathbf{g}}_i, \qquad i = 1, 2, 3, \tag{3.1}$$

where $\hat{\mathbf{g}}_i$ are the unit base vectors in the deformed configuration. If $\mathbf{x}_o = \mathbf{r}_o + \mathbf{y}_o$ is the material vector in the undeformed reference configuration and $\mathbf{x} = \mathbf{r} + \mathbf{y}$ (vectors $\mathbf{y}$ and $\mathbf{y}_o$ are in the cross-section plane) the corresponding vector in the deformed state, they are related by the equation

$$\mathbf{x} = \mathbf{r} + \mathbf{Q} \cdot \mathbf{y}_o. \tag{3.2}$$

The displacement vector $\mathbf{u}$ is then

$$\mathbf{u} = \mathbf{x} - \mathbf{x}_0 = \mathbf{u}_c + (\mathbf{Q} - \mathbf{I}) \cdot \mathbf{y}_o, \tag{3.3}$$

where $\mathbf{u}_c = \mathbf{r} - \mathbf{r}_o$ is the translational displacement vector and $\mathbf{I}$ the unit tensor. The difficulty is to obtain $\mathbf{Q}$. It can be assumed that $\mathbf{Q}$ can be broken down as

$$\mathbf{Q} = \mathbf{Q}_\theta \cdot \mathbf{Q}_\psi \cdot \mathbf{Q}_\phi, \tag{3.4}$$

where $\mathbf{Q}_\phi, \mathbf{Q}_\psi$ and $\mathbf{Q}_\theta$ are the rotation tensors, defining the rotation of magnitude $\phi, -\psi$ and θ about the reference axes $\hat{\mathbf{e}}_1, \hat{\mathbf{e}}_2$ and $\hat{\mathbf{e}}_3$, respectively. Unfortunately, the sequence in which the rotations are performed is crucial.

Keeping in mind, that the kinematical relations for an updated incremental finite element analysis are sought, the rotation tensor (3.4) can be linearized. The component forms of tensors $\mathbf{Q}_\phi, \mathbf{Q}_\psi$ and $\mathbf{Q}_\theta$ are:

$$\mathbf{Q}_\phi = \begin{bmatrix} 1 & 0 & 0 \\ 0 & \cos\phi & -\sin\phi \\ 0 & \sin\phi & \cos\phi \end{bmatrix}, \tag{3.5a}$$

$$\mathbf{Q}_\psi = \begin{bmatrix} \cos\psi & 0 & \sin\psi \\ 0 & 1 & 0 \\ -\sin\psi & 0 & \cos\psi \end{bmatrix}, \tag{3.5b}$$

$$\mathbf{Q}_\theta = \begin{bmatrix} \cos\theta & -\sin\theta & 0 \\ \sin\theta & \cos\theta & 0 \\ 0 & 0 & 1 \end{bmatrix}. \tag{3.5c}$$

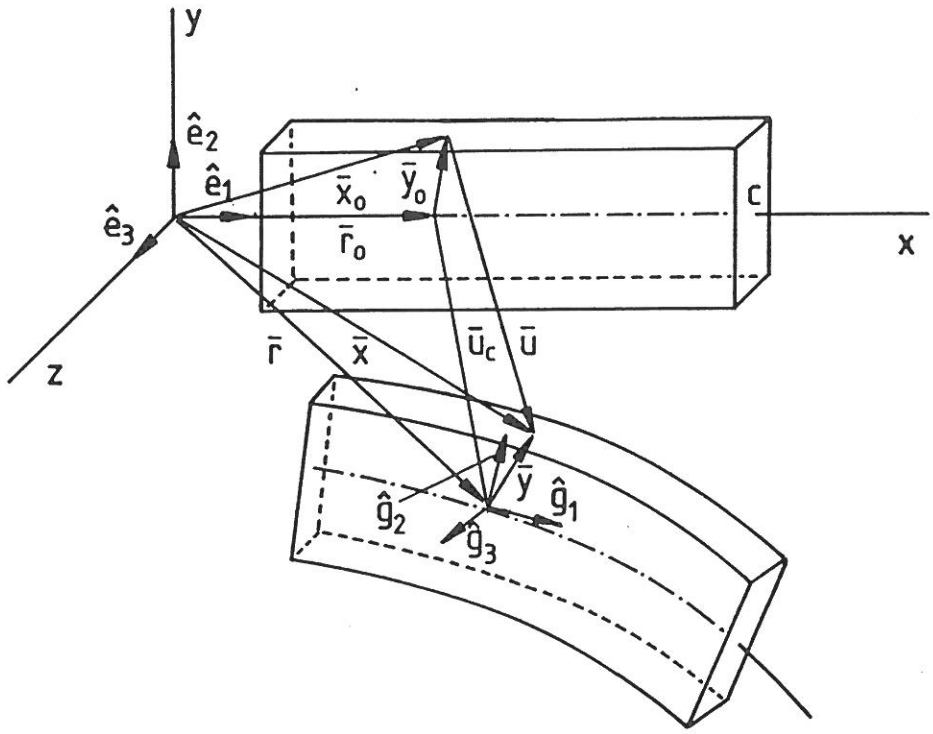

Figure 3.1 Deformation of a beam.

The following expression for the components of $\mathbf{Q}$ with respect to the system $(\hat{\mathbf{e}}_1, \hat{\mathbf{e}}_2, \hat{\mathbf{e}}_3)$ is obtained

$$\mathbf{Q} = \begin{bmatrix} C\psi C\theta & S\phi S\psi C\theta - C\phi S\theta & C\phi S\psi C\theta + S\phi S\theta \\ C\psi S\theta & S\phi S\psi S\theta + C\phi C\theta & C\phi S\psi S\theta - S\phi C\theta \\ -S\psi & S\phi C\psi & C\phi C\psi \end{bmatrix}, \tag{3.6}$$

where the abbreviations for trigonometric functions $C = \cos$ and $S = \sin$ are used. If the rotations are small, $\cos\phi \approx 1 - 1/2\phi^2$ and $\sin\phi \approx \phi$ etc., and the rotation tensor becomes

$$\mathbf{Q} = \begin{bmatrix} 1 - \frac{1}{2}\psi^2 - \frac{1}{2}\theta^2 & -\theta + \phi\psi & \psi + \phi\theta \\ \theta & 1 - \frac{1}{2}\phi^2 - \frac{1}{2}\theta^2 & -\phi + \psi\theta \\ -\psi & \phi & 1 - \frac{1}{2}\phi^2 - \frac{1}{2}\psi^2 \end{bmatrix}$$

where cubic and higher order terms have been omitted. Neglecting the nonlinear terms, the linearized form

$$\mathbf{Q} = \begin{bmatrix} 1 & -\theta & \psi \\ \theta & 1 & -\phi \\ -\psi & \phi & 1 \end{bmatrix} \tag{3.7}$$

is obtained.

The position vector $\mathbf{y}_o$ and the displacement vectors $\mathbf{u}$ and $\mathbf{u}_c$ are

$$\mathbf{y}_o = \begin{bmatrix} 0 \\ y \\ z \end{bmatrix}, \quad \mathbf{u} = \begin{bmatrix} u \\ v \\ w \end{bmatrix}, \quad \mathbf{u}_c = \begin{bmatrix} u_c \\ v_c \\ w_c \end{bmatrix}, \tag{3.8}$$

where u_c, v_c and w_c denote the deflections of the centroid axis in the x, y and z

$(\hat{\mathbf{e}}_1, \hat{\mathbf{e}}_2, \hat{\mathbf{e}}_3)$ directions. Then Equation (3.3) becomes

$$\begin{aligned} u &= u_c - \theta y + \psi z, \\ v &= v_c - \phi z, \\ w &= w_c + \phi y. \end{aligned} \tag{3.9}$$

Equations (3.9) were obtained by assuming, that the cross-section remains planar during the deformation. However, warping displacements take place when the cross-section is twisted. The warping displacement is assumed to depend on the derivative of the angle of twist, Love (1944), according to equation

$$u_\omega = -\omega(y,z)\phi_{,x}, \tag{3.10}$$

where ω is the warping function which depends on the cross-section shape, and can be solved from Laplace equation

$$\begin{aligned} \omega_{,yy} + \omega_{,zz} &= 0 \quad \text{in } A, \\ \text{grad}\omega \cdot \hat{\mathbf{n}} &= 0 \quad \text{on } \partial A. \end{aligned} \tag{3.11}$$

For a rectangular cross-section the warping function has a series expression, Love (1944)

$$\omega(y,z) = yz - 4b^2(\frac{2}{\pi})^3 \sum_{n=0}^{\infty} \frac{(-1)^n}{(2n+1)^3} \frac{\sinh \frac{(2n+1)}{2b}\pi z}{\cosh \frac{(2n+1)}{2b}\pi h} \sin \frac{(2n+1)\pi y}{2b}, \tag{3.12}$$

where b and h are the lengths of the cross-section sides. A close approximation to the expression (3.12) for a narrow section is

$$\omega(y,z) = \omega_1 yz \tag{3.13}$$

and for a square section

$$\omega(y,z) = \omega_2 yz(z^2 - y^2). \tag{3.14}$$

Combining both the approximations (3.13) and (3.14) yields a good approximation to the warping function of a general rectangular cross-section, Bathe and Chaudhary (1982):

$$\omega(y,z) = yz[\omega_1 + \omega_2(z^2 - y^2)]. \tag{3.15}$$

In the finite element analysis the torque is usually constant within an element. Therefore the expression (3.15) contains two additional parameters for each element to be solved. These parameters ω_1 and ω_2 can be eliminated by static condensation prior the assemblage of the element matrices into the global structural matrix, Bathe

and Caudhary (1982). Alternatively, these parameters can be solved a priori from the minimization process of the functional

$$\Pi = \int_A [(y - \omega_{,z})^2 + (z + \omega_{,y})^2] dA, \tag{3.16}$$

which yields the system

$$\begin{bmatrix} a_{11} & a_{12} \\ a_{21} & a_{22} \end{bmatrix} \begin{Bmatrix} \omega_1 \\ \omega_2 \end{Bmatrix} = \begin{Bmatrix} f_1 \\ f_2 \end{Bmatrix}, \tag{3.17}$$

where

$$\begin{aligned} a_{11} &= I_y + I_z, \\ a_{12} &= \frac{A}{80}(h^4 - b^4), \\ a_{21} &= a_{12}, \\ a_{22} &= \frac{A^3}{320}(h^2 + b^2) + \frac{A}{448}(h^6 + b^6), \\ f_1 &= I_z - I_y, \\ f_2 &= \frac{A}{80}(h^4 + b^4) - \frac{A^3}{24}, \\ A &= hb, \\ I_y &= \int_A z^2 dA = \frac{hb^3}{12}, \\ I_z &= \int_A y^2 dA = \frac{bh^3}{12}. \end{aligned} \tag{3.18}$$

An approximation of the torsional rigidity

$$I_t = \int_A [(y - \omega_{,z})^2 + (z + \omega_{,y})^2] dA, \tag{3.19}$$

is obtained from equation

$$I_t = I_y + I_z + \omega_1 f_1 + \omega_2 f_2. \tag{3.20}$$

The final linearized displacement equations are obtained by combining Equations (3.9), (3.10), (3.15) and (3.17)

$$\begin{aligned} u &= u_c - \theta y + \psi z - \omega \phi_{,x}, \\ v &= v_c - \phi z, \\ w &= w_c + \phi y. \end{aligned} \tag{3.21}$$

These linearized equations can be used for incremental displacement assumptions in nonlinear finite element computations. Wunderlich et al. (1986) have retained a nonlinear term for ϕ-rotation

$$\begin{aligned} v &= v_c - \phi z + (\cos\phi - 1) y, \\ w &= w_c + \phi y + (\cos\phi - 1) z, \end{aligned}$$

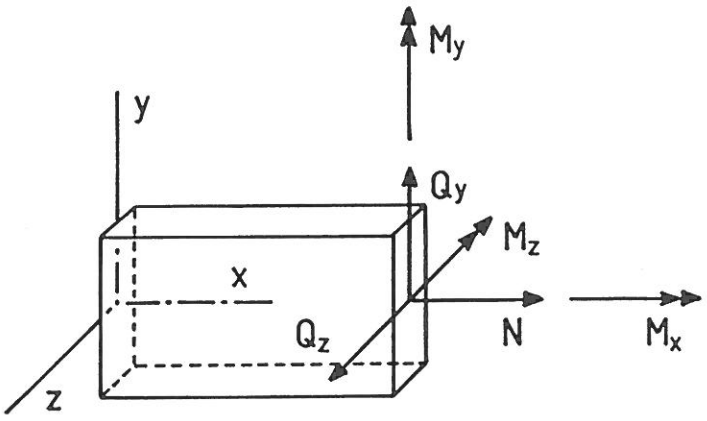

Figure 3.2 Stress resultants of a beam.

and used the two term approximation $\cos\phi \approx 1-\phi^2/2$ in their numerical calculations. Resulting displacement assumptions can be written in the form

$$\begin{aligned} u &= u_c - \theta y + \psi z - \omega\phi_{,x}, \\ v &= v_c - \phi z - \frac{1}{2}\phi^2 y, \\ w &= w_c + \phi y - \frac{1}{2}\phi^2 z. \end{aligned} \tag{3.22}$$

These equations are also used in the present study. However, the effect of the quadratic terms in Equations (3.22) has been found to be neglible in the numerical experiments.

The stress resultants of a three dimensional beam are defined by equations

$$\begin{aligned} N &= \int_A \sigma_x dA, \\ Q_y &= \int_A \tau_{xy} dA, \\ Q_z &= \int_A \tau_{xz} dA, \\ M_x &= \int_A (\tau_{xz} y - \tau_{xy} z) dA, \\ M_y &= \int_A \sigma_x z dA, \\ M_z &= \int_A \sigma_x y dA, \end{aligned} \tag{3.23}$$

which are illustrated in Figure 3.2.

3.2 Beam elements

3.2.1 Elements based on Timoshenko beam theory

For a straight beam element with solid cross-section, the incremental displacement equations, based on displacement assumption in Equation (3.22), are

$$\begin{aligned}
\Delta u(x,y,z) &= \Delta u_c(x) + z\Delta\psi(x) - y\Delta\theta(x) - \omega(y,z)\Delta\phi_{,x}(x),\\
\Delta v(x,y,z) &= \Delta v_c(x) - z\Delta\phi(x) - \frac{1}{2}y[\Delta\phi(x)]^2,\\
\Delta w(x,y,z) &= \Delta w_c(x) + y\Delta\phi(x) - \frac{1}{2}z[\Delta\phi(x)]^2.
\end{aligned} \tag{3.24}$$

The only nonlinear terms which have been retained correspond to the rotation about the centroidal axis of the beam, as done also by Wunderlich et al. (1986). The incremental displacements after some equilibrium iterations will be denoted by $\Delta u^1, \Delta v^1, \Delta w^1, \Delta\phi^1, \Delta\psi^1$ and $\Delta\theta^1$. The iterative changes, which have to be solved are $\delta u, \delta v, \delta w, \delta\phi, \delta\psi$ and $\delta\theta$, and the incremental displacements are

$$\begin{aligned}
\Delta u_c &= \Delta u_c^1 + \delta u_c,\\
\Delta v_c &= \Delta v_c^1 + \delta v_c,\\
\Delta w_c &= \Delta w_c^1 + \delta w_c,\\
\Delta\phi &= \Delta\phi^1 + \delta\phi,\\
\Delta\psi &= \Delta\psi^1 + \delta\psi.\\
\Delta\theta &= \Delta\theta^1 + \delta\theta,
\end{aligned} \tag{3.25}$$

The iterative changes in the Green-Lagrange strain tensor components can be solved from the equations

$$\begin{aligned}
\delta\varepsilon_x &= \Delta\varepsilon_x - \Delta\varepsilon_x^1,\\
\delta\gamma_{xy} &= \Delta\gamma_{xy} - \Delta\gamma_{xy}^1,\\
\delta\gamma_{xz} &= \Delta\gamma_{xz} - \Delta\gamma_{xz}^1,
\end{aligned} \tag{3.26}$$

where $\Delta\varepsilon_x = \Delta\varepsilon_x(\Delta u, \Delta v, \Delta w), \Delta\varepsilon_x^1 = \Delta\varepsilon_x(\Delta u^1, \Delta v^1, \Delta w^1)$ etc. Substitution of the decomposition of incremental displacement vector to Expressions (3.26) yields

$$\begin{aligned}
\delta\varepsilon_x =& (1 + \Delta u_{c,x}^1 - y\Delta\theta_{,x}^1 + z\Delta\psi_{,x}^1)\delta u_{c,x}\\
&+ (\Delta v_{c,x}^1 - z\Delta\phi_{,x}^1 - y\Delta\phi^1\Delta\phi_{,x}^1)\delta v_{c,x}\\
&+ (\Delta w_{c,x}^1 + y\Delta\phi_{,x}^1 - z\Delta\phi^1\Delta\phi_{,x}^1)\delta w_{c,x}\\
&+ \Delta\phi_{,x}^1(r^2\Delta\phi^1\Delta\phi_{,x}^1 - z\Delta w_{c,x}^1 - y\Delta v_{c,x}^1)\delta\phi\\
&+ \{r^2\Delta\phi_{,x}^1[1 + (\Delta\phi^1)^2] - z(\Delta v_{c,x}^1 + \Delta w_{c,x}^1\Delta\phi^1)\\
&- y(\Delta v_{c,x}^1\Delta\phi^1 - \Delta w_{c,x}^1)\}\delta\phi_{,x}
\end{aligned}$$

$$
\begin{aligned}
&+ z(1 + \Delta u^1_{c,x} - y\Delta\theta^1_{,x} + z\Delta\psi^1_{,x})\delta\psi_{,x} \\
&- y(1 + \Delta u^1_{c,x} - y\Delta\theta^1_{,x} + z\Delta\psi^1_{,x})\delta\theta_{,x} \\
&+ \frac{1}{2}\{\delta u^2_{c,x} + \delta v^2_{c,x} + \delta w^2_{c,x} + r^2[1 + (\Delta\phi^1)^2]\delta\phi^2_{,x} \\
&+ r^2(\Delta\phi^1_{,x})^2\delta\phi^2 + z^2\delta\psi^2_{,x} + y^2\delta\theta^2_{,x}\} \\
&- y\delta u_{c,x}\delta\theta_{,x} + z\delta u_{c,x}\delta\psi_{,x} - yz\delta\psi_{,x}\theta_{,x} \\
&- y\Delta\phi^1_{,x}\delta v_{c,x}\delta\phi - z\Delta\phi^1_{,x}\delta w_{c,x}\delta\phi \\
&+ (2r^2\Delta\phi^1\Delta\phi^1_{,x} - y\Delta v^1_{c,x} - z\Delta w^1_{c,x})\delta\phi\delta\phi_{,x}, \qquad (3.27a)
\end{aligned}
$$

$$
\begin{aligned}
\delta\gamma_{xy} = &- \Delta\theta^1\delta u_{c,x} + [1 - (\Delta\phi^1)^2/2]\delta v_{c,x} + \Delta\phi^1\delta w_{c,x} - (z + \omega_{,y})\delta\phi_{,x} \\
&+ (\Delta w^1_{c,x} + \Delta v^1_{c,x}\Delta\phi^1)\delta\phi - (1 + \Delta u^1_{c,x})\delta\theta \\
&- \delta u_{c,x}\delta\theta - \Delta v^1_{c,x}\delta\phi^2/2 - \Delta\phi^1\delta v_{c,x}\delta\phi + \delta w_{c,x}\delta\phi, \qquad (3.27b)
\end{aligned}
$$

$$
\begin{aligned}
\delta\gamma_{xz} = &\Delta\psi^1\delta u_{c,x} + \Delta\phi^1\delta v_{c,x} + [1 - (\Delta\phi^1)^2/2]\delta w_{c,x} + (y - \omega_{,z})\delta\phi_{,x} \\
&- (\Delta v^1_{c,x} + \Delta w^1_{c,x}\Delta\phi^1)\delta\phi + (1 + \Delta u^1_{c,x})\delta\psi \\
&+ \delta u_{c,x}\delta\psi - \delta v_{c,x}\delta\phi, -\Delta\phi^1\delta w_{c,x}\delta\phi - \Delta w^1_{c,x}\delta\phi^2/2, \qquad (3.27c)
\end{aligned}
$$

where the notation $r^2 = y^2 + z^2$ is introduced, and the term $-\omega\delta\phi_{,xx}$ is omitted in the expression for $\delta\varepsilon_x$. Substituting the finite element displacement assumptions

$$
\begin{aligned}
\delta u_c &= \mathbf{N}_u\boldsymbol{\delta}\mathbf{q}_u, \\
\delta v_c &= \mathbf{N}_v\boldsymbol{\delta}\mathbf{q}_v, \\
\delta w_c &= \mathbf{N}_w\boldsymbol{\delta}\mathbf{q}_w, \\
\delta\phi &= \mathbf{N}_\phi\boldsymbol{\delta}\mathbf{q}_\phi, \\
\delta\psi &= \mathbf{N}_\psi\boldsymbol{\delta}\mathbf{q}_\psi, \\
\delta\theta &= \mathbf{N}_\theta\boldsymbol{\delta}\mathbf{q}_\theta,
\end{aligned} \qquad (3.28)
$$

into Equations (3.27a)-(3.27c), the strain increments $\delta\varepsilon_x, \delta\gamma_{xy}$ and $\delta\gamma_{xz}$ are found in terms of the nodal parameters $\boldsymbol{\delta}\mathbf{q}$. The discrete gradient operator i.e. the linear strain displacement matrix is

$$
\mathbf{B} = \begin{bmatrix}
a_1\mathbf{N}_{u,x} & a_2\mathbf{N}_{v,x} & a_3\mathbf{N}_{w,x} & a_4\mathbf{N}_\phi + a_5\mathbf{N}_{\phi,x} & a_6\mathbf{N}_{\psi,x} & a_7\mathbf{N}_{\theta,x} \\
b_1\mathbf{N}_{u,x} & b_2\mathbf{N}_{v,x} & b_3\mathbf{N}_{w,x} & b_4\mathbf{N}_\phi + b_5\mathbf{N}_{\phi,x} & \mathbf{0} & b_7\mathbf{N}_\theta \\
c_1\mathbf{N}_{u,x} & c_2\mathbf{N}_{v,x} & c_3\mathbf{N}_{w,x} & c_4\mathbf{N}_\phi + c_5\mathbf{N}_{\phi,x} & c_6\mathbf{N}_\psi & \mathbf{0}
\end{bmatrix}, \qquad (3.29)
$$

where the abbreviations a_i, b_i and c_i are

$$
\begin{aligned}
a_1 &= 1 + \Delta u^1_{c,x} - y\Delta\theta^1_{,x} + z\Delta\psi^1_{,x},\\
a_2 &= \Delta v^1_{c,x} - \Delta\phi^1_{,x}(z + y\Delta\phi^1),\\
a_3 &= \Delta w^1_{c,x} + \Delta\phi^1_{,x}(y - z\Delta\phi^1),\\
a_4 &= \Delta\phi^1_{,x}(r^2\Delta\phi^1\Delta\phi^1_{,x} - z\Delta w^1_{c,x} - y\Delta v^1_{c,x}),\\
a_5 &= r^2\Delta\phi^1_{,x}[1 + (\Delta\phi^1)^2] - z(\Delta v^1_{c,x} + \Delta w^1_{c,x}\Delta\phi^1) - y(\Delta v^1_{c,x}\Delta\phi^1 + \Delta w^1_{c,x}),\\
a_6 &= za_1,\\
a_7 &= -ya_1,\\
b_1 &= -\Delta\theta^1,\\
b_2 &= 1 - (\Delta\theta^1)^2/2,\\
b_3 &= \Delta\phi^1,\\
b_4 &= \Delta w^1_{c,x} + \Delta v^1_{c,x}\Delta\phi^1,\\
b_5 &= -z - \omega_{,y},\\
b_7 &= -1 - \Delta u^1_{c,x},\\
c_1 &= \Delta\psi^1,\\
c_2 &= -\Delta\phi^1,\\
c_3 &= 1 - (\Delta\theta^1)^2/2,\\
c_4 &= -\Delta v^1_{c,x} - \Delta w^1_{c,x}\Delta\phi^1,\\
c_5 &= y - \omega_{,z},\\
c_6 &= 1 + \Delta u^1_{c,x},
\end{aligned}
\tag{3.30}
$$

Using the linear strain-displacement matrix $\mathbf{B}$ and the constitutive matrix $\mathbf{C}$, matrix $\mathbf{K_1}$ in Equation (2.21) can be written in the form

$$\mathbf{K}_1 = \int_V \mathbf{B}^T\mathbf{C}\mathbf{B}dV, \tag{3.31}$$

and the internal force vector correspondingly

$$\mathbf{R}^1 = \int_V \mathbf{B}^T\tilde{\mathbf{S}}^1 dV, \tag{3.32}$$

where $\tilde{\mathbf{S}}^1$ is the vector of 2nd Piola Kirchhoff stresses $\tilde{\mathbf{S}}^1 = [\,S^1_x \quad S^1_{xy} \quad S^1_{xz}\,]^T$. The geometric stiffness has the form

$$\mathbf{K}_G = \begin{bmatrix}
\mathbf{K}_{Guu} & \mathbf{0} & \mathbf{0} & \mathbf{0} & \mathbf{K}_{Gu\psi} & \mathbf{K}_{Gu\theta}\\
 & \mathbf{K}_{Gvv} & \mathbf{0} & \mathbf{K}_{Gv\phi} & \mathbf{0} & \mathbf{0}\\
 & & \mathbf{K}_{Gww} & \mathbf{K}_{Gw\phi} & \mathbf{0} & \mathbf{0}\\
 & & & \mathbf{K}_{G\phi\phi} & \mathbf{0} & \mathbf{0}\\
 & & & & \mathbf{K}_{G\psi\psi} & \mathbf{K}_{G\psi\theta}\\
\text{s} & \text{y} & \text{m} & \text{m.} & & \mathbf{K}_{G\theta\theta}
\end{bmatrix}, \tag{3.33}$$

in which

$$
\begin{aligned}
\mathbf{K}_{Guu} &= \int_V S^1_x \mathbf{N}^T_{u,x} \mathbf{N}_{u,x} dV, \\
\mathbf{K}_{Gvv} &= \int_V S^1_x \mathbf{N}^T_{v,x} \mathbf{N}_{v,x} dV, \\
\mathbf{K}_{Gww} &= \int_V S^1_x \mathbf{N}^T_{w,x} \mathbf{N}_{w,x} dV, \\
\mathbf{K}_{G\phi\phi} &= \int_V S^1_x \{ r^2 [1 + (\Delta\phi^1)^2] \mathbf{N}^T_{\phi,x} \mathbf{N}_{\phi,x} + r^2 (\Delta\phi^1_{,x})^2 \mathbf{N}^T_\phi \mathbf{N}_\phi \\
&\quad + (2r^2 \Delta\phi^1 \delta\phi^1_{,x} - y\Delta v^1_{c,x} - z\Delta w^1_{c,x})(\mathbf{N}^T_\phi \mathbf{N}_{\phi,x} + \mathbf{N}^T_{\phi,x} \mathbf{N}_\phi) \} dV \\
&\quad - \int_V (S^1_{xy} \Delta w^1_{c,x} + S^1{}_{xz} \Delta v^1_{c,x}) \mathbf{N}^T_\phi \mathbf{N}_\phi dV, \\
\mathbf{K}_{Gw\phi} &= \int_V S^1_x [(y - z\Delta\phi^1) \mathbf{N}^T_{w,x} \mathbf{N}_{\phi,x} - z\Delta\phi^1_{,x} \mathbf{N}^T_{w,x} \mathbf{N}_\phi] dV \\
&\quad + \int_V (S^1_{xy} - S^1_{xz} \Delta\phi^1) \mathbf{N}^T_{w,x} \mathbf{N}_\phi dV, \\
\mathbf{K}_{Gv\phi} &= -\int_V S^1_x [(z + y\Delta\phi^1) \mathbf{N}^T_{v,x} \mathbf{N}_{\phi,x} + y\Delta\phi^1_{,x} \mathbf{N}^T_{v,x} \mathbf{N}_\phi] dV \\
&\quad - \int_V (S^1_{xy} \Delta\phi^1 + S^1_{xz}) \mathbf{N}^T_{v,x} \mathbf{N}_\phi dV, \\
\mathbf{K}_{G\psi\psi} &= \int_V S^1_x z^2 \mathbf{N}^T_{\psi,x} \mathbf{N}_{\psi,x} dV, \\
\mathbf{K}_{Gu\psi} &= \int_V S^1_x z \mathbf{N}^T_{u,x} \mathbf{N}_{\psi,x} dV + \int_V S^1_{xz} \mathbf{N}^T_{u,x} \mathbf{N}_\psi dV, \\
\mathbf{K}_{G\theta\theta} &= \int_V S^1_x y^2 \mathbf{N}^T_{\theta,x} \mathbf{N}_{\theta,x} dV, \\
\mathbf{K}_{G\psi\theta} &= -\int_V S^1_x yz \mathbf{N}^T_{\psi,x} \mathbf{N}_{\theta,x} dV, \\
\mathbf{K}_{Gu\theta} &= -\int_V S^1_x y \mathbf{N}^T_{u,x} \mathbf{N}_{\theta,x} dV - \int_V S^1_{xy} \mathbf{N}^T_{u,x} \mathbf{N}_\theta dV.
\end{aligned}
\tag{3.34}
$$

The integrations along the x-axis direction have to be done by the one point Gaussian quadrature when linear shape functions for each displacement quantity are used. The one point rule integrates exactly the bending stiffness part and makes the shear stiffness singular, thus the element does not lock when the structure becomes slender. The one point integration yields the same linear stiffness matrix as is obtained by using an additional hierarchical parabolic mode for deflection and condensing out this additional degree of freedom.

Also higher order interpolation can be used yielding an subparametric element. In geometrically nonlinear analysis the interpolation of geometry is important. Much better computational effectivity can be achieved by using a linear isoparametric element.

Over the cross-sectional area either Gauss or Simpson integration rules can be used. In the elastic case and when the cross-section is narrow ($h/b \geq 10$) the 2×2 Gaussian or the 3×3 Simpson's rule is sufficient, although these rules underintegrate the torsional rigidity term (3.19)

$$I_t = \int_A [(y - \omega_{,z})^2 + (z + \omega_{,y})^2] dA,$$

when the approximate warping function (3.15) is used. However, the underintegrated torsional rigidity is closer to the exact value than using the 4×4 Gaussian rule, which integrates Expression (3.15) exactly. When the cross-section is a square the 4×4 Gaussian rule gives the best accuracy, see table 3.1.

The consistent mass matrix is

$$\mathbf{M} = \begin{bmatrix} \mathbf{M}_{uu} & & & & & & \\ & \mathbf{M}_{vv} & & & & & \\ & & \mathbf{M}_{ww} & & & & \\ & & & \mathbf{M}_{\phi\phi} & & & \\ & & & & \mathbf{M}_{\psi\psi} & & \\ & & & & & \mathbf{M}_{\theta\theta} & \end{bmatrix}, \tag{3.35}$$

in which the submatrices $\mathbf{M}_{ij}$ are

$$\begin{aligned} \mathbf{M}_{uu} &= \int_V \rho \mathbf{N}_u^T \mathbf{N}_u dV, \\ \mathbf{M}_{vv} &= \int_V \rho \mathbf{N}_v^T \mathbf{N}_v dV, \\ \mathbf{M}_{ww} &= \int_V \rho \mathbf{N}_w^T \mathbf{N}_w dV, \\ \mathbf{M}_{\phi\phi} &= \int_V \rho r^2 \mathbf{N}_\phi^T \mathbf{N}_\phi dV, \\ \mathbf{M}_{\psi\psi} &= \int_V \rho z^2 \mathbf{N}_\psi^T \mathbf{N}_\psi dV, \\ \mathbf{M}_{\theta\theta} &= \int_V \rho y^2 \mathbf{N}_\theta^T \mathbf{N}_\theta dV. \end{aligned} \tag{3.36}$$

For a linear two node element the diagonal mass matrix can be written in the form

$$\mathbf{M} = \begin{bmatrix} \mathbf{M}_d & \\ & \mathbf{M}_d \end{bmatrix}, \tag{3.37}$$

where the submatrice $\mathbf{M}_d$ has the form

$$\mathbf{M}_d = \frac{m}{2} \begin{bmatrix} 1 & & & & & & \\ & 1 & & & & & \\ & & 1 & & & & \\ & & & I_p/A & & & \\ & & & & I_y/A + L^2/12 & & \\ & & & & & I_z/A + L^2/12 & \end{bmatrix}, \tag{3.38}$$

Table 3.1 Accuracy of the numerically evaluated torsional rigidity for a rectangular cross-section when approximate warping function (3.15) is used.

rule		h/b	I_t/hb^3	I_t^{exact}/hb^3	error %	
Gauss	2×2	1	0.091449	0.140577	34.95	
	3×3		0.139012		1.11	
	4×4		0.140741		0.12	$\star$
Simpson	3×3		0.217078		54.42	
	5×5		0.147200		4.71	
	7×7		0.142078		1.07	
Gauss	2×2	2	0.164863	0.228682	27.91	
	3×3		0.223800		2.13	
	4×4		0.230596		0.84	$\star$
Simpson	3×3		0.338634		48.08	
	5×5		0.243985		6.69	
	7×7		0.233483		2.10	
Gauss	2×2	4	0.248022	0.280813	11.68	
	3×3		0.275483		1.90	$\star$
	4×4		0.288537		2.75	
Simpson	3×3		0.367442		30.85	
	5×5		0.306217		9.05	
	7×7		0.292496		4.16	
Gauss	2×2	10	0.313838	0.312325	0.48	$\star$
	3×3		0.317249		1.58	
	4×4		0.323219		3.49	
Simpson	3×3		0.345581		10.65	
	5×5		0.330447		5.80	
	7×7		0.324860		4.01	
Gauss	2×2	100	0.333122	0.331233	0.57	$\star$
	3×2		0.333145		0.58	
	4×2		0.333222		0.60	
Simpson	3×3		0.333481		0.68	
	5×3		0.333314		0.63	
	7×3		0.333243		0.61	

$\star$ smallest error

The notations are $I_p = I_y + I_z, L$ is the length and $m = \rho AL$ is the mass of an element.

The virtual work expression for internal forces can be formulated using stress resultants and the corresponding generalized strain quantities

$$\int_V {}^2S_{ij}\hat{\delta}({}^2E_{ij})dV =$$

$$\int_0^L [{}^2N\hat{\delta}({}^2\varepsilon_c) + {}^2Q_y\hat{\delta}({}^2\gamma_{xy}) + {}^2Q_z\hat{\delta}({}^2\gamma_{xz}) + {}^2M_x\hat{\delta}({}^2\kappa_x) + {}^2M_y\hat{\delta}({}^2\kappa_y) + {}^2M_z\hat{\delta}({}^2\kappa_z)]dx, \tag{3.39}$$

where the stress resultants N, Q_y, Q_z, M_x, M_y and M_z are defined in Equations (3.23). The generalized strain measures, the elongation ε_c at the cross-section center, the shear strains γ_{xy}, γ_{xz}, the twist per unit length κ_x and the bending curvatutes κ_y and κ_z are defined by equations

$$\begin{aligned}
\varepsilon_c &= u_{c,x} + \frac{1}{2}(v_{c,x}^2 + w_{c,x}^2), \\
\gamma_{xy} &= v_{c,x} - \theta + w_{c,x}\phi, \\
\gamma_{xz} &= w_{c,x} + \psi - v_{c,x}\phi, \\
\kappa_x &= \phi_{,x}, \\
\kappa_y &= \psi_{,x} - v_{c,x}\psi, \\
\kappa_z &= -\theta_{,x} + w_{c,x}\psi.
\end{aligned} \tag{3.40}$$

In this case the linearized displacement assumptions

$$\begin{aligned}
u &= u_c - y\theta + z\psi - \omega\phi_{,x}, \\
v &= v_c - z\phi, \\
w &= w_c + y\phi,
\end{aligned} \tag{3.41}$$

are used.

The vectors of stress resultants and generalized strains are denoted by $\mathbf{Q}$ and $\mathbf{e}$, respectively as

$$\begin{aligned}
\mathbf{Q} &= [\,N \quad Q_y \quad Q_z \quad M_x \quad M_y \quad M_z\,]^T, \\
\mathbf{e} &= [\,\varepsilon_c \quad \gamma_{xy} \quad \gamma_{xz} \quad \kappa_x \quad \kappa_y \quad \kappa_z\,]^T.
\end{aligned} \tag{3.42}$$

The constitutive law in the elastic case can be written in an incremental form

$$\Delta\mathbf{Q} = \mathbf{C}\Delta\mathbf{e}, \tag{3.43}$$

with

$$\mathbf{C} = \begin{bmatrix} EA & & & & & \\ & GA_{sy} & & & & \\ & & GA_{sz} & & & \\ & & & GI_t & & \\ & & & & EI_y & \\ & & & & & EI_z \end{bmatrix}, \tag{3.44}$$

in which EA is the axial rigidity, GA_{sy} and GA_{sz} the shear stiffnesses in y and z directions, GI_t the torsional rigidity and EI_y, EI_z the bending stiffnesses about y and z axes, respectively.

Using the incremental decomposition

$$\begin{aligned} {}^2\mathbf{Q} &= {}^1\mathbf{Q} + \Delta\mathbf{Q}^1 + \delta\mathbf{Q}, \\ {}^2\mathbf{e} &= {}^1\mathbf{e} + \Delta\mathbf{e}^1 + \delta\mathbf{e}, \end{aligned} \tag{3.45}$$

where the iterative changes of the generalized strains are

$$\begin{aligned} \delta\varepsilon_c =& \delta u_{c,x} + \Delta v^1_{c,x}\delta v_{c,x} + \Delta w^1_{c,x}\delta w_{c,x} + I_p/A\Delta\phi^1_{,x}\delta\phi_{,x} \\ &+ (\delta v^2_{c,x} + \delta w^2_{c,x} + I_p/A\delta\phi^2_{,x})/2, \\ \delta\gamma_{xy} =& \delta v_{c,x} - \delta\theta + \Delta\phi^1\delta w_{c,x} + \Delta w^1_{c,x}\delta\phi + \delta w_{c,x}\delta\phi, \\ \delta\gamma_{xz} =& \delta w_{c,x} + \delta\psi - \Delta\phi^1\delta v_{c,x} - \Delta v^1_{c,x}\delta\phi - \delta v_{c,x}\delta\phi, \\ \delta\kappa_x =& \delta\phi_{,x}, \\ \delta\kappa_y =& \delta\psi_{,x} - \Delta\phi^1_{,x}\delta v_{c,x} - \Delta v^1_{c,x}\delta\phi_{,x} - \delta v_{c,x}\delta\phi_{,x}, \\ \delta\kappa_z =& -\delta\theta_{,x} + \Delta\phi^1_{,x}\delta w_{c,x} + \Delta w^1_{c,x}\delta\phi_{,x} + \delta w_{c,x}\delta\phi_{,x}, \end{aligned} \tag{3.46}$$

the discretized equilibrium equations (2.21) can be derived. The linearized strain-displacement matrix has thus the form

$$\mathbf{B} = \begin{bmatrix} \mathbf{N}_{u,x} & \Delta v^1_{c,x}\mathbf{N}_{v,x} & \Delta w^1_{c,x}\mathbf{N}_{w,x} & I_p/A\Delta\phi^1_{,x}\mathbf{N}_{\phi,x} & \mathbf{0} & \mathbf{0} \\ \mathbf{0} & \mathbf{N}_{v,x} & \Delta\phi^1\mathbf{N}_{w,x} & \Delta w^1_{c,x}\mathbf{N}_{\phi} & \mathbf{0} & -\mathbf{N}_{\theta} \\ \mathbf{0} & -\Delta\phi^1\mathbf{N}_{v,x} & \mathbf{N}_{w,x} & -\Delta v^1_{c,x}\mathbf{N}_{\phi} & \mathbf{N}_{\psi} & \mathbf{0} \\ \mathbf{0} & \mathbf{0} & \mathbf{0} & \mathbf{N}_{\phi,x} & \mathbf{0} & \mathbf{0} \\ \mathbf{0} & -\Delta\phi^1_{,x}\mathbf{N}_{v,x} & \mathbf{0} & -\Delta v^1_{c,x}\mathbf{N}_{\phi,x} & \mathbf{N}_{\psi,x} & \mathbf{0} \\ \mathbf{0} & \mathbf{0} & \Delta\phi^1_{,x}\mathbf{N}_{w,x} & \Delta w^1_{c,x}\mathbf{N}_{\phi,x} & \mathbf{0} & -\mathbf{N}_{\theta,x} \end{bmatrix}, \tag{3.47}$$

and the internal force vector is calculated using the formula

$$\mathbf{R}^1 = \int_0^L \mathbf{B}^T\mathbf{Q}^1 dx. \tag{3.48}$$

In this case the geometric stiffness matrix has a little simpler form than in Equation (3.33)

$$\mathbf{K}_G = \begin{bmatrix} \mathbf{0} & \mathbf{0} & \mathbf{0} & \mathbf{0} & \mathbf{0} & \mathbf{0} \\ & \mathbf{K}_{Gvv} & \mathbf{0} & \mathbf{K}_{Gv\phi} & \mathbf{0} & \mathbf{0} \\ & & \mathbf{K}_{Gww} & \mathbf{K}_{Gw\phi} & \mathbf{0} & \mathbf{0} \\ & & & \mathbf{K}_{G\phi\phi} & \mathbf{0} & \mathbf{0} \\ & & & & \mathbf{0} & \mathbf{0} \\ \mathrm{s} & \mathrm{y} & \mathrm{m} & \mathrm{m.} & & \mathbf{0} \end{bmatrix}. \tag{3.49}$$

The submatrices are †

$$
\begin{aligned}
\mathbf{K}_{Gvv} &= N \int_0^L \mathbf{N}_{v,x}^T \mathbf{N}_{v,x} dx, \\
\mathbf{K}_{Gww} &= N \int_0^L \mathbf{N}_{w,x}^T \mathbf{N}_{w,x} dx, \\
\mathbf{K}_{G\phi\phi} &= N I_p / A \int_0^L \mathbf{N}_{\phi,x}^T \mathbf{N}_{\phi,x} dx, \\
\mathbf{K}_{Gw\phi} &= M_z \int_0^L \mathbf{N}_{w,x}^T \mathbf{N}_{\phi,x} dx + Q_z \int_0^L \mathbf{N}_{w,x}^T \mathbf{N}_{\phi} dx, \\
\mathbf{K}_{Gv\phi} &= -M_y \int_0^L \mathbf{N}_{v,x}^T \mathbf{N}_{\phi,x} dx - Q_y \int_0^L \mathbf{N}_{v,x}^T \mathbf{N}_{\phi} dx.
\end{aligned}
\tag{3.50}
$$

The internal force vector (3.48), the geometric stiffness (3.49) and the linear stiffness matrix

$$
\mathbf{K}_1 = \int_0^L \mathbf{B}^T \mathbf{C} \mathbf{B} dx \tag{3.51}
$$

can now be integrated with respect to the axial coordinate only. This approach results in a simple way to formulate the finite element equations for a three dimensional beam. It is computationally much more economical than a fully numerically integrated element, Equations (3.29)-(3.34). However, nonlinear material behaviour cannot be modelled as accurately as in the layered model. For example, in elasto-plastic case the yield surface has to be formulated using the stress resultants, which is quite complicated for general cross-sectional shapes. Therefore simple approximate yield surfaces, expressed in terms of stress resultants, have usually been adopted in the analyses. However, the results of this kind of computations have to be interpreted with great care.

3.2.2 Elements based on Euler-Bernoulli beam theory

In the Euler-Bernoulli beam theory the deformations due to transverse shear are neglected. This can be achieved from the Timoshenko beam equations by imposing the constraints

$$
\begin{aligned}
\gamma_{xy} &= v_{c,x} - \theta = 0, \\
\gamma_{xz} &= w_{c,x} + \psi = 0.
\end{aligned}
\tag{3.52}
$$

In the finite element method these constraints can be taken into account by using either Lagrange multipliers or the penalty function method. The advantage of the

† In the elastic case $\int_A S_x^1 r^2 dA = N I_p / A$. If the material behaves nonlinearly, this approximative expression can still be used, but it may slow down the convergence of the iterative process. In the numerical examples, this retardation has found to be insignificant.

penalty method is, that the shape functions of displacement variables can still be C^0-continuous, and the implementation of the constraints to the Timoshenko beam elements is simple.

The beam elements based on the Euler-Bernoulli beam theory are usually formulated using C^1-continuous approximations for deflections

$$\begin{aligned} v(x) &= \mathbf{N}_v(x)\mathbf{q}_v, \\ w(x) &= \mathbf{N}_w(x)\mathbf{q}_w, \end{aligned} \tag{3.53}$$

where $\mathbf{N}_v$ and $\mathbf{N}_w$ contain the cubic Hermitian polynomials

$$\mathbf{N}_v^T = \begin{bmatrix} 1-3\xi^2+2\xi^3 \\ (\xi-2\xi^2+\xi^3)L \\ 3\xi^2-2\xi^3 \\ (-\xi^2+\xi^3)L \end{bmatrix}, \qquad \mathbf{N}_w^T = \begin{bmatrix} 1-3\xi^2+2\xi^3 \\ -(\xi-2\xi^2+\xi^3)L \\ 3\xi^2-2\xi^3 \\ (\xi^2-\xi^3)L \end{bmatrix}, \tag{3.54}$$

in which $\xi = x/L$ and L is the length of an element. The corresponding nodal point parameter vectors are

$$\begin{aligned} \mathbf{q}_v^T &= [\, v_1 \quad \theta_1 \quad v_2 \quad \theta_2 \,] = [\, v_1 \quad v_1' \quad v_2 \quad v_2' \,], \\ \mathbf{q}_w^T &= [\, w_1 \quad \psi_1 \quad w_2 \quad \psi_2 \,] = [\, w_1 \quad -w_1' \quad w_2 \quad -w_2' \,]. \end{aligned} \tag{3.55}$$

If the linearized incremental displacement assumpions

$$\begin{aligned} \Delta u &= \Delta u_c - y\Delta v_{c,x} - z\Delta w_{c,x} - \omega\Delta\phi_{,x}, \\ \Delta v &= \Delta v_c - z\phi, \\ \Delta w &= \Delta w_c + y\phi \end{aligned} \tag{3.56}$$

are used, then the strain increments based on formulas

$$\begin{aligned} \varepsilon_x &= u_{,x} + (v_{,x}^2 + w_{,x}^2)/2, \\ \gamma_{xy} &= u_{,y} + v_{,x} + w_{,x}w_{,y}, \\ \gamma_{xz} &= u_{,z} + w_{,x} + v_{,x}v_{,z}, \end{aligned} \tag{3.57}$$

are

$$\begin{aligned} \delta\varepsilon_x =& \delta u_{c,x} + (\Delta v_{c,x}^1 - z\Delta\phi_{,x}^1)\delta v_{c,x} - y\delta v_{c,xx} \\ &+ (\Delta w_{c,x}^1 + y\Delta\phi_{,x}^1)\delta w_{c,x} - z\delta w_{c,xx} \\ &+ (r^2\Delta\phi_{,x}^1 - z\Delta v_{c,x}^1 + y\Delta w_{c,x}^1)\delta\phi_{,x} \\ &- z\delta v_{c,x}\delta\phi_{,x} + y\delta w_{c,x}\delta\phi_{,x} + (\delta v_{c,x}^2 + \delta w_{c,x}^2 + r^2\delta\phi_{,x}^2)/2, \qquad (3.58a) \\ \delta\gamma_{xy} =& \Delta\phi^1\delta w_{c,x} - (z+\omega_{,y})\delta\phi_{,x} + \Delta w_{c,x}^1\delta\phi + \delta w_{c,x}\delta\phi, \qquad (3.58b) \\ \delta\gamma_{xz} =& -\Delta\phi^1\delta v_{c,x} + (y-\omega_{,z})\delta\phi_{,x} - \Delta v_{c,x}^1\delta\phi - \delta v_{c,x}\delta\phi. \qquad (3.58c) \end{aligned}$$

The linearized strain displacement matrix has the form

$$\mathbf{B} = \begin{bmatrix} \mathbf{N}_{u,x} & a_1\mathbf{N}_{v,x} - y\mathbf{N}_{v,xx} & a_2\mathbf{N}_{w,x} - z\mathbf{N}_{w,xx} & a_3\mathbf{N}_{\phi,x} \\ \mathbf{0} & \mathbf{0} & \Delta\phi^1\mathbf{N}_{w,x} & b_1\mathbf{N}_{\phi,x} + \Delta w^1_{c,x}\mathbf{N}_\phi \\ \mathbf{0} & -\Delta\phi^1\mathbf{N}_{v,x} & \mathbf{0} & c_1\mathbf{N}_{\phi,x} - \Delta v^1_{c,x}\mathbf{N}_\phi \end{bmatrix}, \quad (3.59)$$

where

$$\begin{aligned} a_1 &= \Delta v^1_{c,x} - z\Delta\phi^1_{,x}, \\ a_2 &= \Delta w^1_{c,x} + y\Delta\phi^1_{,x}, \\ a_3 &= r^2\Delta\phi^1_{,x} - z\Delta v^1_{c,x} + y\Delta w^1_{c,x}, \\ b_1 &= -z - \omega_{,y}, \\ c_1 &= y - \omega_{,z}. \end{aligned} \quad (3.60)$$

The derivatives of the incremental displacements $\Delta v^1_{c,x}$ and $\Delta w^1_{c,x}$ prior the current iteration have been calculated using the difference formulas e.g. $\Delta v^1_{c,x} = (\Delta v_2 - \Delta v_1)/L$. This approach has been found to be more effective than evaluating these quantities by the use of shape functions. The axial displacement u and the rotation ϕ about the element axis have been interpolated with linear shape functions. The geometric stiffness matrix is

$$\mathbf{K}_G = \begin{bmatrix} \mathbf{0} & \mathbf{0} & \mathbf{0} & \mathbf{0} \\ & \mathbf{K}_{Gvv} & \mathbf{0} & \mathbf{K}_{Gv\phi} \\ & & \mathbf{K}_{Gww} & \mathbf{K}_{Gw\phi} \\ & \text{symm.} & & \mathbf{K}_{G\phi\phi} \end{bmatrix}, \quad (3.61)$$

where (see footnote for Equation (3.50))

$$\begin{aligned} \mathbf{K}_{Gvv} &= \int_V S^1_x\mathbf{N}^T_{v,x}\mathbf{N}_{v,x}dV = N\int_0^L \mathbf{N}^T_{v,x}\mathbf{N}_{v,x}dV, \\ \mathbf{K}_{Gww} &= \int_V S^1_x\mathbf{N}^T_{w,x}\mathbf{N}_{w,x}dV = N\int_0^L \mathbf{N}^T_{w,x}\mathbf{N}_{w,x}dV, \\ \mathbf{K}_{G\phi\phi} &= \int_V S^1_x r^2\mathbf{N}^T_{\phi,x}\mathbf{N}_{\phi,x}dV = NI_p/A\int_0^L \mathbf{N}^T_{\phi,x}\mathbf{N}_{\phi,x}dV, \\ \mathbf{K}_{Gw\phi} &= \int_V S^1_x y\mathbf{N}^T_{w,x}\mathbf{N}_{\phi,x}dV = M_z\int_0^L \mathbf{N}^T_{w,x}\mathbf{N}_{\phi,x}dV, \\ \mathbf{K}_{Gv\phi} &= -\int_V S^1_x z\mathbf{N}^T_{v,x}\mathbf{N}_{\phi,x}dV = -M_y\int_0^L \mathbf{N}^T_{v,x}\mathbf{N}_{v,x}dV. \end{aligned} \quad (3.62)$$

Similarly to the case of Timoshenko beam, the element stiffness matrices and the internal force vector can be formulated, based on the virtual work equation expressed in terms of stress resultants and the generalized strain quantities:

$$\begin{aligned} \mathbf{Q} &= [\,N \quad M_z \quad M_y \quad M_x\,]^T, \\ \mathbf{e} &= [\,\varepsilon_c \quad \kappa_z \quad \kappa_y \quad \kappa_x\,]^T. \end{aligned} \quad (3.63)$$

The curvatures are

$$\begin{aligned} \kappa_z &= -v_{c,xx}, \\ \kappa_y &= -w_{c,xx}. \end{aligned} \tag{3.64}$$

The constitutive matrix relating $\mathbf{Q}$ and $\mathbf{e}$ is

$$\mathbf{C} = \begin{bmatrix} EA & & & \\ & EI_z & & \\ & & EI_y & \\ & & & GI_t \end{bmatrix}, \tag{3.65}$$

and the linearized strain displacement matrix $\mathbf{B}$ has the form

$$\mathbf{B} = \begin{bmatrix} \mathbf{N}_{u,x} & \Delta v^1_{c,x}\mathbf{N}_{v,x} & \Delta w^1_{c,x}\mathbf{N}_{w,x} & I_p/A\Delta\phi^1_{,x}\mathbf{N}_{\phi,x} \\ \mathbf{0} & -\mathbf{N}_{v,xx} & \Delta\phi^1_{,x}\mathbf{N}_{w,x} & \Delta w^1_{,x}\mathbf{N}_{\phi,x} \\ \mathbf{0} & -\Delta\phi^1_{,x}\mathbf{N}_{v,x} & -\mathbf{N}_{w,xx} & -\Delta v^1_{c,x}\mathbf{N}_{\phi,x} \\ \mathbf{0} & \mathbf{0} & \mathbf{0} & \mathbf{N}_{\phi,x} \end{bmatrix}. \tag{3.66}$$

The consistent mass matrix for the cubic Euler-Bernoulli beam element is

$$\mathbf{M} = \begin{bmatrix} \mathbf{M}_{uu} & & & \\ & \mathbf{M}_{vv} & & \\ & & \mathbf{M}_{ww} & \\ & & & \mathbf{M}_{\phi\phi} \end{bmatrix}, \tag{3.67}$$

in which the submatrices are

$$\begin{aligned} \mathbf{M}_{uu} &= \int_V \rho \mathbf{N}_u^T \mathbf{N}_u dV, \\ \mathbf{M}_{vv} &= \int_V \rho \mathbf{N}_v^T \mathbf{N}_v dV, \\ \mathbf{M}_{ww} &= \int_V \rho \mathbf{N}_w^T \mathbf{N}_w dV, \\ \mathbf{M}_{\phi\phi} &= \int_V \rho r^2 \mathbf{N}_\phi^T \mathbf{N}_\phi dV. \end{aligned} \tag{3.68}$$

The diagonal mass matrix is simply

$$\mathbf{M} = \begin{bmatrix} \mathbf{M}_d & \\ & \mathbf{M}_d \end{bmatrix}, \tag{3.69}$$

where the nodal contributions are of the form

$$\mathbf{M}_d = \frac{m}{2} \begin{bmatrix} 1 & & & & & & \\ & 1 & & & & & \\ & & 1 & & & & \\ & & & I_p/A & & & \\ & & & & L^2/12 & & \\ & & & & & L^2/12 & \end{bmatrix}, \tag{3.70}$$

in which the notations are similar to those in Equation (3.38).

4 Thin-walled beams with open cross-section

4.1 Kinematical relations

The kinematic behaviour of beams with thin-walled open cross-section can be derived, based on the assumption that the projection of the cross-section on a plane normal to the centroidal axis does not distort during deformation, i.e. the cross-section is rigid in its projection plane. According to this assumption, the in plane displacements of an arbitrary point of the cross-section undergoing a small twisting rotation can be expressed by three parameters: two displacement components v, w and the angle of twist ϕ about the longitudinal beam axis, i.e.

$$\begin{aligned} v &= v_c - z\phi, \\ w &= w_c + y\phi. \end{aligned} \tag{4.1}$$

In this study both elastic and inelastic material behaviour has been investigated, so all displacement quantities are referred to a single point of the cross-section. Transforming v and w in Equation (4.1) from the x, y, z coordinate system to the orthogonal x, s, r system gives, see Figure 4.1

$$\begin{aligned} \bar{v} &= v\cos\alpha + w\sin\alpha, \\ \bar{w} &= -v\sin\alpha + w\cos\alpha, \end{aligned} \tag{4.2}$$

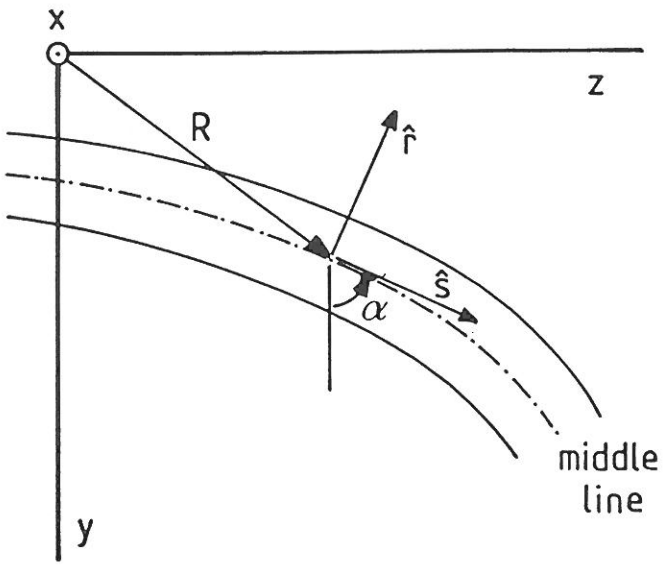

Figure 4.1 Cross-section of a thin-walled beam.

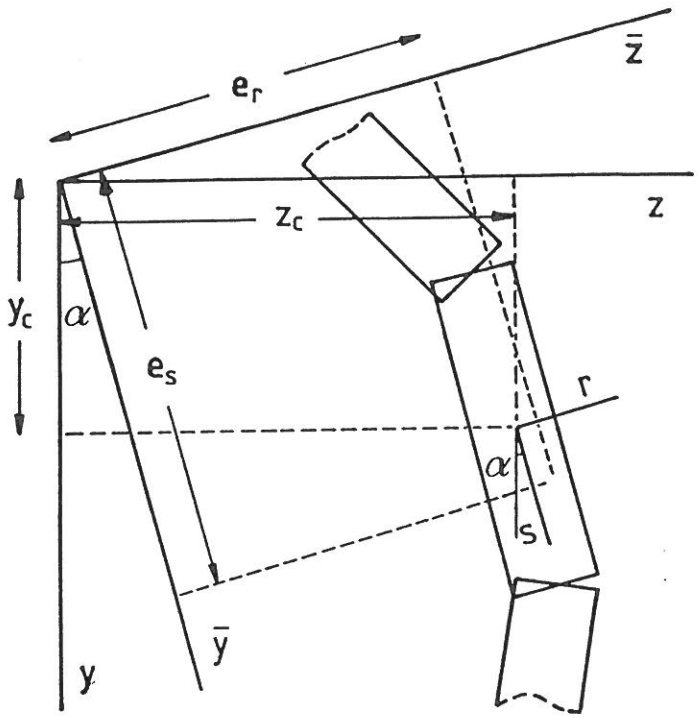

Figure 4.2 Construction of a thin-walled cross-section.

The linear strain-displacement matrix takes the form

$$\mathbf{B} = \begin{bmatrix} a_1\mathbf{N}_{u,x} & a_2\mathbf{N}_{v,x} & a_3\mathbf{N}_{w,x} & a_4\mathbf{N}_{\phi} + a_5\mathbf{N}_{\phi,x} & a_6\mathbf{N}_{\psi,x} & a_7\mathbf{N}_{\theta,x} & a_8\mathbf{N}_{\vartheta,x} \\ b_1\mathbf{N}_{u,x} & b_2\mathbf{N}_{v,x} & b_3\mathbf{N}_{w,x} & b_4\mathbf{N}_{\phi} + b_5\mathbf{N}_{\phi,x} & b_6\mathbf{N}_{\psi} & b_7\mathbf{N}_{\theta} & b_8\mathbf{N}_{\vartheta,x} \end{bmatrix}, \tag{4.32}$$

where

$$\begin{aligned} b_1 &= \Delta\psi^1 \sin\alpha - \Delta\theta^1 \cos\alpha, \\ b_2 &= \cos\alpha - \Delta\phi^1(\sin\alpha + \frac{1}{2}\Delta\phi^1 \cos\alpha), \\ b_3 &= \sin\alpha + \Delta\phi^1(\cos\alpha - \frac{1}{2}\Delta\phi^1 \sin\alpha), \\ b_4 &= \Delta w^1_{c,x}(\cos\alpha - \Delta\phi^1 \sin\alpha) - \Delta v^1_{c,x}(\sin\alpha - \Delta\phi^1 \cos\alpha), \\ b_5 &= -e_r - \omega_{r,s}, \\ b_6 &= (1 + a_1)\sin\alpha, \\ b_7 &= -(1 + a_1)\cos\alpha, \\ b_8 &= -(1 + a_1)\omega_{s,s}. \end{aligned} \tag{4.33}$$

The geometric stiffness $\mathbf{K}_G$ has the same form as presented in Equation (4.24), but the terms written below differ slightly from those listed in Equations (3.34) and

where $\bar{v}$ and $\bar{w}$ are the displacements of an arbitrary point of the cross-section along the s- and r-axes, respectively, while α denotes the angle between y- and s-axes. Equations (4.1) and (4.2) result in

$$\begin{aligned} \bar{v} &= v_c \cos\alpha + w_c \sin\alpha + h_s\phi, \\ \bar{w} &= -v_c \sin\alpha + w_c \cos\alpha + h_r\phi, \end{aligned} \tag{4.3}$$

where

$$\begin{aligned} -h_s &= \mathbf{R}\cdot\hat{\mathbf{r}} = z\cos\alpha - y\sin\alpha, \\ h_r &= \mathbf{R}\cdot\hat{\mathbf{s}} = z\sin\alpha + y\cos\alpha. \end{aligned} \tag{4.4}$$

The unit normal vectors $\hat{\mathbf{s}}, \hat{\mathbf{r}}$ and the radius vector $\mathbf{R}$ are, see Figure 4.1

$$\begin{aligned} \hat{\mathbf{s}} &= \cos\alpha\hat{\mathbf{e}}_y + \sin\alpha\hat{\mathbf{e}}_z, \\ \hat{\mathbf{r}} &= -\sin\alpha\hat{\mathbf{e}}_y + \cos\alpha\hat{\mathbf{e}}_z, \\ \mathbf{R} &= y\hat{\mathbf{e}}_y + z\hat{\mathbf{e}}_z, \end{aligned} \tag{4.5}$$

where $\hat{\mathbf{e}}_y$ and $\hat{\mathbf{e}}_z$ are the unit vectors in the directions of y- and z-axes. Using the linear shear strain expressions

$$\begin{aligned} \gamma_{xs} &= u_{,s} + \bar{v}_{,x}, \\ \gamma_{xr} &= u_{,r} + \bar{w}_{,x}, \end{aligned} \tag{4.6}$$

the axial displacement can be integrated from the total differential

$$\begin{aligned} du =& u_{,s}ds + u_{,r}dr \\ =& (\gamma_{xs} - v_{c,x}\cos\alpha - w_{c,x}\sin\alpha - h_s\phi_{,x})ds \\ &+ (\gamma_{xr} + v_{c,x}\sin\alpha - w_{c,x}\cos\alpha - h_r\phi_{,x})dr. \end{aligned} \tag{4.7}$$

The shear strain γ_{xs} consists of two parts, i.e. parts due to nonuniform bending γ^b_{xs} and torsion γ^t_{xs}, while the strain γ_{xr} has contribution only due to nonuniform bending:

$$\begin{aligned} \gamma_{xs} &= \gamma^b_{xs} + \gamma^t_{xs}, \\ \gamma_{xr} &= \gamma^b_{xr}. \end{aligned} \tag{4.8}$$

Collecting the terms in Equation (4.7) in the form

$$\begin{aligned} du =& \gamma^b_{xy}\cos\alpha ds - \gamma^b_{xy}\sin\alpha dr - v_{c,x}\cos\alpha ds + v_{c,x}\sin\alpha dr \\ &+ \gamma^b_{xz}\sin\alpha ds + \gamma^b_{xz}\cos\alpha dr - w_{c,x}\sin\alpha ds - w_{c,x}ds \\ &- w_{c,x}\cos\alpha dr - (h_s\phi_{,x} - \gamma^t_{xs})ds - h_r\phi_{,x}dr, \end{aligned} \tag{4.9}$$

and using the conventional assumption of the shear strains in the Timoshenko beam theory

$$\begin{aligned} \gamma^b_{xy} &= v_{c,x} - \theta, \\ \gamma^b_{xz} &= w_{c,x} + \psi, \end{aligned} \tag{4.10}$$

with an additional assumption for shear strains due to torsion

$$\gamma_{xs}^{t} = h_s(\phi_{,x} - \vartheta), \tag{4.11}$$

where ϑ is an additional displacement variable describing the variation of warping displacement in the longitudinal axis.

Integrating the differential expression in Equation (4.9) gives the axial displacement

$$u = u_c - y\theta + z\psi - \omega_s\vartheta - \omega_r\phi_{,x}. \tag{4.12}$$

In the above expression, u_c is an arbitrary function depending only on the x-coordinate, and ω_s is the warping function at the middle line of the cross-section of the member

$$\omega_s(s) = \int_0^s h_s ds. \tag{4.13}$$

Further, ω_r is the warping function due to the slab action

$$\omega_r(s,r) = h_r(s)r. \tag{4.14}$$

Derivation of the differential equations of a twisted bar is described in Appendix A1. The total torque is a combination of the pure St. Venant's torque M_{xf} and of the warping torque M_ω

$$\begin{aligned} M_x &= M_{xf} + M_\omega, \\ M_{xf} &= GI_t\phi_{,x}, \\ M_\omega &= GI_s(\phi_{,x} - \vartheta), \end{aligned} \tag{4.15}$$

where the shear constant I_s is defined by expression

$$I_s = \int_A h_s^2 dA. \tag{4.16}$$

The bimoment B is defined by the equation

$$B = -EI_\omega\vartheta_{,x}, \tag{4.17}$$

where the warping rigidity I_ω is

$$I_\omega = \int_A \omega_s^2 dA. \tag{4.18}$$

4.2 Thin-walled beam elements

4.2.1 Elements based on Timoshenko beam theory

For a straight beam element with a thin-walled open cross-section, the incremental displacement expressions are almost identical to the incremental displacement

equations (3.24) used in the case of a beam with a solid cross-section. Only difference is that the warping displacement is divided into two parts,

$$\begin{aligned}
\Delta u(x,y,z) &= \Delta u_c(x) + z\Delta\psi(x) - y\Delta\theta(x) - \omega_s(s)\Delta\vartheta(x) - \omega_r(s,r)\Delta\phi_{,x}(x),\\
\Delta v(x,y,z) &= \Delta v_c(x) - z\Delta\phi(x) - \frac{1}{2}y[\Delta\phi(x)]^2,\\
\Delta w(x,y,z) &= \Delta w_c(x) + y\Delta\phi(x) - \frac{1}{2}z[\Delta\phi(x)]^2.
\end{aligned} \tag{4.19}$$

where $\Delta\vartheta$ is an additional displacement variable. Similarly as in Chapter 3, the iterative changes of the Green-Lagrange strain tensor components are

$$\begin{aligned}
\delta\varepsilon_x =&(1 + \Delta u^1_{c,x} - y\Delta\theta^1_{,x} + z\Delta\psi^1_{,x} - \omega_s\Delta\vartheta^1_{,x})\delta u_{c,x}\\
&+ [\Delta v^1_{c,x} - \Delta\phi^1_{,x}(z + y\Delta\phi^1)]\delta v_{c,x}\\
&+ [\Delta w^1_{c,x} + \Delta\phi^1_{,x}(y - z\Delta\phi^1)]\delta w_{c,x}\\
&+ \Delta\phi^1_{,x}(r^2\Delta\phi^1\Delta\phi^1_{,x} - z\Delta w^1_{c,x} - y\Delta v^1_{c,x})\delta\phi\\
&+ \{r^2\Delta\phi^1_{,x}[1 + (\Delta\phi^1)^2] - z(\Delta v^1_{c,x} + \Delta w^1_{c,x}\Delta\phi^1)\\
&- y(\Delta v^1_{c,x}\Delta\phi^1 - \Delta w^1_{c,x})\}\delta\phi_{,x}\\
&+ z(1 + \Delta u^1_{c,x} - y\Delta\theta^1_{,x} + z\Delta\psi^1_{,x} - \omega_s\Delta\vartheta^1_{,x})\delta\psi_{,x}\\
&- y(1 + \Delta u^1_{c,x} - y\Delta\theta^1_{,x} + z\Delta\psi^1_{,x} - \omega_s\Delta\vartheta^1_{,x})\delta\theta_{,x}\\
&- \omega_s(1 + \Delta u^1_{c,x} - y\Delta\theta^1_{,x} + z\Delta\psi^1_{,x} - \omega_s\Delta\vartheta^1_{,x})\delta\vartheta_{,x}\\
&+ \frac{1}{2}\{\delta u^2_{c,x} + \delta v^2_{c,x} + \delta w^2_{c,x} + r^2[1 + (\Delta\phi^1)^2]\delta\phi^2_{,x}\\
&+ r^2(\Delta\phi^1_{,x})^2\delta\phi^2 + z^2\delta\psi^2_{,x} + y^2\delta\theta^2_{,x} + \omega_s^2\delta\vartheta^2_{,x}\}\\
&- y\delta u_{c,x}\delta\theta_{,x} + z\delta u_{c,x}\delta\psi_{,x} - \omega_s\delta u_{c,x}\delta v_{c,x} - yz\delta\psi_{,x}\theta_{,x}\\
&- z\omega_s\delta\psi_{,x}\delta\vartheta_{,x} + y\omega_s\delta\theta_{,x}\delta\vartheta_{,x} - (z + y\Delta\phi^1)\delta v_{c,x}\delta\phi_{,x}\\
&+ (y - z\Delta\phi^1)\delta w_{c,x}\delta_{,x} - y\Delta\phi^1_{,x}\delta v_{c,x}\delta\phi - z\Delta\phi^1_{,x}\delta w_{c,x}\delta\phi\\
&+ (2r^2\Delta\phi^1\Delta\phi^1_{,x} - y\Delta v^1_{c,x} - z\Delta w^1_{c,x})\delta\phi\delta\phi_{,x}, \qquad (4.20a)\\
\delta\gamma_{xy} =& - \Delta\theta^1\delta u_{c,x} + [1 - (\Delta\phi^1)^2/2]\delta v_{c,x} + \Delta\phi^1\delta w_{c,x} - (z + \omega_{r,y})\delta\phi_{,x}\\
&+ (\Delta w^1_{c,x} + \Delta v^1_{c,x}\Delta\phi^1)\delta\phi - (1 + \Delta u^1_{c,x})\delta\theta - \omega_{s,y}\delta\vartheta\\
&- \delta u_{c,x}\delta\theta - \Delta\phi^1\delta v_{c,x}\delta\phi + \delta w_{c,x}\delta\phi - \Delta v^1_{c,x}\delta\phi^2/2, \qquad (4.20b)\\
\delta\gamma_{xz} =&\Delta\psi^1\delta u_{c,x} + \Delta\phi^1\delta v_{c,x} + [1 - (\Delta\phi^1)^2/2]\delta w_{c,x} + (y - \omega_{r,z})\delta\phi_{,x}\\
&- (\Delta v^1_{c,x} + \Delta w^1_{c,x}\Delta\phi^1)\delta\phi + (1 + \Delta u^1_{c,x})\delta\psi - \omega_{s,z}\delta\vartheta\\
&+ \delta u_{c,x}\delta\psi - \delta v_{c,x}\delta\phi, -\Delta\phi^1\delta w_{c,x}\delta\phi - \Delta w^1_{c,x}\delta\phi^2/2. \qquad (4.20c)
\end{aligned}$$

The twist per unit length is also interpolated within an element by the shape functions

$$\delta\vartheta = \mathbf{N}_\vartheta\delta\mathbf{q}_\vartheta. \tag{4.21}$$

The linear strain-displacement matrix $\mathbf{B}$ can be written in the form

$$\mathbf{B} = \begin{bmatrix} a_1\mathbf{N}_{u,x} & a_2\mathbf{N}_{v,x} & a_3\mathbf{N}_{w,x} & a_4\mathbf{N}_{\phi} + a_5\mathbf{N}_{\phi,x} & a_6\mathbf{N}_{\psi,x} & a_7\mathbf{N}_{\theta,x} & a_8\mathbf{N}_{\vartheta,x} \\ b_1\mathbf{N}_{u,x} & b_2\mathbf{N}_{v,x} & b_3\mathbf{N}_{w,x} & b_4\mathbf{N}_{\phi} + b_5\mathbf{N}_{\phi,x} & \mathbf{0} & b_7\mathbf{N}_{\theta} & b_8\mathbf{N}_{\vartheta,x} \\ c_1\mathbf{N}_{u,x} & c_2\mathbf{N}_{v,x} & c_3\mathbf{N}_{w,x} & c_4\mathbf{N}_{\phi} + c_5\mathbf{N}_{\phi,x} & c_6\mathbf{N}_{\psi} & \mathbf{0} & c_8\mathbf{N}_{\vartheta,x} \end{bmatrix}, \tag{4.22}$$

where the coefficients are presented in Equations (3.30) except

$$\begin{aligned} a_1 &= 1 + \Delta u^1_{c,x} - y\Delta\theta^1_{,x} + z\Delta\psi^1_{,x} - \omega_s\Delta\vartheta^1_{,x}, \\ a_6 &= za_1, \\ a_7 &= -ya_1, \\ a_8 &= -\omega_s a_1, \\ b_5 &= -z - \omega_{r,y}, \\ b_8 &= -\omega_{s,y}, \\ c_5 &= y - \omega_{r,z}, \\ c_8 &= -\omega_{s,z}, \end{aligned} \tag{4.23}$$

The geometric stiffness matrix is

$$\mathbf{K}_G = \begin{bmatrix} \mathbf{K}_{Guu} & \mathbf{0} & \mathbf{0} & \mathbf{0} & \mathbf{K}_{Gu\psi} & \mathbf{K}_{Gu\theta} & \mathbf{K}_{Gu\vartheta} \\ & \mathbf{K}_{Gvv} & \mathbf{0} & \mathbf{K}_{Gv\phi} & \mathbf{0} & \mathbf{0} & \mathbf{0} \\ & & \mathbf{K}_{Gww} & \mathbf{K}_{Gw\phi} & \mathbf{0} & \mathbf{0} & \mathbf{0} \\ & & & \mathbf{K}_{G\phi\phi} & \mathbf{0} & \mathbf{0} & \mathbf{0} \\ & & & & \mathbf{K}_{G\psi\psi} & \mathbf{K}_{G\psi\theta} & \mathbf{K}_{G\psi\vartheta} \\ & & & & & \mathbf{K}_{G\theta\theta} & \mathbf{K}_{G\theta\vartheta} \\ & \text{s} & \text{y} & \text{m} & \text{m.} & & \mathbf{K}_{G\vartheta\vartheta} \end{bmatrix}, \tag{4.24}$$

where the additional terms, compared to Equation (3.33) are

$$\begin{aligned} \mathbf{K}_{G\vartheta\vartheta} &= \int_V S^1_x\omega_s^2\mathbf{N}^T_{\vartheta,x}\mathbf{N}_{\vartheta,x}dV, \\ \mathbf{K}_{G\theta\vartheta} &= \int_V S^1_x y\omega_s\mathbf{N}^T_{\theta,x}\mathbf{N}_{\vartheta,x}dV, \\ \mathbf{K}_{G\psi\vartheta} &= -\int_V S^1_x z\omega_s\mathbf{N}^T_{\psi,x}\mathbf{N}_{\vartheta,x}dV, \\ \mathbf{K}_{Gu\vartheta} &= -\int_V S^1_x\omega_s\mathbf{N}^T_{u,x}\mathbf{N}_{\vartheta,x}dV. \end{aligned} \tag{4.25}$$

An element stiffness matrix and internal force vector are integrated using the one point Gaussian quadrature in x-axis direction when the linear shape functions are used. Each part of a cross-section has to be integrated at least the 2×2 Gaussian rule. For inelastic analysis higher order rules have to be used.

The consistent mass matrix contains also an additional block, i.e.

$$\mathbf{M} = \begin{bmatrix} \mathbf{M}_{uu} & & & & & & & \\ & \mathbf{M}_{vv} & & & & & & \\ & & \mathbf{M}_{ww} & & & & & \\ & & & \mathbf{M}_{\phi\phi} & & & & \\ & & & & \mathbf{M}_{\psi\psi} & & & \\ & & & & & \mathbf{M}_{\theta\theta} & & \\ & & & & & & \mathbf{M}_{\vartheta\vartheta} \end{bmatrix}, \tag{4.26}$$

where

$$\mathbf{M}_{\vartheta\vartheta} = \int_V \rho\omega_s^2 \mathbf{N}_\vartheta^T \mathbf{N}_\vartheta dV. \tag{4.27}$$

The other submatrices are presented in Equation (3.35). The lumped diagonal mass matrix for a two noded element has the same form as in Equation (3.37), where the nodal submatrix $\mathbf{M}_d$ is

$$\mathbf{M}_d = \frac{m}{2} \begin{bmatrix} 1 & & & & & & & \\ & 1 & & & & & & \\ & & 1 & & & & & \\ & & & I_p/A & & & & \\ & & & & I_y/A + L^2/12 & & & \\ & & & & & I_z/A + L^2/12 & & \\ & & & & & & I_{\omega_s}/A \end{bmatrix}. \tag{4.28}$$

A thin-walled beam element can also be constructed using two strain components only, the axial strain and the shear strain paraller to the middle line of the cross-section, and the corresponding stress quantities. In the incremental displacement assumptions (4.19) the increments Δv and Δw are now measured for each part of the cross-section in local coordinate system $\bar{y}, \bar{z}$, which is paraller to the local axes s, r, see Figure 4.2,

$$\begin{aligned} \Delta\bar{v}(x,y,z) &= \Delta v_c(x)\cos\alpha + \Delta w_{c,x}(x)\sin\alpha - e_r\Delta\phi(x) - \frac{1}{2}e_s[\Delta\phi(x)]^2, \\ \Delta\bar{w}(x,y,z) &= \Delta w_c(x)\cos\alpha - \Delta v_{c,x}\sin\alpha + e_s\Delta\phi(x) - \frac{1}{2}e_r[\Delta\phi(x)]^2. \end{aligned} \tag{4.29}$$

The notations

$$\begin{aligned} e_r &= z_c\cos\alpha - y_c\sin\alpha + r, \\ e_s &= z_c\sin\alpha + y_c\cos\alpha + s, \end{aligned} \tag{4.30}$$

are introduced in which y_c and z_c are the coordinates of the centroid of a cross-section part and α is the angle between the axes y and $\bar{y}$. The strain increments are evaluated using the formulas

$$\begin{aligned} \Delta\varepsilon_x &= \Delta u_{,x} + (\Delta u_{,x}^2 + \Delta\bar{v}_{,x}^2 + \Delta\bar{w}_{,x}^2)/2, \\ \Delta\gamma_{xs} &= \Delta u_{,s} + \Delta\bar{v}_{,x} + \Delta u_{,x}\Delta u_{,s} + \Delta\bar{v}_{,x}\Delta\bar{v}_{,s} + \Delta\bar{w}_{,x}\Delta\bar{w}_{,s}. \end{aligned} \tag{4.31}$$

(4.25):

$$
\begin{aligned}
\mathbf{K}_{G\phi\phi} = & \int_V S_x^1\{r^2[1+(\Delta\phi^1)^2]\mathbf{N}_{\phi,x}^T\mathbf{N}_{\phi,x} + r^2(\Delta\phi^1)^2\mathbf{N}_\phi^T\mathbf{N}_\phi \\
& + (2r^2\Delta\phi^1\Delta\phi_{,x}^1 - y\Delta v_{c,x}^1 - z\Delta w_{c,x}^1)(\mathbf{N}_\phi^T\mathbf{N}_{\phi,x} + \mathbf{N}_{\phi,x}^T\mathbf{N}_\phi)\}dV \\
& - \int_V S_{xs}^1(\cos\alpha\Delta v_{c,x}^1 + \sin\alpha\Delta w_{c,x}^1)\mathbf{N}_\phi^T\mathbf{N}_\phi dV, \\
\mathbf{K}_{Gw\phi} = & \int_V S^1[(y - z\Delta\phi^1)\mathbf{N}_{w,x}^T\mathbf{N}_{\phi,x} - z\Delta\phi_{,x}^1\mathbf{N}_{w,x}^T\mathbf{N}_\phi]dV \\
& + \int_V S_{xs}^1(\cos\alpha - \Delta\phi^1\sin\alpha)\mathbf{N}_{w,x}^T\mathbf{N}_\phi dV, \\
\mathbf{K}_{Gv\phi} = & -\int_V S^1[(z + y\Delta\phi^1)\mathbf{N}_{v,x}^T\mathbf{N}_{\phi,x} + y\Delta\phi_{,x}^1\mathbf{N}_{v,x}^T\mathbf{N}_\phi]dV \\
& + \int_V S_{xs}^1(\Delta\phi^1\cos\alpha - \sin\alpha)\mathbf{N}_{v,x}^T\mathbf{N}_\phi dV.
\end{aligned}
\tag{4.34}
$$

A thin-walled beam element can also be formulated using the stress resultants and the corresponding generalized strain quantities. The internal virtual work expression for a thin-walled beam is

$$
\int_V {}^2S_{ij}\hat{\delta}({}^2E_{ij})dV =
$$

$$
\begin{aligned}
& \int_0^L [{}^2N\hat{\delta}({}^2\varepsilon_c) + {}^2Q_y\hat{\delta}({}^2\gamma_{xy}) + {}^2Q_z\hat{\delta}({}^2\gamma_{xz}) + {}^2M_{xf}\hat{\delta}({}^2\kappa_x) \\
& + {}^2M_y\hat{\delta}({}^2\kappa_y) + {}^2M_z\hat{\delta}({}^2\kappa_z) + {}^2B\hat{\delta}({}^2\kappa_\omega) + {}^2M_\omega\hat{\delta}({}^2\gamma_\omega)]dx.
\end{aligned}
\tag{4.35}
$$

The generalized strain measures $\varepsilon_c, \gamma_{xy}, \gamma_{xz}, \kappa_x, \kappa_y$ and κ_z are defined in Equations (3.40) and in addition

$$
\begin{aligned}
\kappa_\omega &= -\vartheta_{,x} \\
\gamma_\omega &= \phi_{,x} - \vartheta.
\end{aligned}
\tag{4.36}
$$

As in the case of a beam with solid cross-section, the linearized displacement assumptions

$$
\begin{aligned}
u &= u_c - y\theta + z\psi - \omega_r\phi_{,x} - \omega_s\vartheta, \\
v &= v_c - z\phi, \\
w &= w_c + y\phi,
\end{aligned}
\tag{4.37}
$$

are adopted. Denoting the vector of stress resultants by $\mathbf{Q}$ and the vector of generalized strains by $\mathbf{e}$

$$
\begin{aligned}
\mathbf{Q} &= [\,N \quad Q_y \quad Q_z \quad M_{xf} \quad M_y \quad M_z \quad B \quad M_\omega\,]^T, \\
\mathbf{e} &= [\,\varepsilon_c \quad \gamma_{xy} \quad \gamma_{xz} \quad \kappa_x \quad \kappa_y \quad \kappa_z \quad \kappa_\omega \quad \gamma_\omega\,]^T,
\end{aligned}
\tag{4.38}
$$

the constitutive law in the elastic case can be written in an incremental form

$$
\mathbf{\Delta Q} = \mathbf{C\Delta e}, \tag{4.39}
$$

where the constitutive matrix has the form

$$\mathbf{C} = \begin{bmatrix} EA & & & & & & & \\ & GA_{sy} & & & & & & \\ & & GA_{sz} & & & & & \\ & & & GI_t & & & & \\ & & & & EI_y & & EI_{y\omega} & \\ & & & & & EI_z & EI_{z\omega} & \\ & & & & EI_{\omega y} & EI_{\omega z} & EI_{\omega} & \\ & & & & & & & GI_s \end{bmatrix}. \tag{4.40}$$

Using the incremental decomposition, as in Equation (3.45), the linearized strain-displacement matrix

$$\mathbf{B} = \begin{bmatrix} \mathbf{N}_{u,x} & \Delta v^1_{c,x}\mathbf{N}_{v,x} & \Delta w^1_{c,x}\mathbf{N}_{w,x} & I_p/A\Delta\phi^1_{,x}\mathbf{N}_{\phi,x} & \mathbf{0} & \mathbf{0} & \mathbf{0} \\ \mathbf{0} & \mathbf{N}_{v,x} & \Delta\phi_1\mathbf{N}_{w,x} & \Delta w^1_{c,x}\mathbf{N}_{\phi} & \mathbf{0} & -\mathbf{N}_{\theta} & \mathbf{0} \\ \mathbf{0} & -\Delta\phi^1\mathbf{N}_{v,x} & \mathbf{N}_{w,x} & -\Delta v^1_{c,x}\mathbf{N}_{\phi} & \mathbf{N}_{\psi} & \mathbf{0} & \mathbf{0} \\ \mathbf{0} & \mathbf{0} & \mathbf{0} & \mathbf{N}_{\phi,x} & \mathbf{0} & \mathbf{0} & \mathbf{0} \\ \mathbf{0} & -\Delta\phi^1_{,x}\mathbf{N}_{v,x} & \mathbf{0} & -\Delta v^1_{c,x}\mathbf{N}_{\phi,x} & \mathbf{N}_{\psi,x} & \mathbf{0} & \mathbf{0} \\ \mathbf{0} & \mathbf{0} & \Delta\phi^1_{,x}\mathbf{N}_{w,x} & \Delta w^1_{c,x}\mathbf{N}_{\phi,x} & \mathbf{0} & -\mathbf{N}_{\theta,x} & \mathbf{0} \\ \mathbf{0} & \mathbf{0} & \mathbf{0} & \mathbf{0} & \mathbf{0} & \mathbf{0} & \mathbf{N}_{\vartheta,x} \\ \mathbf{0} & \mathbf{0} & \mathbf{0} & \mathbf{N}_{\phi,x} & \mathbf{0} & \mathbf{0} & -\mathbf{N}_{\vartheta} \end{bmatrix} \tag{4.41}$$

is obtained. The internal force vector is presented in the formula (3.48). The geometric stiffness has the form

$$\mathbf{K}_G = \begin{bmatrix} \mathbf{0} & \mathbf{0} & \mathbf{0} & \mathbf{0} & \mathbf{0} & \mathbf{0} & \mathbf{0} \\ & \mathbf{K}_{Gvv} & \mathbf{0} & \mathbf{K}_{Gv\phi} & \mathbf{0} & \mathbf{0} & \mathbf{0} \\ & & \mathbf{K}_{Gww} & \mathbf{K}_{Gw\phi} & \mathbf{0} & \mathbf{0} & \mathbf{0} \\ & & & \mathbf{K}_{G\phi\phi} & \mathbf{0} & \mathbf{0} & \mathbf{0} \\ & & & & \mathbf{0} & \mathbf{0} & \mathbf{0} \\ & & & & & \mathbf{0} & \mathbf{0} \\ & \text{s} & \text{y} & \text{m} & \text{m.} & & \mathbf{0} \end{bmatrix}, \tag{4.42}$$

where the submatrices are given in Equations (3.50)

An element based on Vlasov's classical theory of torsion concerning thin-walled members can be simply constructed from the presented elements by using a penalty method. In an element, formulated by using the stress-resultants and generalized strain quantities, the Vlasov's constraint

$$\phi_{,x} - \vartheta = 0 \tag{4.43}$$

can be included in the constitutive matrix C by substituting term αGI_s instead of GI_s, where α is suitably chosen penalty parameter ($\alpha \gg 1$). To other elements, the constraint (4.43) can be included by adding a term

$$\alpha GI_s \int_0^L (\phi_{,x}\hat{\delta}\phi_{,x} - \phi_{,x}\hat{\delta}\vartheta - \vartheta\hat{\delta}\phi_{,x} + \vartheta\hat{\delta}\vartheta)dx \tag{4.44}$$

in the variational equations.

4.2.2 Elements based on Euler-Bernoulli beam theory

The most common procedure to formulate a thin-walled beam element is to use Vlasov's theory, Vlasov (1963), for thin-walled beams with open non-deformable cross-section. In this theory the shear strains in the middle line of the cross-section is assumed to be zero, i.e. in linearized form

$$\gamma_{xs} = u_{,s} + v_{,x} = 0. \tag{4.45}$$

In the finite element method the incremental displacement assumptions

$$\begin{aligned} \Delta u &= \Delta u_c - y\Delta v_{c,x} - z\Delta w_{c,x} - \omega\Delta\phi_{,x}, \\ \Delta v &= \Delta v_c - z\Delta\phi, \\ \Delta w &= \Delta w_c + y\Delta\phi, \end{aligned} \tag{4.46}$$

can be used in formulating the equilibrium equations in the updated incremental Lagrangian description. The warping function ω contains now both parts ω_r and ω_s. The bending displacements v_c and w_c are interpolated within an element by the cubic Hermitian polynomials (3.54). The angle of twist ϕ is interpolated by the same shape functions as the translational displacement v_c, so possessing C^1-continuity. For the axial displacement u_c the linear interpolation is used. The displacement field is described by equations

$$\begin{aligned} u_c &= \mathbf{N}_u\mathbf{q}_u, \\ v_c &= \mathbf{N}_v\mathbf{q}_v, \\ w_c &= \mathbf{N}_w\mathbf{q}_w, \\ \phi &= \mathbf{N}_\phi\mathbf{q}_\phi, \end{aligned} \tag{4.47}$$

where

$$\begin{aligned} \mathbf{q}_u^T &= [\, u_1 \quad u_2 \,], \\ \mathbf{q}_\phi^T &= [\, \phi_1 \quad \phi_1' \quad \phi_2 \quad \phi_2' \,], \end{aligned} \tag{4.48}$$

and $\mathbf{q}_v$ and $\mathbf{q}_w$ are given in Equations (3.54). Using the displacement assumptions (4.46), the strain increments are

$$\begin{aligned} \delta\varepsilon_x =& \delta u_{c,x} + (\Delta v_{c,x}^1 - z\Delta\phi_{,x}^1)\delta v_{c,x} - y\delta v_{c,xx} \\ &+ (\Delta w_{c,x}^1 + y\Delta\phi_{,x}^1)\delta w_{c,x} - z\delta w_{c,xx} \\ &+ (r^2\Delta\phi_{,x}^1 - z\Delta v_{c,x}^1 + y\Delta w_{c,x}^1)\delta\phi_{,x} - \omega\delta_{,xx} \\ &- z\delta v_{c,x}\delta\phi_{,x} + y\delta w_{c,x}\delta\phi_{,x} + (\delta v_{c,x}^2 + \delta w_{c,x}^2 + r^2\delta\phi_{,x}^2)/2, \end{aligned} \tag{4.49a}$$

$$\delta\gamma_{xy} = \Delta\phi^1\delta w_{c,x} - (z + \omega_{,y})\delta\phi_{,x} + \Delta w_{c,x}^1\delta\phi + \delta w_{c,x}\delta\phi, \tag{4.49b}$$

$$\delta\gamma_{xz} = -\Delta\phi^1\delta v_{c,x} + (y - \omega_{,z})\delta\phi_{,x} - \Delta v_{c,x}^1\delta\phi - \delta v_{c,x}\delta\phi, \tag{4.49c}$$

based on strain measures in Equation (3.57). Substituting the displacement interpolations, Equation (4.47), into the expressions (4.49a)-(4.49c), the linear part of the strains are related to the nodal point displacement parameters through the strain-displacement matrix

$$\mathbf{B} = \begin{bmatrix} \mathbf{N}_{u,x} & a_1\mathbf{N}_{v,x} - y\mathbf{N}_{v,xx} & a_2\mathbf{N}_{w,x} - z\mathbf{N}_{w,xx} & a_3\mathbf{N}_{\phi,x} - \omega\mathbf{N}_{\phi,xx} \\ \mathbf{0} & \mathbf{0} & \Delta\phi^1\mathbf{N}_{w,x} & b_1\mathbf{N}_{\phi,x} + \Delta w^1_{c,x}\mathbf{N}_\phi \\ \mathbf{0} & -\Delta\phi^1\mathbf{N}_{v,x} & \mathbf{0} & c_1\mathbf{N}_{\phi,x} - \Delta v^1_{c,x}\mathbf{N}_\phi \end{bmatrix}, \quad (4.50)$$

where the abbreviations a_1, a_2, a_3, b_1 and c_1 are the same as in Equation (3.60). The geometric stiffness matrix is similar to Equation (3.61), now only the shape functions for the angle of twist ϕ have been changed to cubic polynomials.

The internal virtual work, expressed in terms of generalized strain quantities and stress resultants is

$$\int_V {}^2S_{ij}\hat{\delta}({}^2E_{ij})dV =$$

$$\int_0^L [{}^2N\hat{\delta}({}^2\varepsilon_c) + {}^2M_{xf}\hat{\delta}({}^2\kappa_x) + {}^2M_y\hat{\delta}({}^2\kappa_y) + {}^2M_z\hat{\delta}({}^2\kappa_z) + {}^2B\hat{\delta}({}^2\kappa_\omega)]dx, \quad (4.51)$$

where

$$\kappa_\omega = -\phi_{,xx}, \quad (4.52)$$

and the other terms have the same meaning as in Equations (4.35) and (3.64). The linearized incremental displacement assumptions (4.37) have been adopted. The vector of stress resultants and the generalized strains are now

$$\begin{aligned} \mathbf{Q} &= [\,N \quad M_z \quad M_y \quad M_{xf} \quad B\,]^T, \\ \mathbf{e} &= [\,\varepsilon_c \quad \kappa_z \quad \kappa_y \quad \kappa_x \quad \kappa_\omega\,]^T. \end{aligned} \quad (4.53)$$

The constitutive matrix relating the increments of $\mathbf{Q}$ and $\mathbf{e}$ is

$$\mathbf{C} = \begin{bmatrix} EA & & & & \\ & EI_z & & & EI_{z\omega} \\ & & EI_y & & EI_{y\omega} \\ & & & GI_t & \\ & EI_{\omega z} & EI_{\omega y} & & EI_\omega \end{bmatrix}. \quad (4.54)$$

The linearized strain-displacement matrix has the form

$$\mathbf{B} = \begin{bmatrix} \mathbf{N}_{u,x} & \Delta v^1_{c,x}\mathbf{N}_{v,x} & \Delta w^1_{c,x}\mathbf{N}_{w,x} & I_p/A\Delta\phi^1_{,x}\mathbf{N}_{\phi,x} & \mathbf{0} \\ \mathbf{0} & -\mathbf{N}_{v,xx} & \Delta\phi^1_{,x}\mathbf{N}_{w,x} & \Delta w^1_{w,x}\mathbf{N}_{\phi,x} & \mathbf{0} \\ \mathbf{0} & -\Delta\phi^1_{,x}\mathbf{N}_{v,x} & -\mathbf{N}_{w,xx} & -\Delta v^1_{c,x}\mathbf{N}_{\phi,x} & \mathbf{0} \\ \mathbf{0} & \mathbf{0} & \mathbf{0} & \mathbf{N}_{\phi,x} & \mathbf{0} \\ \mathbf{0} & \mathbf{0} & \mathbf{0} & \mathbf{0} & \mathbf{N}_{\phi,xx} \end{bmatrix}. \quad (4.55)$$

and the geometric stiffness matrix is similar to the previous one.

5 TRANSFORMATION BETWEEN LOCAL AND GLOBAL COORDINATE SYSTEMS

Orientation of a beam is completely defined in the global X, Y, Z space, if the beam axis and the two directions of the cross-section perpendicular to the beam axis are known. The orthonormal base vectors in the global coordinate system are denoted by $\hat{\mathbf{G}}_1, \hat{\mathbf{G}}_2\ \hat{\mathbf{G}}_3$ and the orthonormal base vectors in the beams initial local coordinate system x, y, z by $\hat{\mathbf{g}}_1, \hat{\mathbf{g}}_2, \hat{\mathbf{g}}_3$ in the directions of X, Y, Z and x, y, z axes, respectively, see Figure 5.1. The initial orientation matrix of a beam can be defined by

$$\mathbf{R}_o = \begin{bmatrix} \hat{\mathbf{g}}_1 \cdot \hat{\mathbf{G}}_1 & \hat{\mathbf{g}}_1 \cdot \hat{\mathbf{G}}_2 & \hat{\mathbf{g}}_1 \cdot \hat{\mathbf{G}}_3 \\ \hat{\mathbf{g}}_2 \cdot \hat{\mathbf{G}}_1 & \hat{\mathbf{g}}_2 \cdot \hat{\mathbf{G}}_2 & \hat{\mathbf{g}}_2 \cdot \hat{\mathbf{G}}_3 \\ \hat{\mathbf{g}}_3 \cdot \hat{\mathbf{G}}_1 & \hat{\mathbf{g}}_3 \cdot \hat{\mathbf{G}}_2 & \hat{\mathbf{g}}_3 \cdot \hat{\mathbf{G}}_3 \end{bmatrix}, \tag{5.1}$$

i.e. the matrix $\mathbf{R}_o$ contains the direction cosines

$$R_{oij} = \cos(\hat{\mathbf{g}}_i, \hat{\mathbf{G}}_j) \tag{5.2}$$

and transfers the global base vectors into the local ones

$$\hat{\mathbf{g}}_i = \mathbf{R}_o \hat{\mathbf{G}}_i. \tag{5.3}$$

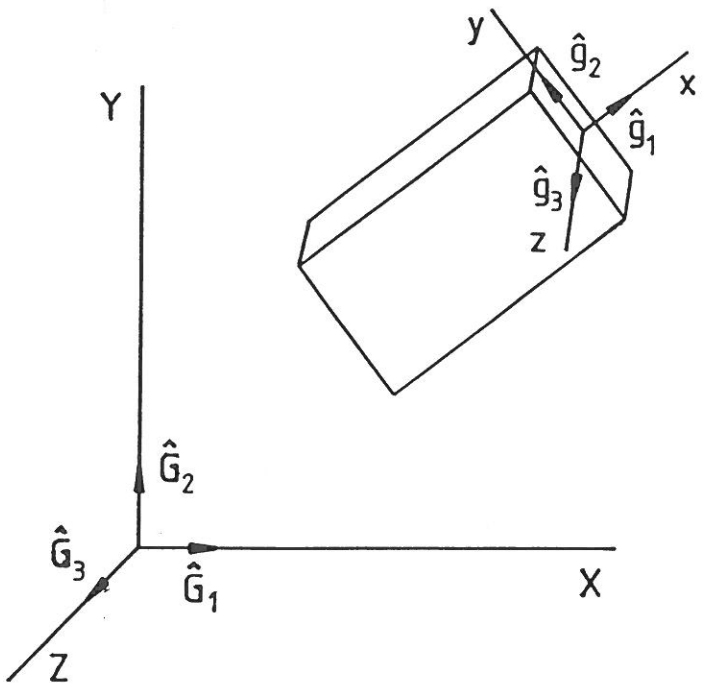

Figure 5.1 Orientation of a beam.

At some equilibrium configuration C_2, reached after $n+1$ steps, the rotation matrix $\mathbf{R}_{n+1}$ can be obtained from the rotation matrix at previous equilibrium

configuration C_1 (at step n) by the formula

$$\mathbf{R}_{n+1} = \mathbf{\Delta R}\mathbf{R}_n, \tag{5.4}$$

where the incremental rotation matrix $\mathbf{\Delta R}$ is calculated from the incremental displacements as explained in the following.

Defining the Eulerian angles α, β and γ, see Figure 5.2, between configurations C_1 and C_2, the rotation matrix $\mathbf{\Delta R}$ is obtained after three consecutive rotations of magnitude $\alpha, -\beta$ and γ with respect to axes z_n, x_α and x_{n+1}. The resulting matrix is

$$\mathbf{\Delta R} = \begin{bmatrix} C\beta C\alpha & C\beta S\alpha & S\beta \\ -S\gamma S\beta C\alpha - C\gamma S\alpha & -S\gamma S\beta S\alpha + C\gamma C\alpha & S\gamma C\beta \\ -C\gamma S\beta C\alpha - S\gamma S\alpha & -C\gamma S\beta S\alpha - S\gamma C\alpha & C\gamma C\beta \end{bmatrix}, \tag{5.5}$$

in which the notations $C\alpha = \cos\alpha, S\alpha = \sin\alpha$ etc. have been used. The rigid body rotation angles can be calculated from equations

$$\begin{aligned} \cos\alpha &= \Delta u_c / \sqrt{\Delta u_c^2 + \Delta v_c^2}, \\ \sin\alpha &= \Delta v_c / \sqrt{\Delta u_c^2 + \Delta v_c^2}, \\ \cos\beta &= \sqrt{\Delta u_c^2 + \Delta v_c^2}/L, \\ \sin\beta &= \Delta w_c / L, \\ \gamma &= \Delta\phi. \end{aligned} \tag{5.6}$$

In the computer program the initial rotation matrix $\mathbf{R}_o$ is formed from the information included in two vectors, the tangent vector of the beam axis $\hat{\mathbf{g}}_1$ and the normal vector of the primary bending plane, or some other given direction of the cross-section plane, $\hat{\mathbf{g}}_3$. Othonormal base of the triple

$$\hat{\mathbf{g}}_1, \hat{\mathbf{g}}_2 = \hat{\mathbf{g}}_1 \times \hat{\mathbf{g}}_3 \quad \text{and} \quad \hat{\mathbf{g}}_3$$

forms the initial rotation matrix $\mathbf{R}_o$. If the vector $\hat{\mathbf{g}}_3$ is not normal to the principal bending plane, forming an angle φ, the initial rotation matrix is obtained from the orthonormal base $\hat{\mathbf{g}}_1, \hat{\mathbf{g}}_2, \hat{\mathbf{g}}_3$, and the resulting matrix is

$$\mathbf{R}_o = [\, \hat{\mathbf{g}}_1 \quad \cos\varphi\hat{\mathbf{g}}_2 - \sin\varphi\hat{\mathbf{g}}_3 \quad \sin\varphi\hat{\mathbf{g}}_2 + \cos\varphi\hat{\mathbf{g}}_3 \,]. \tag{5.7}$$

If the element stiffness matrices and the internal force vector are integrated numerically over the cross-sectional area, the transformation (5.7) is not necessarily needeed.

The element stiffness matrix $\bar{\mathbf{K}}$ and the internal force vector $\bar{\mathbf{R}}$, evaluated in the local coordinate system, are transformed into global coordinate system by formulas

$$\begin{aligned} \mathbf{K} &= \mathbf{T}^T \bar{\mathbf{K}} \mathbf{T}, \\ \mathbf{R} &= \mathbf{T}^T \bar{\mathbf{R}}, \end{aligned} \tag{5.8}$$

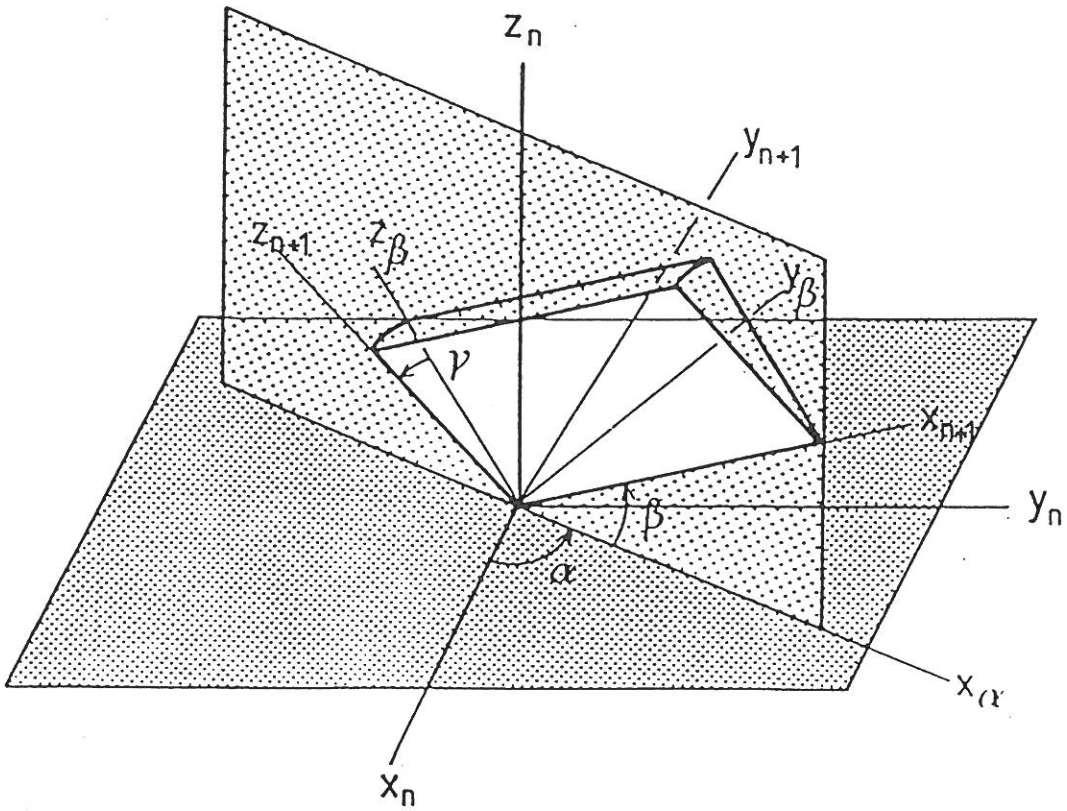

Figure 5.2 Euler angles.

where the transformation matrix $\mathbf{T}$ is composed of the rotation matrices

$$\mathbf{T} = \begin{bmatrix} \mathbf{R} & & \\ & \ddots & \\ & & \mathbf{R} \end{bmatrix}, \tag{5.9}$$

where the number of blocks in the diagonal is twice the number of the nodal points in an element. In the case of a thin-walled beam element the transformation matrix has the form, Bažant and El-Nimeiri (1973)

$$\mathbf{T} = \begin{bmatrix} \mathbf{R} & & & & & & \\ & \mathbf{R} & & & & & \\ & & 1 & & & & \\ & & & \ddots & & & \\ & & & & \mathbf{R} & & \\ & & & & & \mathbf{R} & \\ & & & & & & 1 \end{bmatrix}, \tag{5.10}$$

where the unit element corresponds to the warping degree of freedom.

6 CONSTITUTIVE MODELS

6.1 Elasto-plastic material model

Incremental constitutive equations which are suitable for computational purposes are usually based on a rate-type plasticity theory by Hill (1959). The strain rate $\mathbf{D}$ is decomposed into elastic and plastic parts

$$\mathbf{D} = \mathbf{D}^e + \mathbf{D}^p. \tag{6.1}$$

The elastic part $\mathbf{D}^e$ is related to the corotational Zaremba-Jaumann rate of Cauchy stress tensor $\mathbf{T}$ by a linear law

$$\overset{*}{\mathbf{T}} = \mathbf{C}^e : \mathbf{D}^e = \mathbf{C}^e : (\mathbf{D} - \mathbf{D}^p), \tag{6.2}$$

in which $\mathbf{C}^e$ is the elastic constitutive tensor. For an isotropic material the components of $\mathbf{C}^e$ are

$$C^e_{ijkl} = \frac{E}{1+\nu}(\delta_{ik}\delta_{jl} + \frac{\nu}{1-2\nu}\delta_{ij}\delta_{kl}), \tag{6.3}$$

where E is Young's modulus, ν Poisson's ratio and δ_{pq} is the Kronecker delta. In the J_2-flow theory, the yield function is

$$f = \sqrt{3J_2} - \sigma(\kappa), \tag{6.4}$$

where J_2 is the second invariant of the deviatoric Cauchy stress tensor

$$J_2 = -T'_{II} = \frac{1}{2}\mathrm{tr}(\mathbf{T}')^2, \qquad \mathbf{T}' = \mathbf{T} - (\frac{1}{3}\mathrm{tr}\mathbf{T})\mathbf{I}, \tag{6.5}$$

and κ is a hardening parameter. The plastic part of the strain rate is obtained from the plastic potential by the normality law

$$\mathbf{D}^p = \dot{\lambda}\frac{\partial f}{\partial \mathbf{T}} = \dot{\lambda}\mathbf{n}. \tag{6.6}$$

Using the consistency condition during plastic flow, i.e.

$$\dot{f} = 0 \tag{6.7}$$

$\dot{\lambda}$ is obtained and Equation (6.2) gives

$$\overset{*}{\mathbf{T}} = (\mathbf{C}^e - \frac{1}{h}\mathbf{b}\mathbf{b}) : \mathbf{D} = \mathbf{C}^{ep} : \mathbf{D}, \tag{6.8}$$

where

$$\begin{aligned} \mathbf{b} &= \mathbf{C}^e : \mathbf{n}, \\ h &= \mathbf{n} : \mathbf{C}^e : \mathbf{n} + E_p. \end{aligned} \tag{6.9}$$

The plastic hardening modulus E_p is obtained from the tangent modulus E_t and the modulus of elasticity E by the formula

$$E_p = \frac{EE_t}{E - E_t}, \qquad E_t = \frac{d\sigma_y}{d\bar{\varepsilon}^p}. \tag{6.10}$$

The yield stress σ_y is obtained from tension tests as a function of the logarithmic inelastic strain

$$\bar{\varepsilon}^p = \int \sqrt{\frac{2}{3}\mathbf{D}^p : \mathbf{D}^p}\, dt, \tag{6.11}$$

where t is time or in static analyses a load parameter. In the Lagrangian description a relationship between the 2nd Piola-Kirchhoff stress and the Green-Lagrange strain

$$\dot{\mathbf{S}} = \mathbf{C}_L : \dot{\mathbf{E}} \tag{6.12}$$

is needed. Taking the time derivative from the expression

$$\mathbf{S} = J\mathbf{F}^{-1} \cdot \mathbf{T} \cdot \mathbf{F}^{-T}, \tag{6.13}$$

where $J = \rho_o/\rho$ is the determinant of the deformation gradient $\mathbf{F}$, and using the relationship between the strain rate $\mathbf{D}$ and the rate of Green-Lagrange strain

$$\dot{\mathbf{E}} = \mathbf{F}^T \cdot \mathbf{D} \cdot \mathbf{F}, \tag{6.14}$$

yield Equation (6.12). If small strain assumption is made, the deformation gradient contains only the rigid body rotation, i.e.

$$\mathbf{F} \approx \mathbf{R},$$

and $J = 1$. So, the time derivative of the 2nd Piola-Kirchhoff stress is

$$\dot{\mathbf{S}} = (\mathbf{R}^T \cdot \mathbf{T} \cdot \mathbf{R})^{\cdot} = \mathbf{R}^T \cdot (\dot{\mathbf{T}} - \mathbf{W} \cdot \mathbf{T} - \mathbf{T} \cdot \mathbf{W}^T) \cdot \mathbf{R} = \mathbf{R}^T \cdot \overset{*}{\mathbf{T}} \cdot \mathbf{R}, \tag{6.15}$$

where $\mathbf{W}$ is the rate of rotation tensor. Equation (6.14) has now the form

$$\dot{\mathbf{E}} = \mathbf{R}^T \cdot \mathbf{D} \cdot \mathbf{R}. \tag{6.16}$$

Substituting Equation (6.8) into Equation (6.15) and taking Equation (6.16) into account, the relationship between the rate of the 2nd Piola-Kirchhoff stress and the Green-Lagrange strain is obtained

$$\dot{\mathbf{S}} = \mathbf{C}^{ep} : \dot{\mathbf{E}}. \tag{6.17}$$

6.2 Viscoplastic material model

For rate-dependent material behaviour the strain rate is decomposed into elastic and viscoplastic parts

$$\mathbf{D} = \mathbf{D}^e + \mathbf{D}^{vp}. \tag{6.18}$$

Perzyna (1966) has given the following expression for the viscoplastic part

$$\mathbf{D}^{vp} = \gamma \langle \frac{f}{\sigma_y} - 1 \rangle^p \frac{\partial f}{\partial \mathbf{T}} \tag{6.19}$$

where $f = \sqrt{3J_2}$, γ is the viscosity coefficient, σ_y the static yield limit and p is a material parameter. The notation $\langle x \rangle$ has the meaning

$$\langle x \rangle = \begin{cases} 0, & \text{if } x \leq 0; \\ x & \text{if } x > 0. \end{cases} \tag{6.20}$$

For isotropic hardening the static yield limit is taken as function of the effective plastic strain $\bar{\varepsilon}^p$

$$\begin{aligned} \sigma_y(\bar{\varepsilon}^p) &= \sigma_{yo} + E_p \bar{\varepsilon}^p, \\ \bar{\varepsilon}^p &= \int_{t_o}^{t} \sqrt{\frac{2}{3} \mathbf{D}^{vp} : \mathbf{D}^{vp}} dt. \end{aligned} \tag{6.21}$$

6.3 Thermo-elasto-plastic material

At high temperatures the material parameters, the modulus of elasticity and yield stress decrease. Considering small strain ε and infinitesimal stress σ the rate form of Equation (6.2) is

$$\dot{\sigma} = \mathbf{C}^e : \dot{\varepsilon}^e + \frac{\partial \mathbf{C}^e}{\partial \theta} : \varepsilon \dot{\theta}, \tag{6.22}$$

where θ is the temperature. The rate of deformation is decomposed into elastic, plastic and thermal parts

$$\dot{\varepsilon} = \dot{\varepsilon}^e + \dot{\varepsilon}^p + \dot{\varepsilon}^\theta. \tag{6.23}$$

The J_2-flow theory is used to evaluate the plastic strain rate

$$\dot{\varepsilon}^p = \dot{\lambda} \frac{\partial f}{\partial \sigma} = \dot{\lambda} \mathbf{n}, \tag{6.24}$$

and the thermal strain rate is

$$\dot{\varepsilon}^\theta = \alpha \dot{\theta} \mathbf{I}, \tag{6.25}$$

where α is the coefficient of thermal expansion. The yield condition is expressed by the formula

$$f = \sqrt{3J_2} - \sigma_y(\kappa, \theta), \tag{6.26}$$

where the yield stress σ_y depends on a hardening parameter κ and temperature θ. According to the consistency condition during the plastic flow

$$\dot{f} = \frac{\partial f}{\partial \boldsymbol{\sigma}} : \dot{\boldsymbol{\sigma}} + \frac{\partial f}{\partial \kappa}\dot{\kappa} + \frac{\partial f}{\partial \theta}\dot{\theta} = 0, \tag{6.27}$$

and the flow rule, Equation (6.24), together with Equations (6.22) and (6.23) yield

$$\dot{\boldsymbol{\sigma}} = (\mathbf{C}^e - \frac{1}{h}\mathbf{bb}) : (\dot{\boldsymbol{\varepsilon}} - \dot{\boldsymbol{\varepsilon}}^\theta) + \frac{1}{h}\mathbf{b}(\frac{\partial \sigma_y}{\partial \theta}\dot{\theta} - \mathbf{n} : \frac{\partial \mathbf{C}^e}{\partial \theta} : \boldsymbol{\varepsilon}^e\dot{\theta}) + \frac{\partial \mathbf{C}^e}{\partial \theta} : \boldsymbol{\varepsilon}^e\dot{\theta}, \tag{6.28}$$

where $h, \mathbf{n}, \mathbf{b}$ are defined in Equations (6.6) and (6.9).

Thermodynamically consistent constitutive laws in plasticity and viscoplasticity have been considered for instance by Lehmann (1983) and the computational procedures by Kojič and Bathe (1987a,b), Riff and Simitses (1988) and Ray and Utku (1989).

6.4 Yield surfaces expressed in terms of stress resultants

Denoting the vector of stress resultants and the corresponding generalized strains by $\mathbf{Q}$ and $\mathbf{e}$, the yield function (6.4) can be expressed in the form

$$f(\mathbf{Q}) = 0. \tag{6.29}$$

For a three dimensional beam with arbitrary cross-sectional shape the function f would be very complex. Yang et al. (1989) have discussed the form of the yield surface for a double symmetric I-sections under five active forces N, M_x, M_y, M_z and B. However, in analysing the response under strong transient loadings, the effect of shear forces becomes important and cannot be neclected from the yield function expression. Simo et al. (1988) have proposed a stress resultant yield function for a plane Timoshenko beam containing the shear force. In this study two simple approximate yield functions have been used. The first one, hypershere has the form

$$\sum_{i=1}^{n_r}(\frac{\mathbf{Q}_i}{\mathbf{Q}_{pi}})^2 = 1, \tag{6.30}$$

where n_r is the number of stress resultants. The second one, hypercube yield surface is

$$\left|\frac{\mathbf{Q}_i}{\mathbf{Q}_{pi}}\right| = 1, \qquad i = 1, ..., n_r. \tag{6.31}$$

In Equations (6.30) and (6.31) $\mathbf{Q}_{pi}$ is the fully plastic value of the corresponding stress resultant. Evaluation of the plastic strains $\Delta\boldsymbol{\varepsilon}^p$ and the constitutive matrix $\mathbf{C}^{ep}$ is formed similarly to the ones presented in Chapters 6.1 and 6.2.

7 ON THE PENALTY METHOD

A constraint equation can be handled in a simple way by using the penalty method. It is an alternative to the method of Lagrange multipliers. In this chapter the effect of the penalty parameter variations to the accuracy of the solution is studied in a simple example problem of torsion of a thin-walled beam.

The potential energy functional of the thin-walled torsion bar, based on the theory described in section 4.2.1 is

$$\Pi_P(\phi,\vartheta) = \frac{1}{2}\int_0^L [M_x\phi_{,x} + B\vartheta_{,x} + M_\omega(\phi_{,x} - \vartheta)]dx - \int_0^L m_t\phi dx, \tag{7.1}$$

where m_t is the distributed torque along the axis of the bar. Taking into account the relationship between the stress resultants M_x, B, M_ω and the generalized strain quantities $\phi_{,x}, \vartheta_{,x}$ and $\phi_{,x} - \vartheta$, the functional (7.1) becomes

$$\Pi_P(\phi,\vartheta) = \frac{1}{2}\int_0^L (GI_t\phi_{,x}^2 + EI_\omega\vartheta_{,x}^2)dx + \frac{1}{2}\int_0^L GI_s(\phi_{,x} - \vartheta)^2 dx - \int_0^L m_t\phi dx. \tag{7.2}$$

The Vlasov's contraint of the vanishing shear strain along the middle line of the cross-section, i.e.

$$\gamma_{xs} = \phi_{,x} - \vartheta = 0 \tag{7.3}$$

can be introduced into the functional (7.2) by replacing term GI_s with αGI_s, where α is the penalty parameter. The correct choice of the penalty parameter is an essential question in the penalty method; if it is too large, numerical truncation errors could destroy the accuracy of the solution, and if it is too small the constraint equation is not properly satisfied. For remedy of these shortcomings a variable penalty method was proposed by Kheshgi and Scriven (1985) or an iterative improvement of the penalty parameter by Salonen (1976).

As a simple example, a clamped beam with a consentrated torque at the midspan of the beam. Linear interpolation functions are used for both ϕ and ϑ in the FE discretization of the functional (7.2). The penalty term has to be underintegrated in order to avoid a locking phenomenon. The error in bimoment $B = -EI_\omega\vartheta_{,x}$ is of interest. It is measured by the maximum norm

$$\|B - B_h\|_\infty = \max_e |B(x_c^e) - B(x_c^e)|, \tag{7.4}$$

where B is the exact bimoment, B_h the finite element approximation and x_c^e the midpoint of an element e. Relative errors

$$e_r(B) = \frac{\|B - B_h\|_\infty}{\|B\|_\infty} \tag{7.5}$$

as a function of penalty parameter are shown schematically in Figure 7.1 from a coarse and a fine mesh computations. This figure shows, that in a small region of the values of the penalty parameter, the error has a minimum. These minimum values are considerably lower compared to the error values when larger 'safe' values of the penalty parameter are used. The convergence of the bimoment for the particular problem is shown in Figure 7.2. Also results from a numerical convergence test of an element based on functional

$$\Pi_P(\phi) = \frac{1}{2}\int_0^L [M_x\phi_{,x} + B\phi_{,xx}]dx - \int_0^L m_t\phi dx, \tag{7.6}$$

are shown in Figure 7.2. In this element cubic Hermitian polynomials are used for the angle of twist ϕ. The convergence rate is of order 2 for both linear penalty and cubic element. However, the error constant is greater for the linear penalty element if the penalty parameter does not have optimum value. For the optimal penalty parameter the following relation is obtained

$$\alpha^{-1} = Ch^2, \tag{7.7}$$

where h is the length of an element and C is a constant. For the determination of the optimum penalty parameter, no simple algorithm exists.

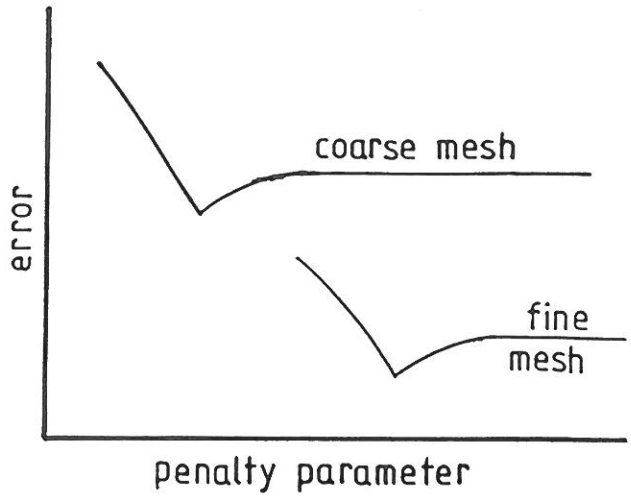

Figure 7.1 Error as a function of penalty parameter.

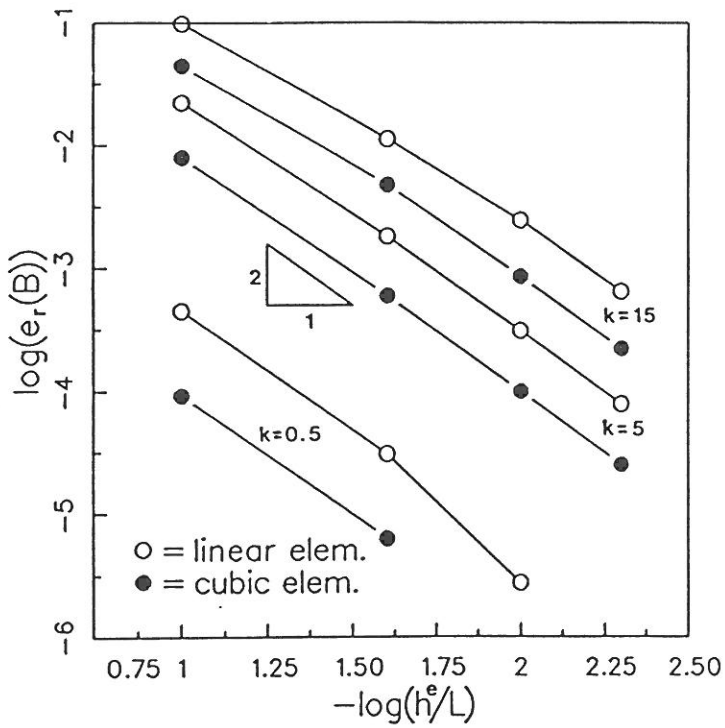

Figure 7.2 Convergence of bimoment. Computations are performed using three values of the dimensionless parameter $k = L\sqrt{GI_t/EI_\omega}$, which characterizes the torsional behaviour of the beam.

8 SOLUTION PROCEDURES OF NONLINEAR EQUILIBRIUM EQUATIONS

8.1 Continuation methods

8.1.1 Basic procedure

Discretization of nonlinear equations of a static equilibrium yields a n-dimensional nonlinear algebraic equation system

$$\mathbf{F}(\mathbf{q}, \boldsymbol{\lambda}) = \mathbf{0}, \tag{8.1}$$

where $\mathbf{q}$ is a n-dimensional vector of displacement quantities, also called a state variable vector, and $\boldsymbol{\lambda}$ is a m-dimensional parameter vector. The parameter vector can consist of loads, imperfections and/or material parameters. Solution of the multidimensionally parametrized nonlinear equilibrium surface requires complicated algorithms, Rheinboldt (1988). Thus it is not surprising that the dimension of the parameter space is usually reduced to one. In structural and solid mechanics, the system (8.1) is often written in the form

$$\mathbf{F}(\mathbf{q}, \lambda) \equiv \lambda \mathbf{Q}_r(\mathbf{q}) - \mathbf{R}(\mathbf{q}) = \mathbf{0}, \tag{8.2}$$

where $\mathbf{R}$ is the vector of internal resistance forces, $\mathbf{Q}_r$ the reference load vector and λ the load parameter, which now alone characterizes the parametrization of the problem.

Iterative methods have to be used to solve the nonlinear system (8.2). Usually the $(\mathbf{q}, \lambda)$ path is followed incrementally proceeding from a known equilibrium state $({}^1\mathbf{q}, {}^1\lambda)$ to an adjacent configuration $({}^2\mathbf{q}, {}^2\lambda)$. The incremental form of Equation (8.2) is then

$$\frac{\partial \mathbf{F}}{\partial \mathbf{q}} \Delta\mathbf{q} + \frac{\partial \mathbf{F}}{\partial \lambda} \Delta\lambda + \mathbf{F}({}^1\mathbf{q}, {}^1\lambda) = \mathbf{0}. \tag{8.3}$$

The more familiar notation in structural applications is

$${}^1\mathbf{K}\Delta\mathbf{q} = {}^2\mathbf{Q} - {}^1\mathbf{R}, \tag{8.4}$$

in which ${}^1\mathbf{K}$ is the tangent stiffness matrix at configuration 1

$$\mathbf{K} = -\frac{\partial \mathbf{F}}{\partial \mathbf{q}} = \frac{\partial \mathbf{R}}{\partial \mathbf{q}} - \frac{\partial \mathbf{Q}}{\partial \mathbf{q}}, \tag{8.5}$$

${}^2\mathbf{Q} \approx {}^2\mathbf{Q}({}^1\mathbf{q}) = {}^2\lambda \mathbf{Q}_r({}^1\mathbf{q}) = ({}^1\lambda + \Delta\lambda)\mathbf{Q}_r({}^1\mathbf{q}) = {}^2\lambda\, {}^1\mathbf{Q}_r$ is the approximation of the load vector at configuration 2, and ${}^1\mathbf{R} = \mathbf{R}({}^1\mathbf{q})$ is the internal force vector at configuration 1. The last term in Equation (8.5) $\partial\mathbf{Q}/\partial\mathbf{q}$ is the load stiffness matrix (see Chapter 2). If external loads do not depend on the deformed

configuration, the load vector ${}^2\mathbf{Q}$ is uniquely determined by the value of the load parameter ${}^2\lambda$. In the incremental procedure two strategies have to be chosen: how to proceed from configuration 1 to the next configuration 2 (prediction), and how to improve the predicted solution (correction). The first question is crucial. It has direct influence to the behaviour of the corrector algorithm and so to the cost of computation. Also, depending on the kinematical assumptions made in the formulation of Equation (8.4), the accuracy of the solution and the reliability of the whole computation process is to a great extent determined by the prediction phase. Thus, the construction of a reliable predictor algorithm is of primary interest and it will be discussed in Section 8.1.4.

The simplest procedure is the Newton-Raphson or the modified Newton-Raphson iteration, in which the load increment $\Delta\lambda = {}^2\lambda - {}^1\lambda$ is kept constant, and the choice of the load increment size is the primary question. The prediction and the correction to the displacements are performed using the same scheme

$$\begin{aligned} \Delta\mathbf{q}^1 &= {}^1\mathbf{K}^{-1}({}^2\lambda\,{}^1\mathbf{Q}_r - {}^1\mathbf{R}), \\ \delta\mathbf{q}^i &= (\mathbf{K}^{-1})^{i-1}({}^2\lambda\mathbf{Q}_r^{i-1} - \mathbf{R}^{i-1}), \qquad i = 2,3..., \end{aligned} \tag{8.6}$$

where $\delta\mathbf{q}^i$ is the correction to the previous estimate ${}^2\mathbf{q}^{i-1}$ i.e. ${}^2\mathbf{q}^i = {}^1\mathbf{q} + \Delta\mathbf{q}^i = {}^2\mathbf{q}^{i-1} + \delta\mathbf{q}^i$, and $\mathbf{R}^{i-1} = \mathbf{R}({}^2\mathbf{q}^{i-1})$. Simplicity and the quadratic convergence are the main advantages of the full Newton-Raphson iteration, but the cost of the computation could be very high, due to the reforming and triangulation of the tangent stiffness matrix at each iteration step. In the last decade a lot of attention has been paid to the development of the so called quasi-Newton methods. They have better convergence characteristics than the modified Newton method and are, in principle, computationally more effective than the full Newton method. However, in geometrically highly nonlinear problems the quasi-Newton methods usually fail to converge, and so they cannot be regarded as robust corrector algorihms, Kouhia (1986). An excellent survey of the mathematical properties of different quasi-Newton methods can be found in Reference Dennis and More (1977). Numerical experiments of the quasi-Newton methods in the structural finite element applications can be found in References Matthies and Strang (1979), Crisfield (1979,1982,1984). Eriksson (1987) has used the idea of eigenvector projections to speed up the convergence of the corrector iteration.

The corrector iterations in the constant load incrementing methods fail to converge near limit points, where the tangent stiffness matrix becomes singular. A simple remedy is to add a constraint equation

$$c(\Delta\mathbf{q}, \Delta\lambda) = 0 \tag{8.7}$$

relating displacement and load quantities, and to solve the changes of load and displacements from the extended system, Haselgrove (1961), Wempner (1971),

Riks (1972,1974,1977,1984)

$$\mathbf{G}(\mathbf{q},\lambda) = \begin{cases} \dfrac{\partial \mathbf{F}}{\partial \mathbf{q}}\Delta\mathbf{q} + \dfrac{\partial \mathbf{F}}{\partial \lambda}\Delta\lambda + \mathbf{F}({}^1\mathbf{q}, {}^1\lambda) = \mathbf{0} \\ \dfrac{\partial c}{\partial \mathbf{q}}\Delta\mathbf{q} + \dfrac{\partial c}{\partial \lambda}\Delta\lambda + c({}^1\mathbf{q}, {}^1\lambda) = 0 \end{cases} \tag{8.8}$$

The Jacobian matrix of the extended system (8.8) is not necessarily symmetric and the banded nature of the Jacobian of the mapping $\mathbf{F}$ is not preserved in the Jacobian of $\mathbf{G}$. Algorithms which take the special form of the system (8.8) into account, should be used to solve the linearized equation system of $n+1$ unknowns. Ramm (1980) and Crisfield (1981) solved the system (8.8) by splitting the incremental displacement vector into two parts and using the Jacobian of mapping $\mathbf{F}$, i.e. the conventional tangent stiffness matrix to obtain these two parts. The constraint equation (8.7) can be written briefly in the form

$$c(\Delta\mathbf{q}, \Delta\lambda) = \mathbf{t}^T\mathbf{C}\mathbf{n} + \theta. \tag{8.9}$$

Different possibilities exist to choose the form of the tangent vector $\mathbf{t}$, vector $\mathbf{n}$ and scalar θ, Ramm (1980), Crisfield (1981), Fried (1984), Schweizerhof and Wriggers (1986), Forde and Stiemer (1987). A positive definite, or at least positive semidefinite, diagonal weighting matrix is used to make the load parameter and the different displacement quantities commensurable. It is in partitioned form

$$\mathbf{C} = \begin{bmatrix} \mathbf{W} & \\ & \alpha^2 \end{bmatrix}, \tag{8.10}$$

where the diagonal matrix $\mathbf{W}$ contains the weighting terms of displacements and α is a scaling factor. Matrix $\mathbf{W}$ can also be updated, Tuomala and Kouhia (1986), during the computation in order to adapt the solution algorithm to the particular problem in question. For instance, the emergence of local instabilities could be detected better by the continuation method if the procedure could control more closely those degrees of freedom which change most rapidly. The choices of the weighting terms and the updating process are described in Section 8.1.4.1.

The arc length Δs between configurations 1 and 2 is defined by equation

$$(\Delta s)^2 = \mathbf{t}^T\mathbf{C}\mathbf{t}, \tag{8.11}$$

where $\mathbf{t}^T = [\Delta\mathbf{q}^T \quad \Delta\lambda]$. The prediction step to next configuration can be determined from equations

$$\begin{aligned} \Delta\mathbf{q}_Q^1 &= ({}^1\mathbf{K}^{-1}){}^1\mathbf{Q}_r, \\ \Delta\lambda^1 &= \mathrm{sign}({}^1\mathbf{K})\frac{\Delta s}{\sqrt{(\Delta\mathbf{q}_Q^1)^T\mathbf{W}\Delta\mathbf{q}_Q^1 + \alpha^2}}, \\ \Delta\mathbf{q}^1 &= \Delta\lambda^1\Delta\mathbf{q}_Q^1, \end{aligned} \tag{8.12}$$

where the signum operation is defined

$$\text{sign}(\mathbf{K}) = \begin{cases} +1, & \text{if } \mathbf{K} \text{ positive definite;} \\ -1, & \text{otherwise.} \end{cases} \tag{8.13}$$

A family of corrector algoritms are expressed in the form: solve the iterative changes $\delta\mathbf{q}^i$ and $\delta\lambda^i$ from

$$\begin{aligned} \mathbf{K}^{i-1}\delta\mathbf{q}^i &= \delta\lambda^i\mathbf{Q}_r^{i-1} - \mathbf{F}^{i-1}, \\ c(\Delta\mathbf{q}^i, \Delta\lambda^i) &= (\mathbf{t}^i)^T\mathbf{C}\mathbf{n}^i + \theta^i = 0, \\ \delta\mathbf{q}^i &= \delta\lambda^i\delta\mathbf{q}_Q^i + \delta\mathbf{q}_F^i, \\ \delta\mathbf{q}_Q^i &= (\mathbf{K}^{i-1})^{-1}\mathbf{Q}_r^{i-1}, \\ \delta\mathbf{q}_F^i &= (\mathbf{K}^{i-1})^{-1}\mathbf{F}^{i-1}. \end{aligned} \tag{8.14}$$

In this study Fried's orthogonal trajectory method, Fried (1984), is used. It is simple and linear for solving the load parameter change. Vectors $\mathbf{t}, \mathbf{n}$ and scalar θ are

$$\mathbf{t}^i = \begin{bmatrix} \delta\mathbf{q}_Q^i \\ 1 \end{bmatrix}, \qquad \mathbf{n}^i = \begin{bmatrix} \delta\mathbf{q}^i \\ \delta\lambda^i \end{bmatrix}, \qquad \theta^i = 0. \tag{8.15}$$

With a certain choice of the weighting matrix $\mathbf{W}$, Equations (8.14) and (8.15) can be identified with single displacement control method, Batoz and Dhatt (1979). If the choice of the controlling displacement is determined independently at each step, the method is similar to Rheinboldt's continuation procedure, Rheinboldt (1986), which also has proved to be reliable and effective, Eriksson (1989). Substituting Equation (8.15) into Equations (8.14), the iterative change of load parameter is computed from the equation

$$\delta\lambda^i = \frac{(\delta\mathbf{q}_Q^i)^T\mathbf{W}\delta\mathbf{q}_F^i}{(\delta\mathbf{q}_Q^i)^T\mathbf{W}\delta\mathbf{q}_Q^i + \alpha^2}. \tag{8.16}$$

The geometrical interpretation of Fried's orthogonal trajectory method is shown in a one dimensional case in Figure 8.1. It should be noted that if the tangent stiffness matrix is not updated in the corrective iteration process, Fried's method coincides with the normal plane method, suggested by Ramm (1980) and which is similar to the original method proposed by Riks (1974).

8.1.2 Detection of singular points

The solution of Equation $(8.14)_1$ can be achieved as long as the Jacobian $\mathbf{K}$ is regular. When a critical point is attained, the condition

$$\mathbf{K}\boldsymbol{\phi} = \mathbf{0} \tag{8.17}$$

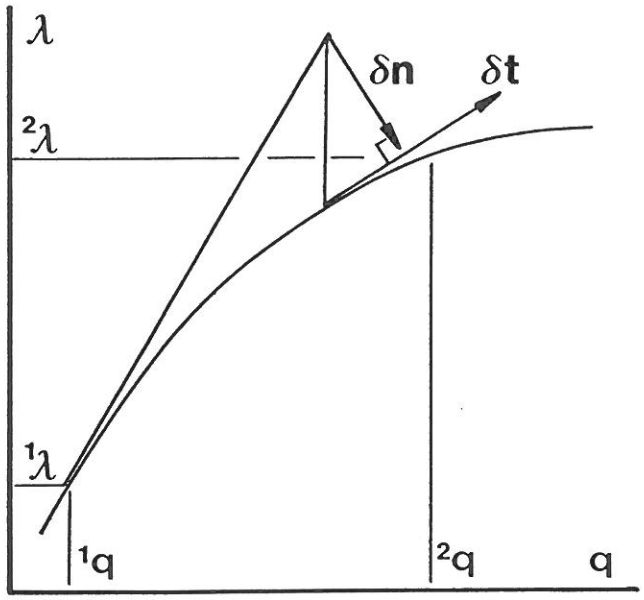

Figure 8.1 Orthogonal trajectory method.

is satisfied, where ϕ is the eigenvector belonging to the eigenvalue $\omega = 0$. By symmetry of $\mathbf{K}$ ϕ also satisfies $\phi^T\mathbf{K} = \mathbf{0}^T$. The solvability condition of Equation $(8.14)_1$ is then

$$\Delta\lambda^1\phi^T\mathbf{Q}_r = 0 \tag{8.18}$$

($\mathbf{F} = \mathbf{0}$ at equilibrium configuration). If a simple critical point where

$$\dim(\ker\mathbf{K}) = 1 \tag{8.19}$$

is in question, there are two possibilities to satisfy Equation (8.18), either $\Delta\lambda^1 = 0$ (limit point) or $\phi^T\mathbf{Q}_r = 0$ (bifurcation point). In numerical computations, the conditions (8.17) and (8.18) are never exactly satisfied. Also, near the singular point the system of equations is ill conditioned and large round of errors can deteriorate the accuracy of the computed equilibrium path. Then, it is preferable to keep away from the singular point as far as possible, and the nearby existence of the critical point should be estimated in the continuation method as early as possible. On the other hand, the classification of limit and bifurcation points is more reliable when small increments are used near the critical point. It could be preferable to use a deflated decomposition method to solve the nearly singular system $(8.14)_1$ as pointed out by Rheinboldt (1977,1986). The deflated decomposition algorithm and it's use in the continuation procedure is discussed in more detail in Section (8.1.4).

Possibly the most reliable way to estimate the forthcoming critical point, is to extrapolate the zero point of the smallest eigenvalue (absolute value). Monitoring

the evolution of the smallest eigenvalues of $\mathbf{K}$ as a function of the path parameter

$$s_n = \sum_{k=1}^{n} \Delta s_k, \tag{8.20}$$

is quite expensive; especially in cases where one critical point is reached and an unstable post-critical equilibrium path is followed. In this case at least two lowest eigenvalues have to be determined. In most of the practical computations, the determinant of the tangent stiffness matrix gives sufficient information. It is an easy byproduct of the normal continuation process, so the additional computational work is minimal. The only drawback is that the determinant is a product of all eigenvalues and so the rate of change in its value can be high in areas which are quite far from the critical point, see Figure 8.2. However, this could indicate that some of the higher modes (at the present moment) will be the critical ones after some subsequent steps, for instance in the case of example 4 by Eriksson (1989).

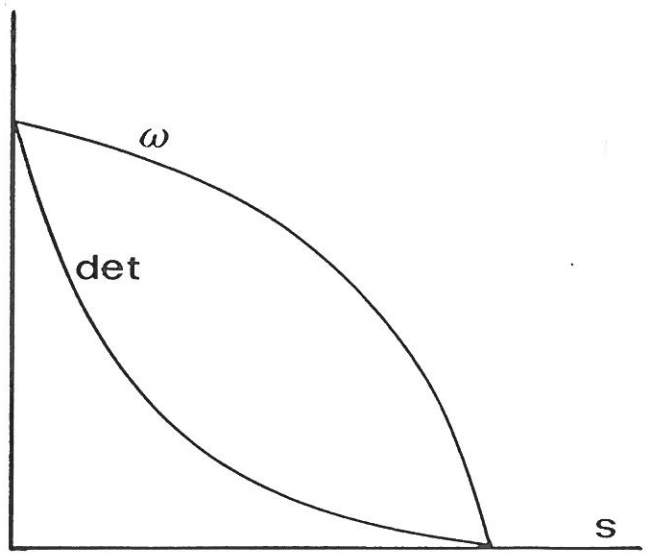

Figure 8.2 Determinant and the smallest eigenvalue as a function of path parameter.

The determinant of the Jacobian $\mathbf{K}$ can be computed from the triangular decomposition of $\mathbf{K} = \mathbf{L}\mathbf{D}\mathbf{L}^T$

$$\det \mathbf{K} = \prod_{i=1}^{n} D_{ii} = \prod_{i=1}^{n} \omega_i, \tag{8.21}$$

where D_{ii} is the i-th term of the diagonal matrix $\mathbf{D}$ and ω_i is the i-th eigenvalue of matrix $\mathbf{K}$. The signum function of the stiffness matrix (8.13) can be determined

from $\mathbf{D}$ as

$$\text{sign}(\mathbf{K}) = \begin{cases} +1, & \text{if} \quad \forall \quad D_{ii} > 0 \ ; \\ -1, & \text{if} \quad \exists \quad D_{ii} \leq 0 \ . \end{cases} \tag{8.22}$$

An alternative definition is also deduced from Equation (8.21)

$$\text{sign}(\mathbf{K}) = \begin{cases} +1, & \text{if} \quad \forall \quad \omega_i > 0 \ ; \\ -1, & \text{if} \quad \exists \quad \omega_i \leq 0. \end{cases} \tag{8.23}$$

Change in the numbers of negative elements is considered as an evidence of the existence of a critical point inside this step.

If the critical point is noticed during the step $\Delta\mathbf{q}_n, \Delta\lambda_n, \Delta s_n$, the condition of the existence of limit point is first checked, i.e. whether a point $s_{cr} \in (s_{n-1}, s_n)$ exists with the property $d\lambda/ds = 0$. This can be done by using an interpolation polynomial for $\lambda = \lambda(s)$ through the previous computed points. In this study parabolic interpolation is used and so the data from three equilibrium points is needed. If the product $\Delta\lambda_{n-1}\Delta\lambda_n$ is negative, it is clear that the limit point is reached, see Figure 8.3a, but also if it is positive, a possibility of the existence of limit point still exists, Figure 8.3b. In this case an estimate for the critical value of s_{cr} can be obtained from the interpolation polynomial.

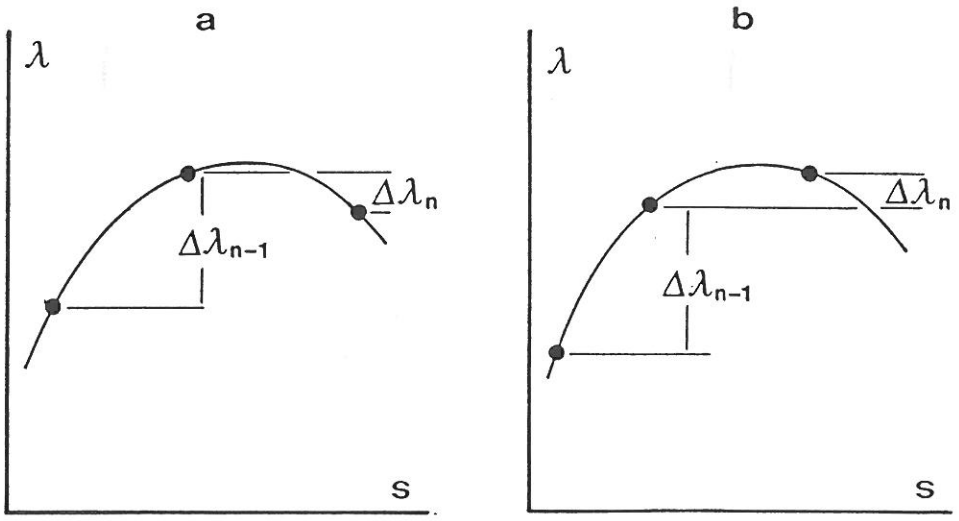

Figure 8.3 Two possibilities which satisfy the limit point condition.

If the criteria for the existence of limit point is not satisfied, the critical eigenvector is needed to verify the condition of bifurcation point, which is satisfied if

$$\frac{\boldsymbol{\phi}^T \mathbf{Q}_r}{\|\boldsymbol{\phi}\| \|\mathbf{Q}_r\|} < TOL, \tag{8.24}$$

where TOL is a prescribed tolerance, the value of which 10^{-2} is used in the numerical computations of this study. The critical load is computed by using linear interpolation

$$\lambda_{cr} = \lambda_n - \frac{\lambda_n - \lambda_{n-1}}{\tilde{d}_n - \tilde{d}_{n-1}} \tilde{d}_n, \tag{8.25}$$

where $\tilde{d}$ is the modified determinant value, $\tilde{d}_{n-1} = \text{sign}(\mathbf{K}_{n-1})|\det \mathbf{K}_{n-1}|, \tilde{d}_n = \text{sign}(\mathbf{K}_n)|\det \mathbf{K}_n|$. The critical load value can also be interpolated from the critical eigenvalue-load relationship, if the lowest eigenvalues are calculated during the continuation process. If neither the bifurcation nor the limit point condition is not satisfied, despite that a change in the number of negative terms in $\mathbf{D}$ is noticed, the situation could be due to the round of errors in the triangulation algorithm or it is due to the inconsistency of the tangent stiffness matrix with respect to the internal force vector. In these situations special care should be paid to the decision of the continuation of the computation. Bergan (1981) and Eriksson (1988) have discussed the construction of some steering parameters for nonlinear computations of equilibrium paths.

8.1.3 Branching onto the secondary path

When the bifurcation point $(\mathbf{q}_{cr}, \lambda_{cr})$ is determined, the direction of the branch is needeed in order to follow the post critical equilibrium path. The solution of Equation $(8.14)_1$ is written as a sum of the particular solution $\mathbf{p}$ and an arbitrary multiple of the eigenvector ϕ associated with the critical state

$$\delta\mathbf{q} = \eta\mathbf{p} + \xi\phi. \tag{8.26}$$

The solution of the unknown scalar multipliers η and ξ can be determined using the second order equation, Riks (1974), Rheinboldt (1977)

$$\frac{d^2\mathbf{F}}{ds^2} = \frac{\partial\mathbf{F}}{\partial\mathbf{q}}\frac{d^2\mathbf{q}}{ds^2} + \frac{\partial\mathbf{F}}{\partial\lambda}\frac{d^2\lambda}{ds^2} + \left[\left(\frac{d}{ds}\frac{\partial\mathbf{F}}{\partial\mathbf{q}}\right)\frac{d\mathbf{q}}{ds} + \left(\frac{d}{ds}\frac{\partial\mathbf{F}}{\partial\lambda}\right)\frac{d\lambda}{ds}\right] = 0. \tag{8.27}$$

At the bifurcation point the Jacobian $\partial\mathbf{F}/\partial\mathbf{q}$ is singular and the term $\partial\mathbf{F}/\partial\lambda$ is orthogonal to the critical eigenmode. Thus the last term in brackets multiplied with the eigenmode should vanish. This leads to the scalar equation

$$a_1\xi^2 + 2a_2\xi\eta + a_3\eta^2 = 0, \tag{8.28}$$

where the abbreviations are

$$\begin{aligned} a_1 &= \phi^T\left[\left(\frac{\partial^2\mathbf{F}}{\partial\mathbf{q}^2}\phi\right)\phi\right], \\ a_2 &= \phi^T\left[\left(\frac{\partial^2\mathbf{F}}{\partial\mathbf{q}^2}\mathbf{p}\right)\phi\right], \\ a_3 &= \phi^T\left[\left(\frac{\partial^2\mathbf{F}}{\partial\mathbf{q}^2}\mathbf{p}\right)\mathbf{p}\right]. \end{aligned} \tag{8.29}$$

If the particular solution $\mathbf{p}$ is chosen to be the tangent vector of the primary path, the coefficient a_3 vanishes, Riks (1974).

Two different situations arise. In the case of symmetric bifurcation the coefficient a_1 is zero, Thompson and Hunt (1973), Riks (1974), so $\eta = 0$ and ξ can be chosen to be the next arc-length Δs ($\|\phi\| = 1$). When antisymmetric bifurcation is in question, $a_1 \neq 0$ and the unknown parameters η and ξ can be solved from Equation (8.28) by use of a suitable constraint equation.

When the dimension n of the mapping $\mathbf{F}$ is large, the direct evaluation of the second order derivative $\partial^2\mathbf{F}/\partial\mathbf{q}^2$ is out of question. The computation of the coefficients a_i has to be carried out approximatively. Several ways to compute these quantities are presented by Riks (1974), Rheinboldt (1977), Eriksson (1990). The problem of the decision whether a_1 is zero or not is obvious. Therefore it seems preferable to construct a procedure which does not require the estimation of parameters a_i. Rheinboldt (1978) has developed a refined branching algorithm which does not need the coefficients a_i. In this method a point onto the branch is iterated from a perturbed state $\mathbf{q} = \mathbf{q}_{cr} + \xi\phi$, where ξ is an a priori chosen small parameter. Rheinboldt's numerical experiments show that the procedure is not very sensitive to the choise of ξ. Kouhia and Mikkola (1989) have developed a similar algorithm where the parameter ξ which multiplies the eigenvector is concidered as an unknown. An initial value of ξ is set to $\xi_o = \Delta s$ and an iteration process with Crisfield's elliptical constraint equation is adopted.

Probably the simplest and most reliable way to branch is to use Fried's orthogonal trajectory method from the perturbed critical state $\mathbf{q} = \mathbf{q}_{cr} + \Delta s\phi$. Because this method does not require a known equilibrium point as a starting value, the iteration onto the branch can be started from the perturbed state which is not an equilibrium state. The branching procedure is illustrated in one dimensional case in Figure 8.4.

8.1.4 Some computational aspects

8.1.4.1 Determination of the arc-length and weighting factors

The first value of the arc-length can be determined at the first iteration cycle of the first load step by the formula

$$\Delta s_1 = \Delta\lambda_0\sqrt{(\delta\mathbf{q}^1_{Q1})^T\mathbf{W}\delta\mathbf{q}^1_{Q1} + \alpha^2}, \tag{8.30}$$

where $\Delta\lambda_1$ is given as an input data. Scaling parameter α is determined from equation

$$(\delta\mathbf{q}^1_{Q1})^T\mathbf{W}\delta\mathbf{q}^1_{Q1} = \alpha^2(\delta\lambda_0)^2, \tag{8.31}$$

and it is then kept constant. Also other possibilities to determine the first arc-length exist, Bathe and Dvorkin 1983. From the point of view of succesful and

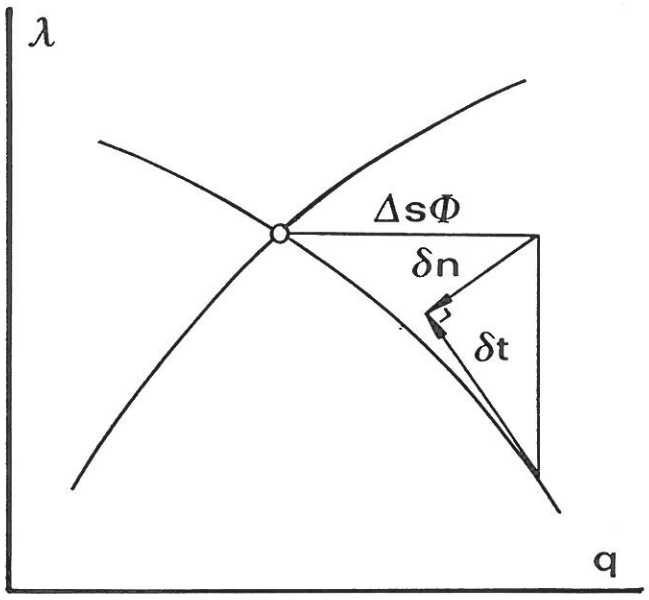

Figure 8.4 Branching onto the secondary path.

economical computation, the question of determining the arc-length for subsequent steps is essential. Ramm (1980) proposed a simple formula to the arc-length control

$$\Delta s_{n+1} = \Delta s_n (\frac{I^d}{I_n})^p, \tag{8.32}$$

where I^d is the number of desired iterations per load step and I_n the corresponding number at step n. The damping parameter p is usually set to $1/2$. This approach could in some cases produce uneconomically small increments. To circumvent this drawback the arc-length is modified only if

$$I_n < I^d_{lower} \quad \text{or} \quad I_n > I^d_{upper}. \tag{8.33}$$

The values between $I^d_{lower} = 3 \ldots 4$ and $I^d_{upper} = 4 \ldots 10$ are used in numerical computations of this study.

Chaisomphob et al. (1988) have proposed an incrementing algorithm which is based on the curvature changes of the equilibrium path. In their formulation restriction $\Delta s_n \leq \Delta s_1$ has been made and, practically, it's use is limited only to certain types of problems.

The initial values of the terms in the diagonal weighting matrix $\mathbf{W}$ in the arc-length constraint equation (8.9) are determined after the first iteration cycle. A simple choice is, Schweizerhof and Wriggers (1986)

$$W_{kk} = [(\delta q_{Qk})_1]^{-1}. \tag{8.34}$$

Another possibility, which has proven to be more stable and efficient in the numerical computations is presented by Kouhia and Mikkola (1989). Vector

$$\delta \mathbf{q}_{Q1} = \left\{ \begin{array}{c} \delta \mathbf{q}_{Q1,1} \\ \vdots \\ \delta \mathbf{q}_{Q1,np} \end{array} \right\} \tag{8.35}$$

is partitioned to groups containing local degrees of freedom at each nodal point (np is the total number of nodes). Then the vector $\boldsymbol{\delta q}_{Q1,i}$ of the i-th node contains elements

$$\boldsymbol{\delta q}_{Q1,i} = \left\{ \begin{array}{c} \delta q_{Q1,i,1} \\ \vdots \\ \delta q_{Q1,i,ndof} \end{array} \right\}, \tag{8.36}$$

where $ndof$ is the number of degrees of freedom in the i-th node. Then

$$W_{kk} = \underset{i}{\text{ave}}(\delta q_{Q1,i,j})^{-2}, \tag{8.37}$$

where the notation ave is the average over all nodes, and the global degree of freedom k can be determined from the local degree of freedom j. Also the average in Equation (8.37) can be determined based on different grouping of the nodal values as in Equation (8.36). One possibility is to split the nodal degrees of freedom to rotational and translational displacement groups and then take the average over the mesh in these groups in Equation (8.37). De Borst (1987) used a weighting matrix $\mathbf{W}$ with the diagonal terms either 1 or 0 in analysing the complex behaviour of concrete structures.

Updating of the weighting matrix $\mathbf{W}$ is often advantageous in order to maintain the ability to controll those degrees of freedom which change most rapidly. For instance, the emergence of local instabilities will be better detected by the continuation method. It is updated by the formula

$$(W_{kk})_{n+1} = \xi \sqrt{\frac{|(v_k)_{n+1}|}{|(v_k)_n|}} (W_{kk})_n, \tag{8.38}$$

where the vector

$$\mathbf{v} = \frac{\partial \mathbf{q}}{\partial s} \approx \frac{\boldsymbol{\Delta q}}{\Delta s}. \tag{8.39}$$

The scalar parameter ξ follows from the condition

$$\text{tr}(\mathbf{W}_{n+1}) = \text{tr}(\mathbf{W}_n). \tag{8.40}$$

8.1.4.2 Convergence estimation of corrector iterations

Full Newton-Raphson iteration has the quadratic convergence property, i.e.

$$\|\mathbf{q}^{i+1} - \mathbf{q}^*\| < \delta \|\mathbf{q}^i - \mathbf{q}^*\|^2, \tag{8.41}$$

where $\mathbf{q}^*$ is the exact solution, δ positive real number and $\|\cdot\|$ some vector norm, Ortega and Rheinboldt (1970). Watson and Holzer (1983) have proved the quadratic convergence of Crisfield's method. During the iterative process it

could be preferable to try to estimate the number of subsequent iterations needeed for the convergence. If the number of estimated iterations is too high, it is possible to shorten the arc-length during an increment. Also, it could guide the decision process of updating the stiffness matrix if modified or quasi-Newton methods are used. In elasto-plastic problems it is usually more economical to use modified versions of Newton iteration However, in strongly geometrically nonlinear problems the full Newton method is essential in order to get converged solution. Denoting ϵ the ratio

$$\epsilon^i = \frac{\|\delta \mathbf{q}^i\|}{\|\Delta \mathbf{q}^i\|}, \tag{8.42}$$

or some other measure which characterizes the residual, the estimate for the convergence rate at some iteration stage i is

$$p^i = \frac{\log \epsilon^i}{\log \epsilon^{i-1}}, \tag{8.43}$$

and the estimate for subsequent iterations to get converged solution is

$$N = \frac{\log(\frac{\log TOL}{\log \epsilon^i})}{\log p^i}, \tag{8.44}$$

where the notation TOL means the required error tolerance. Different convergence quality estimators has been presented by Rheinboldt (1986).

8.1.4.3 Solution of nearly singular equation system

Close to the limit- and bifurcation points the stiffness matrix is nearly singular and the system of equations becomes ill conditioned. Near such a point the solution of the system (8.14) may produce large relative errors, as pointed out by Rheinboldt (1986). Chan (1984) has proposed deflation techniques for stabilizing the algorithm. Considering the nearly singular symmetric system

$$\mathbf{K}\mathbf{q} = \mathbf{b}. \tag{8.45}$$

It is preferable to compute the solution $\mathbf{q}$ decomposed in the form, Rheinboldt (1977), Chan (1984)

$$\mathbf{q} = \mathbf{y} + \nu\boldsymbol{\phi}, \qquad \mathbf{y}^T\boldsymbol{\phi} = 0, \tag{8.46}$$

where $\boldsymbol{\phi}$ is the normalized singular vector corresponding to the smallest singular value σ of $\mathbf{K}$

$$\mathbf{K}\boldsymbol{\phi} = \sigma\boldsymbol{\phi} \tag{8.47}$$

and ν is a multiplier. Due to symmetry also the condition $\mathbf{K}^T\boldsymbol{\phi} = \sigma\boldsymbol{\phi}$ holds. The inverse iteration can be used to compute the singular vector rather efficiently, i.e.

starting with an initial guess ϕ_0, † and iterating

$$\begin{aligned} \mathbf{K}\tilde{\phi}^{i+1} &= \phi^i, \\ \phi^{i+1} &= \frac{\tilde{\phi}^{i+1}}{\|\tilde{\phi}^{i+1}\|}, \\ \sigma^{i+1} &= \frac{1}{\|\tilde{\phi}^{i+1}\|}. \end{aligned} \tag{8.48}$$

For the deflated solution $\mathbf{y}$ the process

$$\begin{aligned} \mathbf{y}^o &= \mathbf{0} \qquad j = 0, 1, 2, ..., \\ \mathbf{c}^j &= \mathbf{b} - \mathbf{K}\mathbf{y}^j, \\ \mathbf{K}\tilde{\mathbf{y}}^j &= \mathbf{c}^j - (\phi^T \mathbf{c}^j)\phi, \\ \mathbf{y}^{j+1} &= \mathbf{y}^j + \tilde{\mathbf{y}}^j - (\phi^T \tilde{\mathbf{y}}^j)\phi, \end{aligned} \tag{8.49}$$

converges quickly to the deflated solution $\mathbf{y}$ of Equation (8.45). The corresponding deflated decomposition is given by

$$\mathbf{q} = \mathbf{y} + \frac{\phi^T(\mathbf{b} - \mathbf{K}\mathbf{y})}{\sigma}\phi. \tag{8.50}$$

8.2 Time integration methods

8.2.1 Central difference method

The semi discrete equations of motion (2.26)

$$\mathbf{M}^2\ddot{\mathbf{q}} = {}^2\mathbf{Q} - {}^1\mathbf{R} \tag{8.51}$$

can be solved by a direct time integration method. The explicit central difference method, based on the central difference formulas for the velocity $\dot{\mathbf{q}}$ and for the acceleration $\ddot{\mathbf{q}}$ at time t_n

$$\begin{aligned} \dot{\mathbf{q}}_n &= (\mathbf{q}_{n+1} - \mathbf{q}_{n-1})/2\Delta t, \\ \ddot{\mathbf{q}}_n &= (\mathbf{q}_{n+1} - 2\mathbf{q}_n + \mathbf{q}_{n-1})/\Delta t^2, \end{aligned} \tag{8.52}$$

gives

$$\mathbf{q}_{n+1} = \Delta t^2 \mathbf{M}^{-1}(\mathbf{Q}_n - \mathbf{R}_n) + 2\mathbf{q}_n - \mathbf{q}_{n-1}. \tag{8.53}$$

---

† The initial vector ϕ_0 could be taken as $\phi_0 = \tilde{\mathbf{z}}/\|\tilde{\mathbf{z}}\|, \tilde{\mathbf{z}}^T = [1 \quad 1 \quad \ldots \quad 1]$ or $\phi_0 = \text{diag}(\mathbf{K})/\|\text{diag}(\mathbf{K})\|$.

In Equation (8.53) there is an addition of the form $\mathcal{O}(1) + \mathcal{O}(\Delta t^2)$, which gives unfavourable rounding errors when Δt is small, Dahlquist and Björck (1974). It is preferable to use the summed form of the method, where

$$\dot{\mathbf{q}}_{n+\frac{1}{2}} = (\mathbf{q}_{n+1} - \mathbf{q}_n)/\Delta t. \tag{8.54}$$

Noticing that

$$\dot{\mathbf{q}}_{n+\frac{1}{2}} - \dot{\mathbf{q}}_{n-\frac{1}{2}} = (\mathbf{q}_{n+1} - 2\mathbf{q}_n + \mathbf{q}_{n-1})/\Delta t$$

gives the summed form of the central difference (CD) formulas

$$\begin{aligned} \dot{\mathbf{q}}_{n+\frac{1}{2}} &= \dot{\mathbf{q}}_{n-\frac{1}{2}} + \Delta t \ddot{\mathbf{q}}_n, \\ \mathbf{q}_{n+1} &= \mathbf{q}_n + \Delta t \dot{\mathbf{q}}_{n+\frac{1}{2}}, \\ \ddot{\mathbf{q}}_{n+1} &= \mathbf{M}^{-1}(\mathbf{Q}_{n+1} - \mathbf{R}_{n+1}), \end{aligned} \tag{8.55}$$

in which $t_{n+\frac{1}{2}} = t_n + (\Delta t)/2$.

The central difference method is only conditionally stable, and the time step is limited to

$$\Delta t \leq \Delta t_{cr} = \frac{2}{\omega_{max}}, \tag{8.56}$$

where ω_{max} is the highest natural frequency of the structure.

8.2.2 Newmark family

For implicit methods the equation of motion (2.24) is written in the form

$$\mathbf{K}_{n+1}^{i-1} \delta \mathbf{q}_{n+1}^i + \mathbf{M} \ddot{\mathbf{q}}_{n+1}^i = \mathbf{Q}_{n+1} - \mathbf{R}_{n+1}^{i-1}, \tag{8.57}$$

where $\delta \mathbf{q}_{n+1}^i = \Delta \mathbf{q}_{n+1}^i - \Delta \mathbf{q}_{n+1}^{i-1}$. In Newmark method the difference formulas used are

$$\begin{aligned} \mathbf{q}_{n+1} &= \mathbf{q}_n + \Delta t \dot{\mathbf{q}}_n + \Delta t^2 [(\frac{1}{2} - \beta) \ddot{\mathbf{q}}_n + \beta \ddot{\mathbf{q}}_{n+1}], \\ \dot{\mathbf{q}}_{n+1} &= \dot{\mathbf{q}}_n + \Delta t [(1 - \gamma) \ddot{\mathbf{q}}_n + \gamma \ddot{\mathbf{q}}_{n+1}], \end{aligned} \tag{8.58}$$

where β and γ are parameters. Substituting Equations (8.58) into Equation (8.57) yields

$$\mathbf{K}_s \delta \mathbf{q}_{n+1}^i = \mathbf{F}_s. \tag{8.59}$$

Here

$$\begin{aligned} \mathbf{K}_s &= \mathbf{K}_{n+1}^{i-1} + \frac{1}{\beta \Delta t^2} \mathbf{M}, \\ \mathbf{F}_s &= \mathbf{Q}_{n+1} - \mathbf{R}_{n+1}^{i-1} + \mathbf{M} \left[-\frac{1}{\beta \Delta t^2} (\mathbf{q}_{n+1}^{i-1} - \mathbf{q}_n) + \frac{1}{\beta \Delta t} \dot{\mathbf{q}}_n + \frac{(\frac{1}{2} - \beta)}{\beta} \ddot{\mathbf{q}}_n \right], \end{aligned} \tag{8.60}$$

are the effective stiffness matrix and the effective load vector, respectively. For the choise $\gamma = 1/2$ and $\beta = 1/4$ the implicit average acceleration method, or as

also known by the name trapezoidal rule, is obtained. Also the central difference method (8.53) is obtained from Equations (8.59) and (8.60) if $\gamma = 1/2$ and $\beta = 0$.

In a midpoint version of the trapezoidal rule, the effective load vector can be written in the form, Mikkola and Tuomala (1989)

$$\mathbf{F}_s = 2(\mathbf{Q}_{n+\frac{1}{2}} - \mathbf{R}^i_{n+\frac{1}{2}}) - \frac{4}{\Delta t^2}\mathbf{M}\left[(\mathbf{q}^i_{n+1} - \mathbf{q}_n) - \Delta t\dot{\mathbf{q}}_n\right], \tag{8.61}$$

where

$$\begin{aligned} \mathbf{Q}_{n+\frac{1}{2}} &= \mathbf{Q}(t_{n+\frac{1}{2}}), \\ \mathbf{R}^1_{n+\frac{1}{2}} &= \mathbf{R}(\mathbf{q}^i_{n+\frac{1}{2}}), \\ \mathbf{q}^i_{n+\frac{1}{2}} &= (\mathbf{q}^i_{n+1} + \mathbf{q}_n)/2, \\ t_{n+\frac{1}{2}} &= (t_{n+1} + t_n)/2. \end{aligned} \tag{8.62}$$

In nonlinear problems the midpoint rule is more stable than the trapezoidal rule.

8.2.3 Energy balance

In materially nonlinear cases an energy balance check is essential. If T, U and W denote the kinetic, internal and external energies, the energy balance check can be stated as

$$\Delta E = \Delta U + \Delta T - \Delta W < TOLE(U + T), \tag{8.63}$$

where the notation $TOLE$ is a tolerance. The energy increments can be calculated by using the trapezoidal integration, Mikkola and Tuomala (1989),

$$\begin{aligned} \Delta U &= \mathbf{\Delta q}^T(\mathbf{R}_n + \mathbf{R}_{n+1})/2, \\ \Delta T &= \mathbf{\Delta \dot{q}}^T\mathbf{M}(\dot{\mathbf{q}}_n + \dot{\mathbf{q}}_{n+1})/2, \\ \Delta W &= \mathbf{\Delta q}^T(\mathbf{Q}_n + \mathbf{Q}_{n+1})/2, \end{aligned} \tag{8.64}$$

where $\mathbf{\Delta q}$ is the incremental displacement vector between steps $n+1$ and n. Denoting E_n by the cumulating energy error at time t_n

$$E_n = \sum_{i=1}^{n} \frac{\Delta E_i}{U_i + T_i}, \tag{8.65}$$

the solution is feasible if E_n is smaller than the value of $10^{-3} - 10^{-2}$.

9 NUMERICAL EXAMPLES

9.1 Torsional behaviour of elasto-plastic beams

A cantilever beam with a square cross-section under a consentrated torque in it's free end is analysed. The J_2-flow theory is used for modelling the plastic material properties. Results obtained are shown in Figures 9.1 and 9.2. When the 4×4 Gaussian integration rule over the cross-sectional area is used, the onset of plasticity is noticed at so high load level as 1.35 times the exact yield load. However, the error compared to calculations with higher order quadratures, is diminishing when yielding continues. Also Simpson's integration rule is used, see Figure 9.1.

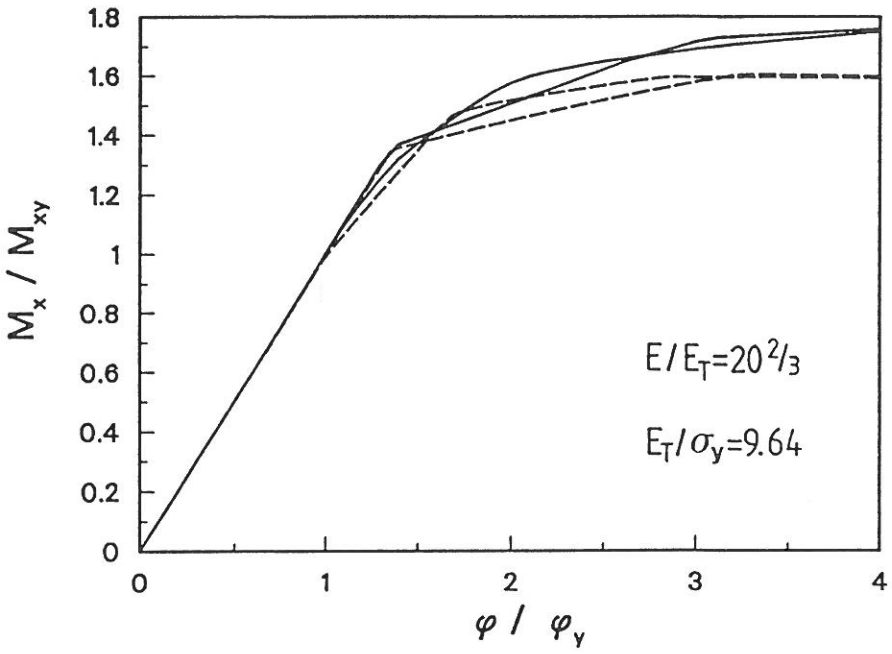

Figure 9.1 Elasto-plastic torsional behaviour of a beam with a square cross-section. Dashed lines correspond to the ADINA calculations. About 50 load increments are used in the computations. The 4×4 Gaussian and the 7×7 Simpson's rules are used to integrate over the cross-sectional area. Solid curves indicate calculations with present formulation, in which the 4×4 and the 9×9 Gaussian rules are used.

Reference calculations, dashed lines in Figure 9.1, are performed with the general purpose finite element code ADINA, with both the 4×4 Gaussian and the 7×7 Simpson's integration rules over the cross-sectional area. Elasto-plastic isotropically hardening material model is used and the equilibrium equations are solved by ADINA's automatic load incrementation procedure. Surprisingly, the ADINA computations show a limit point behaviour, i.e. the load is decreasing after reaching the value $\phi/\phi_y = 3.2$, in which $\phi_y = M_{xy}L/GI_t, M_{xy} = \tau_y W_x, \tau_y =$

$\sigma_y/\sqrt{3}$ and $W_x = 0.208b^3$ where b is the side length of the cross-section. In the present computations the length of the beam is ten times the side length of the cross-section. One linear element is used to model the structure. The problem has also been analysed by Bathe and Chaundhary (1982).

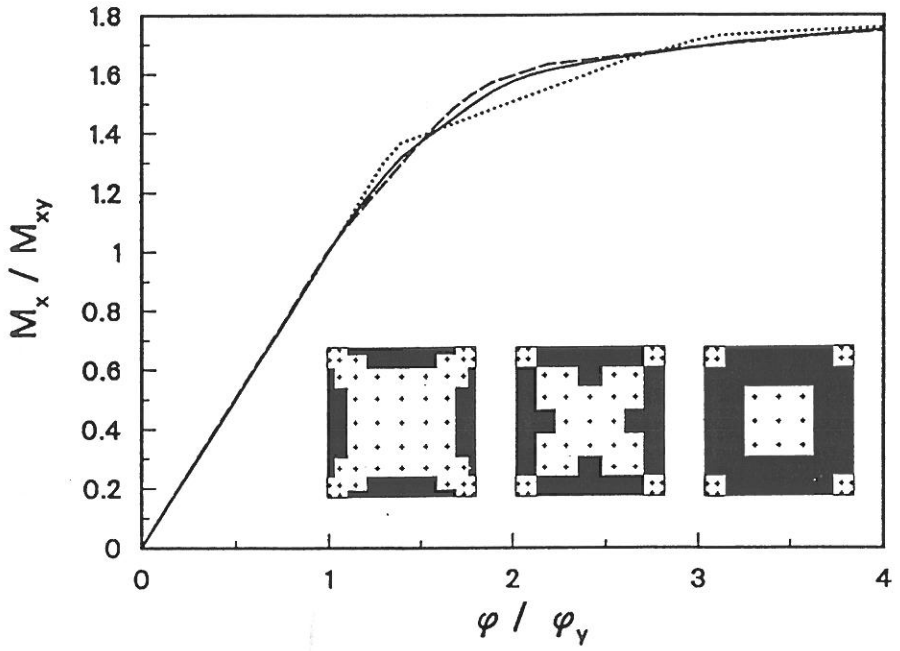

Figure 9.2 Elasto-plastic torsional behaviour of a beam with a square cross-section. Solid curve indicates calculation with the 9×9 Gaussian rule, dashed line the 7×7 Simpson's rule and dotted line the 4×4 Gaussian rule. Fourty increments were used in the computation. The plastic area of the cross-section is shown at load levels $M_x/M_{xy} = 1.4, 1.55$ and 1.6 in the case when the 9×9 Gaussian rule is used.

Also a beam with a solid cross-section with section proportion $h/b = 2$ is analysed using elastic perfectly plastic material model. The fully plastic torque M_{xp}, predicted by the Nadai's sand heap analogy is

$$M_{xp} = \tau_y W_{xp}, \qquad W_{xp} = \frac{b^2}{6}(3h - b) = \frac{5}{6}b^3.$$

Present formulation for the warping of the beam gives fairly good results compared to the analytical, Smith and Sidebottom (1965), and numerical solutions made by a cellular analogy method, Johnson (1988). The computed maximum load was 1.03 M_{xp} after 30 load increments at the point where the angle of twist per unit lenght has the value $\phi' = 2M_{xp}/GI_t$. Calculations with ADINA program failed to converge at the point where $\phi' \approx M_{xp}/GI_t$ after the load has decreased for some increments. Calculated load displacement curves are shown in Figure 9.3.

Elasto-plastic torsional behaviour of a cantilever beam with a thin-walled I-section is also studied. When there are no warping restraints, the torque is carried

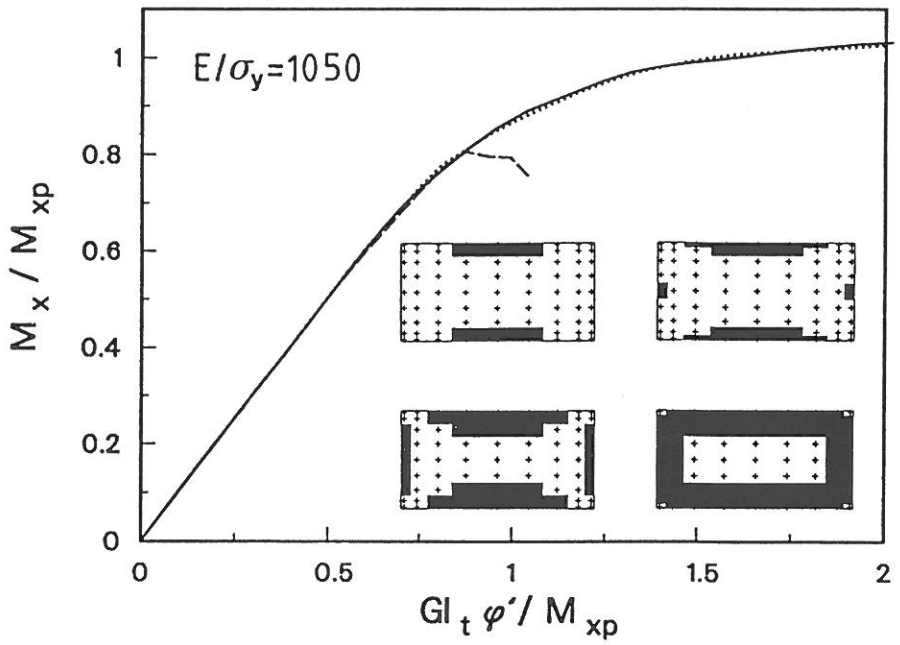

Figure 9.3 Elasto-plastic torsional response of a beam with a rectangular cross-section. Solid curve indicates computations with the 9×9 Gaussian integration, dotted line the 9×9 Simpson's rule and dashed line ADINA computation with the 7×7 Simpson's rule. The plastic areas are shown at load levels $M_x/M_{xp} = 0.7, 0.8, 0.9$ and 0.98.

by the St. Venant shear stresses, and the fully plastic solution is given by the sand heap analogy. For a thin-walled I-beam a close approximation to the fully plastic sand heap torque is

$$M_{xp} = \frac{t_w^2}{6}(3h - t_w) + \frac{t_f^2}{3}(3b - t_f), \tag{9.1}$$

where t_w and t_f are the web and flange thicknesses, h the depth of a beam between flange centroids and b the breadth of flanges. However, in most structures in which torsion is significant, there are warping restraints at the ends of the members. It is known that the maximum load carrying capacity of a twisted I-beam with warping restraints is higher than the sand heap value, but there is no exact theoretical solution. An upper bound for the total torque M_{xo} at plastic collapse is given by

$$M_{xo} = M_{xp} + Q_f h,$$

where Q_f is the flange shear force, Dinno and Merchant (1965). The flange bending moment M_f cannot exceed the plastic hinge moment

$$M_{fp} = \frac{\sigma_y t_f b^2}{4},$$

so the shear force Q_f cannot exceed the value

$$Q_f = M_{fp}/L,$$

where L is the length of the cantilever. The total torque is

$$M_{xo} = M_{xp} + \frac{h}{L}\sigma_y \frac{t_f b^2}{4}. \tag{9.2}$$

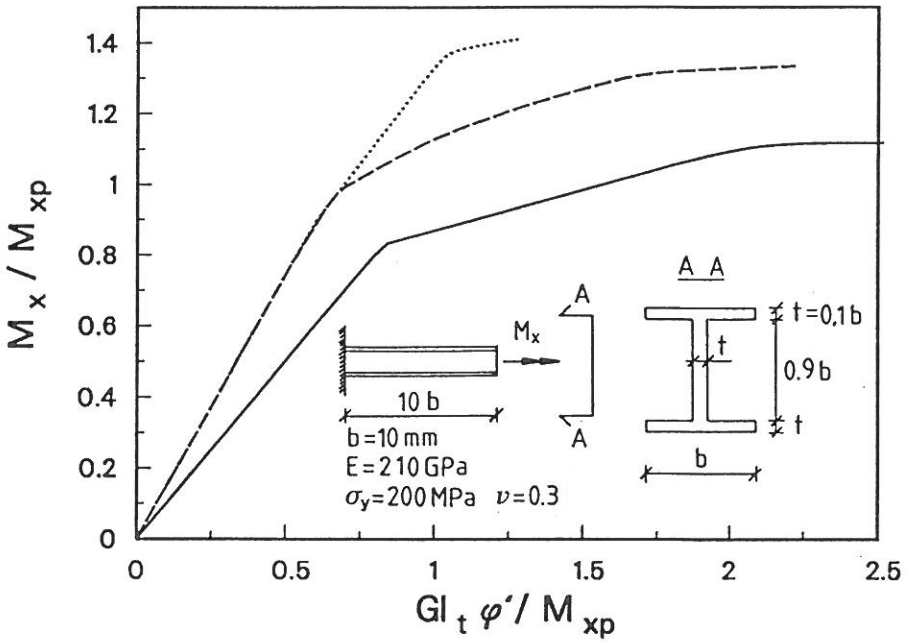

Figure 9.4 Elasto plastic behaviour of a cantilever I-beam. Solid curve corresponds to the pure St. Venant's torsional behaviour and dashed line indicates the load-deflection curve computed with elements containing warping degrees of freedom. The 4×4 Gaussian integration rule in every cross-section part is used. Dotted line is the result of computation with the 2×2 Gaussian rule at each cross-section part.

The cantilever beam shown in Figure 9.4 is analysed using a four element mesh where the nodal point coordinates x_j have been graded polynomially according to the grading function

$$\Gamma(x_j) = x_j^{\beta}, \tag{9.3}$$

where $\beta = 3$, see Appendix A2, Babuška and Szabo (1983). The cross-section is constructed of five rectangular parts in which the 4×4 Gaussian integration rule is used in each part, separately. The calculated load-deflection curve is shown in Figure 9.4. The maximum torque obtained in the present calculation was 1.33 M_{xp}, which is slightly greater than Dinno's and Merchant's upper bound value 1.31 M_{xp}. The spread of plastic area is shown in Figure 9.5. At the clamped

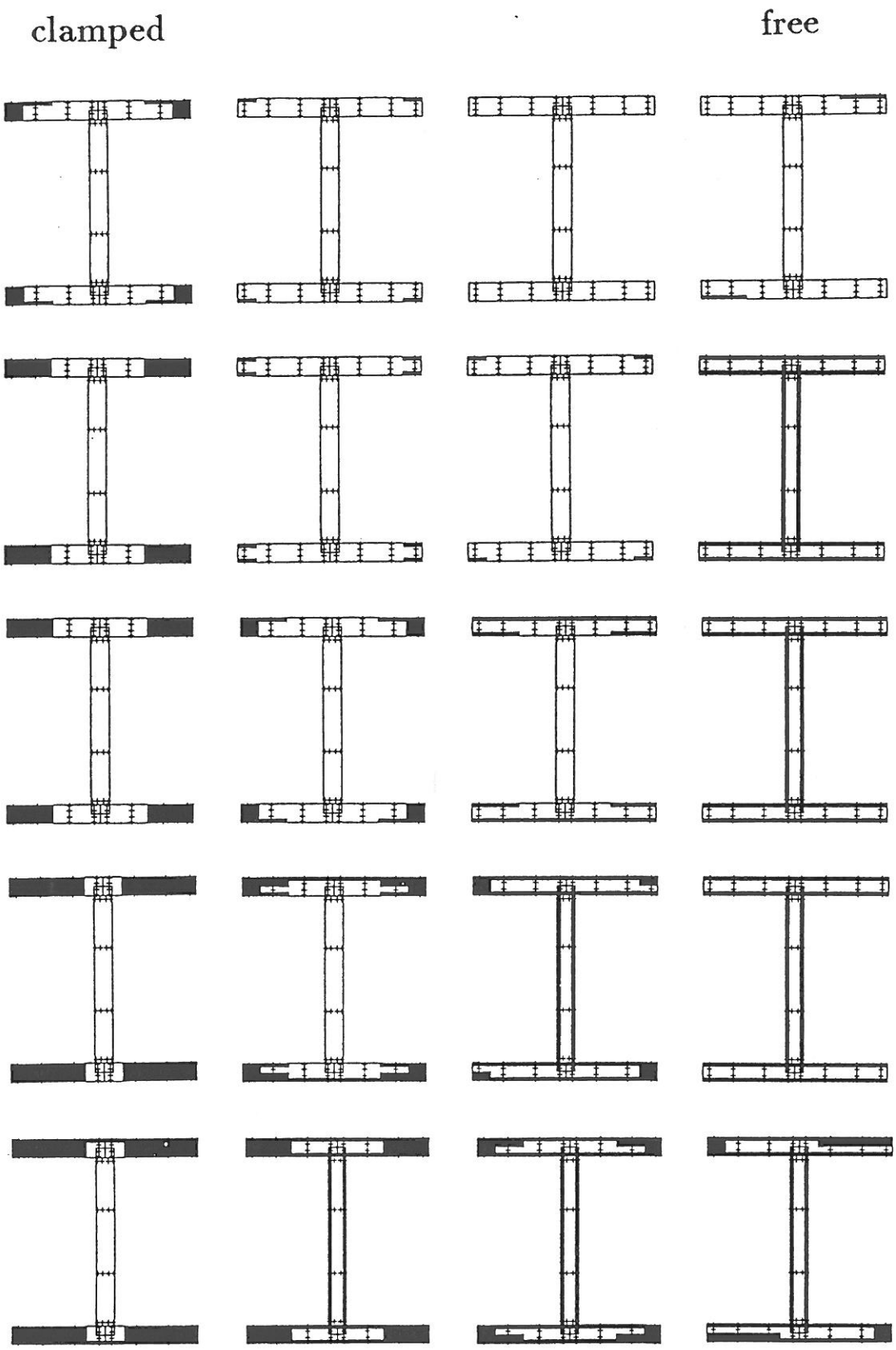

Figure 9.5 Spread of plasticity in cantilevered I-beam, subjected to twisting end moment. The places of figures from up to down correspond to the values of $M_x/M_{xp} = 0.9, 1.0, 1.1, 1.2$ and 1.3.

end on the left hand side of the beam, the spread of plasticity can be seen to be governed by warping i.e. flange bending. At the free end (on the right hand side) the effects of St. Venant torsional stresses dominate. The problem is also analysed using the element which does not contain the warping degrees of freedom. The corresponding load-deflection curve is shown in Figure 9.4 by solid line and the collapse torque obtained is 1.12 M_{xp} when the 4×4 Gaussian rule is used in each part of the cross-section. The same problem has also been analysed by Bathe and Wiener (1983). They have constructed the web and flanges from nine 4 noded isoparametric beam elements with 6 degrees of freedom at each node and used constraint equations to tie the parts together. The results obtained in the present study are in good agreement with the results obtained by Bathe and Wiener (1983).

9.2 Large deflection analysis of a circular bend

The response of a cantilever 45-degree bend subjected to a concentrated end load is calculated. The bend is modelled with eight straight linear elements and the total force, 7.2 EI/R^2, is divided into 10, 20 or 60 equal load increments. The pure load controlled Newton method is used to solve the nonlinear equations of equilibrium. The load-tip deflection curves are shown in Figure 9.6, when 20 equal load increments are used. In the figure also the results from calculation with 8 beam-column elements, Virtanen and Mikkola (1985), is presented. They agree well with the present results. Calculated tip deflections are compared to those reported in Bathe and Bolourchi (1979), Simo and Vu-Quoc (1986), Dvorkin et al. (1988), Surana and Sorem (1989) and Sandhu et al. (1990) in Table 9.1.

Performance of the convergence of the iterative solution procedure is significantly improved when the nonlinear shear terms are omitted, which is usually done in the nonlinear analyses of planar frames. In 3-D problems the nonlinear shear terms are required especially in lateral buckling problems. When the load is divided into 10 increments the solution diverge after the first converged load step if the nonlinear shear terms are included, but if they are omitted 4 to 8 stiffness matrix evaluations per increment are needeed to obtain converged solution. In the analysis with the smallest load increment (60 steps) 3 to 4 stiffness matrix evaluations per load step are needed when the nonlinear shear terms are included and only 3 when they are omitted

9.3 Instability analysis of a shallow hexagonal frame

Snap-through instability characterizes the large deformation behaviour of a shallow hexagonal dome under a point load shown in Figure 9.7a. The experimental limit load from a plexiglas model frame is 251 N, Chu and Rampetsreiter (1973). The same frame has also been analysed in References Connor et al. (1968),

Table 9.1 Comparison of tip deflections of a circular bend.

	NEL	shape f.	$NINC$	$-u/R$	$-v/R$	w/R
present	8	linear	10	0.135	0.231	0.533
present	8	linear	20	0.137	0.230	0.533
present	8	linear	60	0.137	0.229	0.532
Bathe and Bolourchi	8	cubic	60	0.134	0.235	0.534
Simo and Vu-Quoc	8	linear	3	0.135	0.235	0.534
Cardona and Geradin	8	linear	6	0.138	0.237	0.535
Dvorkin et al.	5	parabolic	10	0.136	0.235	0.533
Surana and Sorem	8	parabolic	7	0.133	0.230	0.530
Sandhu et al.	8	linear	3	0.134	0.234	0.533

NEL : number of elements
$NINC$: number of load steps

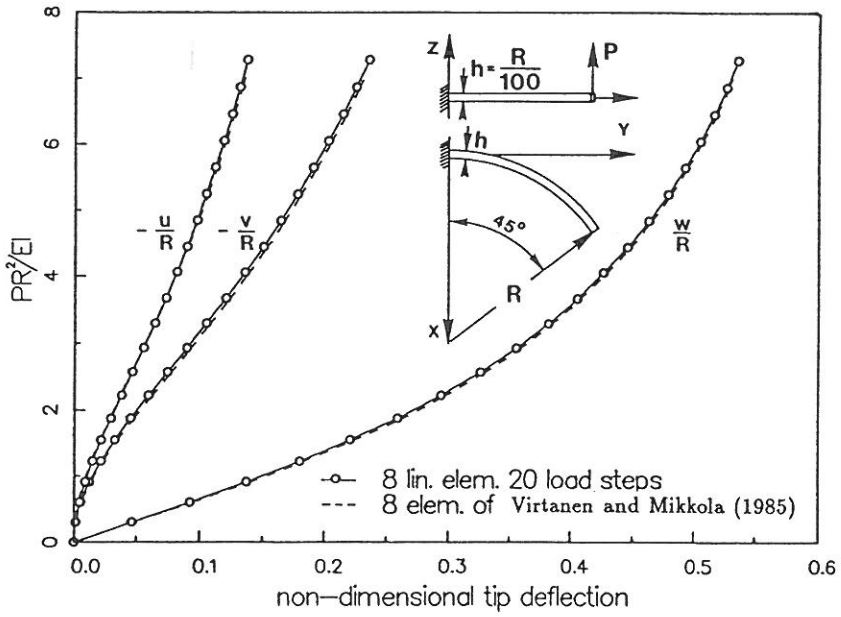

Figure 9.6 Large deflection analysis of a circular bend.

Papadrakakis (1981), Meek and Tan (1984), Virtanen and Mikkola (1985), Nee and Haldar (1988) and Chan (1988). Comparisons with other results have been made in Table 9.2.

If the vertical supports are not free to move in the horizontal direction, bifurcation occurs in the equilibrium path before the limit point. Due to the

symmetry the multiplicity of the critical point is two. In order to follow the post-critical equilibrium path, a symmetry condition has to be chosen. In the present calculations the rotation of the apex about the direction of the point load and one horizontal displacement component are restrained. In figure 9.7b the load-deflection curves are shown. Using four elements per a member and the initial load step of 50 kN, the bifurcation load, 358 kN, is reached after 14 load steps. If the horizontal deflections and the rotation about the vertical axis are restrained, the symmetric deformation mode has a fold point at load level 373 kN This is considerably lower value than the one obtained by Meek and Tan 415 kN, but is quite close to the result obtained by Hasegawa et al. (1987a), 365 kN, or by Nee and Haldar 380 kN. Hasegawa et al. have used 16 elements for one sixth of the dome. This problem is not particularly tricky for the continuation algorithm. When analysing the symmetric deformation mode the modified Newton-Raphson scheme (2-3 corrector iterations per load increment) can be used through the whole equilibrium path shown in the Figures 9.7a and 9.7b. Only near the bifurcation point in the post buckling regime the full Newton method was required to archive convergence.

Table 9.2 Comparison of limit loads.

	NEL	element type	ΔP_0/kN	P_{cr}/kN	
experimental				251	
present anal.	4	linear Tim.	50	260	
present anal.	8	linear Tim.	50	253	
present anal.	4	cubic E-B	50	253	
Chu and Rampetsreiter		BC-element		270	
Papadrakakis	4	BC-element		253	(*)
Meek and Tan	1	cubic E-B		277	(*)
Virtanen and Mikkola	1	BC-element	50	253	
Nee and Haldar		cubic E-B	50	247	(*)
Chan	2	BC-element		264	(*)

NEL : number of elements per a member
$NINC$: number of load steps
(*) measured from figure

9.4 Instability analysis of a framed dome

The static responce of a framed dome shown in Figure 9.8 is analysed. Two

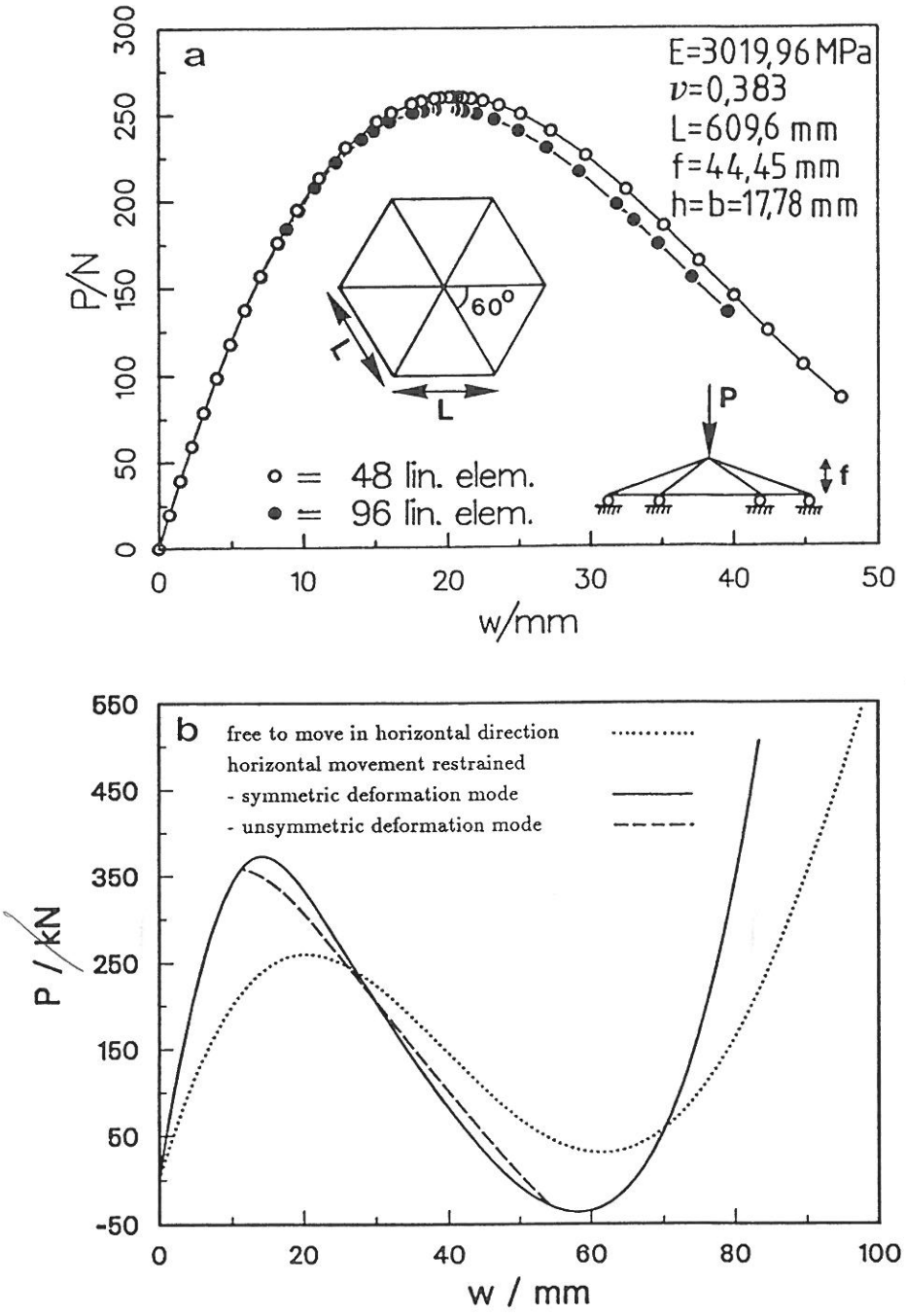

Figure 9.7 Load-vertical deflection of the apex of a shallow dome.

different loading conditions are considered. The first loading system consists of concentrated vertical loads of equal magnitude placed at the crown and at the end points of the horizontal members, while the second loading type is a single concentrated load at the crown point. This dome has been analysed also by Chu and Rampetsreiter (1972), Remseth (1979) and Shi and Atluri (1988). The dome is modelled using 90 linear Timoshenko beam elements i.e. five elements for each member. No symmetry conditions are used.

In the first loading case bifurcation occurs at the load level of 18.2 MN,

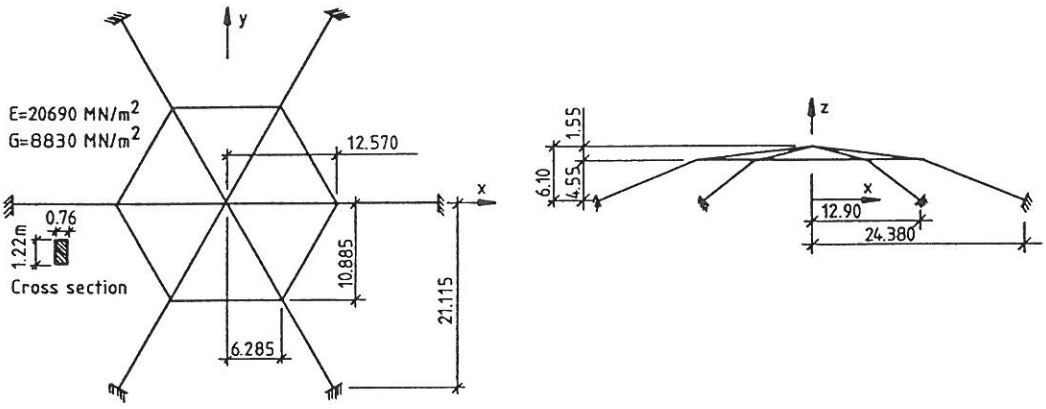

Figure 9.8 Framed dome.

which is quite close to the value (18.0 MN) given by Chu and Rampersreiter. The buckling mode is a rotational mode about z-axis, see Figure 9.9. Shi and Atluri have possibly used some symmetry conditions or their finite element mesh is too crude to describe the lowest buckling mode. In their calculations only one element per a member has been used, and so the vertical displacement of the crown point starts to increase rapidly after reaching the load value 55 MN. The resulting load-displacement curve from the present calculation is in Figure 9.9.

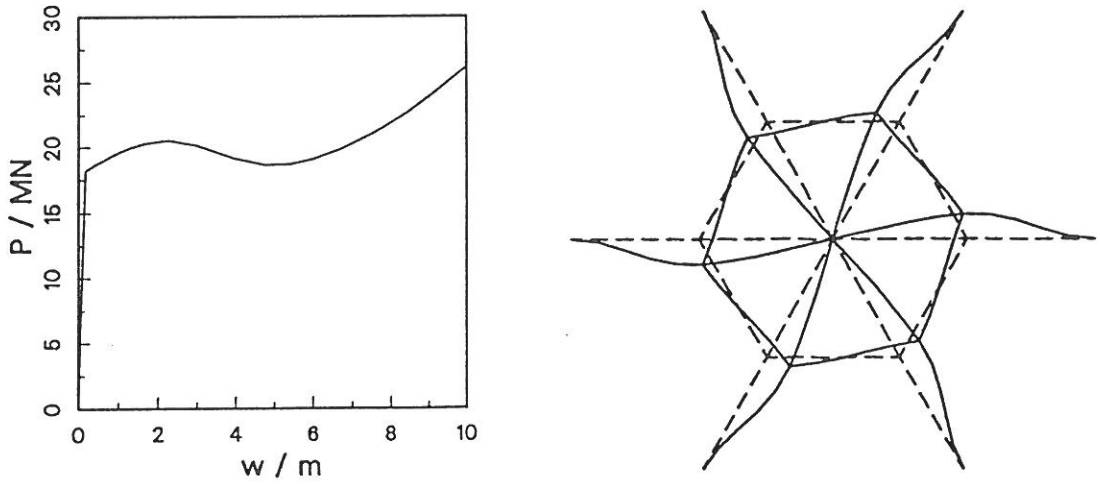

Figure 9.9 Framed dome, vertical displacement of the apex vs. load and the rotational buckling mode.

In the second loading case a branching point with the rotational buckling mode is noticed at the load value of 78.6 MN. Remseth has also studied this loading type but his results differ significantly from the present ones. The results of the present calculations are quite similar to the results obtained by Shi and Atluri, however, they have not noticed the bifurcation point. Load deflection

curve from the unstable symmetric deformation mode is drawn with dashed line in Figure 9.10. The result from the computation of the symmetric deformation mode is in good agreement with Shi's and Atluri's result.

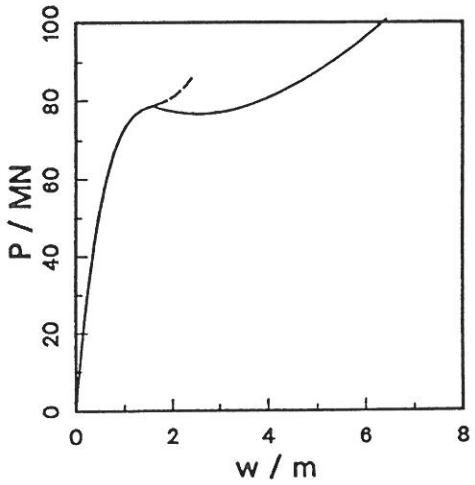

Figure 9.10 Load-displacement curve of a framed dome when a concentrated load alone acts at the crown point.

9.5 Tezcan's frame

A high frame, shown in Figure 9.11 is analysed. The behaviour of the same frame has also been studied by Tezcan and Mahapatra (1969) and Virtanen and Mikkola (1985). The frame is modelled using 72 linear Timoshenko beam elements (eight elements for a column and four for a beam). The values of 206 GPa and 0.25 for Young's modulus and Poisson's ratio are used.

In the present computation a bifurcation point occurred at the load level of 1235 kN, which is not noticed in the other studies. The post buckling behaviour contains the rotational mode about the vertical axis (z-axis) and also small horizontal deflections in the x-axis direction, however, the determination of the post-buckling behaviour did not succeed. Preventing the displacement in y-axis direction and the rotation about z-axis, the equilibrium path shown in Figure 9.12 is computed. During the load step between the load values of 1348 kN and 1507 kN two eigenvalues became negative. The bifurcation condition (8.24) is not satisfied and the computation is continued onto the basic path. Despite of the existence of negative eigenvalues the load-deflection curve is increasing. The load-deflection curve deviates significantly from the one obtained by Tezcan and Mahapatra but is qualitatively similar to the result presented by Virtanen and Mikkola. In those analyses a coarse mesh in which only one element per a member is used. If the problem is analysed using two elements per a member (Virtanen and Mikkola beam-column element) the result seems to converge to that of present analysis.

(a)

(b)

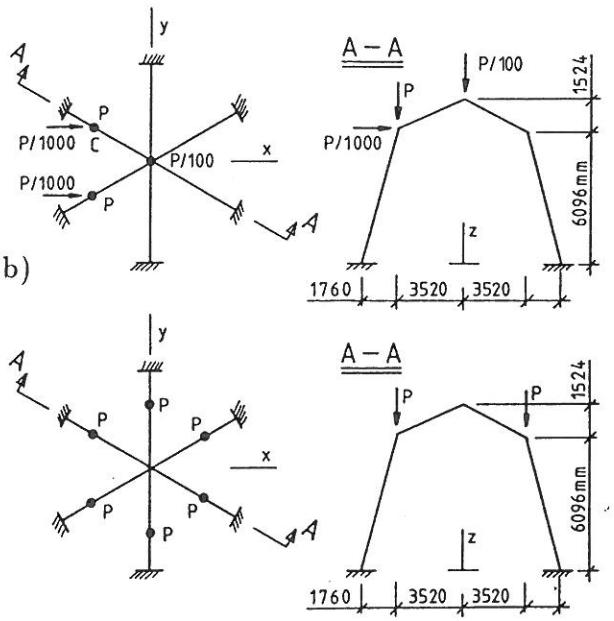

	columns	beams
A / 10^3 mm^2	22.806	11.006
I_t / 10^6 mm^4	5.4651	1.4027
I_y / 10^6 mm^4	143.64	31.176
I_z / 10^6 mm^4	446.88	94.776

Figure 9.11 Geometry and loadings of the Tezcan's frame: (a) unsymmetric loading case analysed in the present study and by Tezcan and Mahapatra (1969) and Virtanen and Mikkola (1985), (b) symmetric loading case analysed in the present study.

The deflected shape of the frame at the load level of 1960 kN is shown in Figure 9.12. It can be seen from the figure that the two colums bearing the vertical loads P buckle.

In the case of symmetric loading, a bifurcation occurred at the load level of 1035 kN, and the post buckling deformation shape was the rotational mode about the vertical axis. The deflected shape of the frame is shown at the load level of 1550 kN in the post buckling regime in Figure 9.13. In this case there is no difficulty in branching onto the secondary path.

9.6 Lateral buckling analysis of cantilever beams

In this section various analyses concerning the behaviour of cantilever beams have been made. First example is a long beam with a narrow solid cross-section ($h/b = 16.129, L/h = 40$). This example has been studied both theoretically and experimentally by Woolcock and Trahair (1974). The lateral displacement-load curves shown in Figure 9.14 are in close agreement with the results of Woolcock and Trahair. The beam is modelled by ten equal Timoshenko beam elements and the initial load increment used is $\Delta P_0 = 0.5\sqrt{EI_y GI_t}/L^2$. The obtained

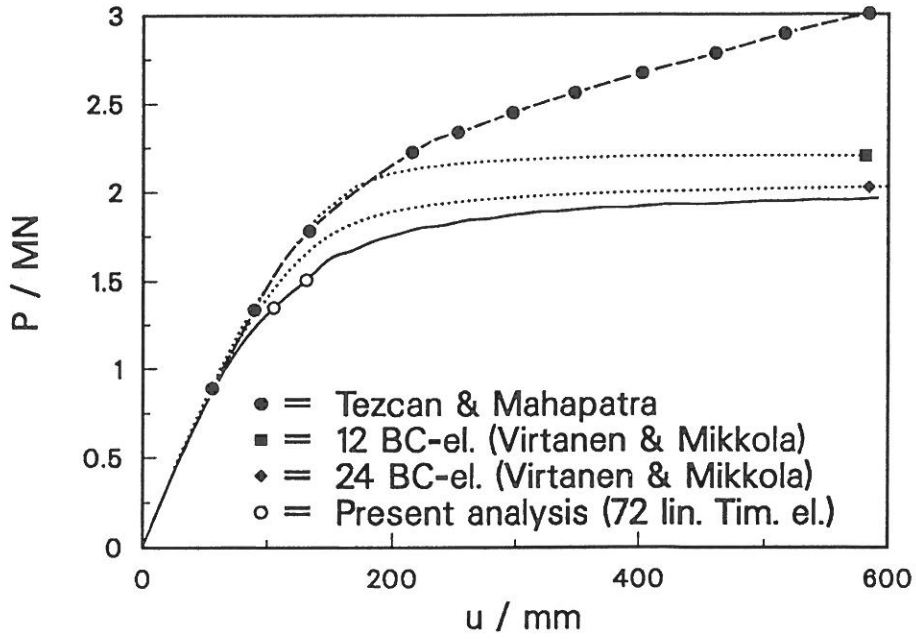

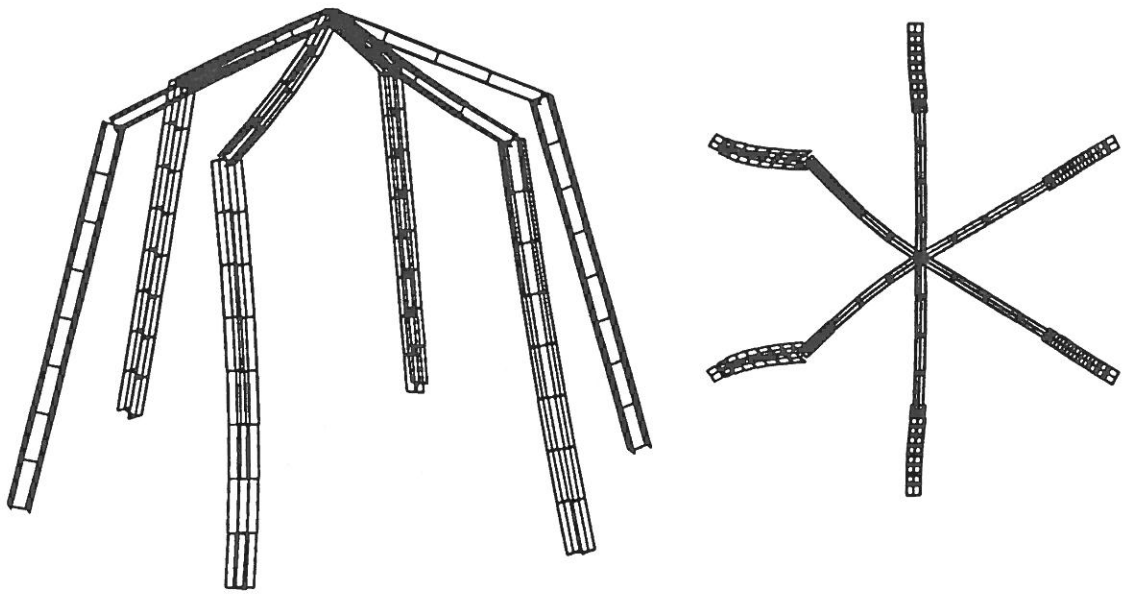

Figure 9.12 Displacement in x-axis direction at the point C vs. load. The blanked circles indicate the load step in which negative eigenvalues are noticed. Deformed shape at load level P=1960 kN

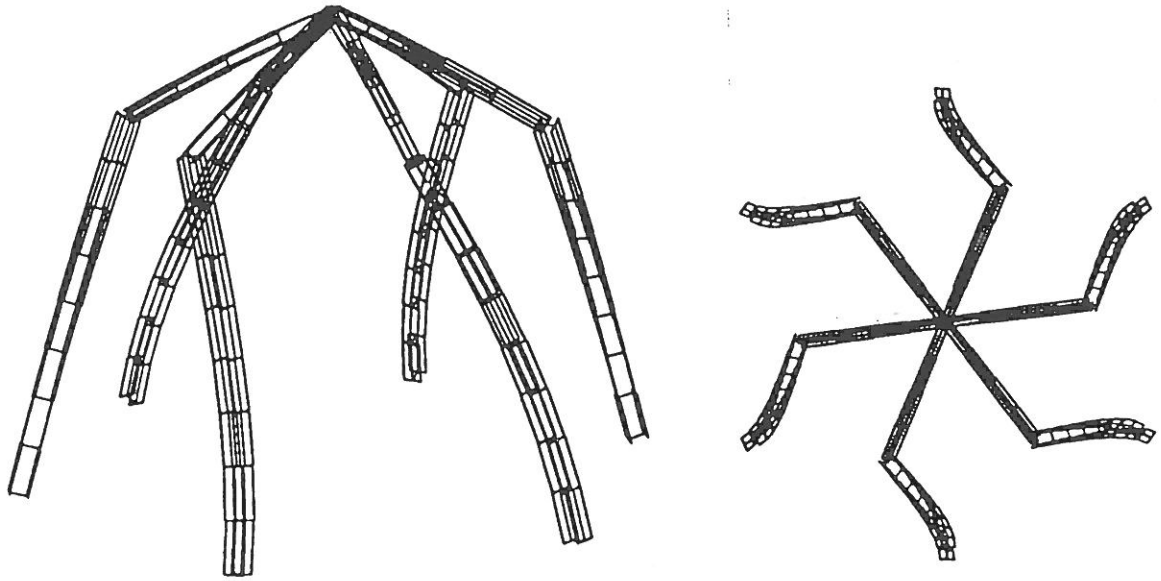

Figure 9.13 Deformed shape at load level P=1550 kN in the symmetric loading case. The rotation of the top point with respect to the vertical axis is 23 degrees.

bifurcation loads are $P_{cr} = 4.085\sqrt{EI_y GI_t}/L^2$ without the effect of the selfweight and $P_{cr} = 3.159\sqrt{EI_y GI_t}/L^2$ including it. As a classical result, without selfweight, the load factor is 4.13, Timoshenko and Gere (1963). The exact critical load including the effect of in plane deformations is 4.036 and when the effect of the selfweight is included it is 3.091, Woolcock and Trahair (1974). †

Elasto-plastic behaviour of a cantilever beam shown in Figure 9.15 is studied. A graded mesh with four elements is used. Polynomial grading is chosen and the parameter β has the value $\beta = 1.4$. The calculations with layered material model description are compared to the results obtained by using different kind of stress-resultant yield functions. Two different values of the yield stress have been used, resulting in different types of post-buckling behaviour. In the first case the yield stress is so high that the yielding starts in the post-buckling regime. In the other one the yield stress is lower and the yielding starts at the pre-buckling

† There are some discrepancies between the data given in Reference Woolcock and Trahair (1974) at page 160 in Tables 1 and 2. If the value of the expression $\sqrt{EI_y GI_t}/L^2$ is calculated from the information given in the section property table, it will be 1.76229 lbf and if it is calculated from the value given to the classical critical load 7.01 lbf (self weight excluded) in the member detail table, it is 7.01 lbf/4.013 = 1.74682 lbf.

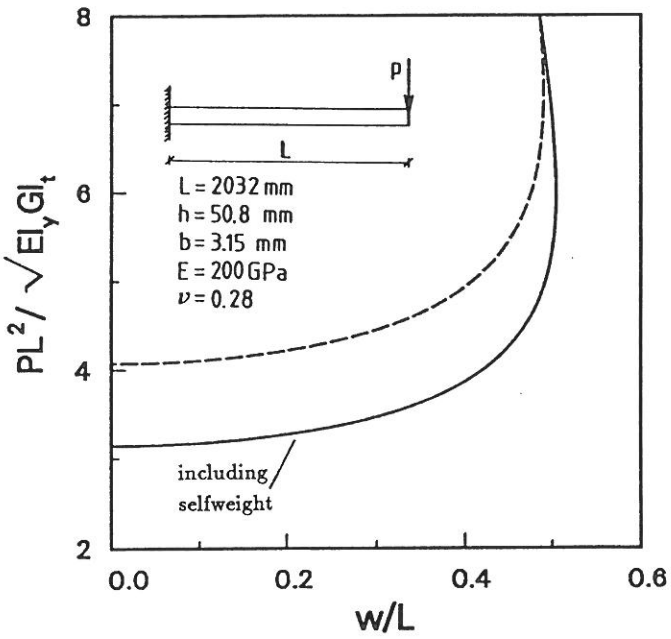

Figure 9.14 Lateral tip deflections of a narrow rectangular cantilever

state so lowering the buckling load. In the computations with layered model seven quadrature points are used in the height direction of the cross-section, and the effect of the number of integration points used over the width direction is investigated. From Figure 9.15 it can be concluded that the Simpson's rule with three points in the width direction yields considerably different result compared to the use of higherorder quadratures. The result obtained from calculation where the 7×3 Gauss quadrature is used has reasonably good accuracy in the plastic post-buckling region. The use of the 7×4 Gauss or the 7×5 Simpson's rules, or higher ones, yield almost identical results. The use of the hypercube yield function differs greatly from the other calculations when the smaller yield stress value is used. In this case there are no excess of lateral displacements, so the collapse enters before lateral buckling.

Figure 9.16 shows a load-deflection curve is shown from an analysis of a cantilever beam loaded by a concentrated load at the free end. The load is placed either on the top or on the bottom point of the cross-section. Timoshenko and Gere (1963) give the approximative formula for calculating the critical load

$$P_{cr} = 4.013\frac{\sqrt{EI_yGI_t}}{L^2}(1 \mp \frac{a}{L}\sqrt{\frac{EI_y}{GI_t}}). \tag{9.4}$$

In this formula a denotes the distance of the point of application of the load vertically from the centroid. If the point of application of the load is above the centroid the minus sign is chosen. Table 9.3 shows the bifurcation loads obtained from an analysis using ten equal Timoshenko beam elements. The length of the

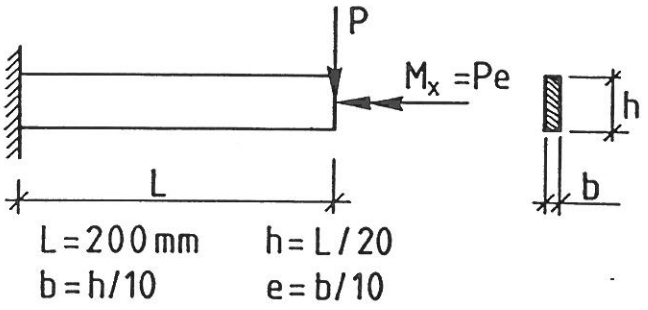

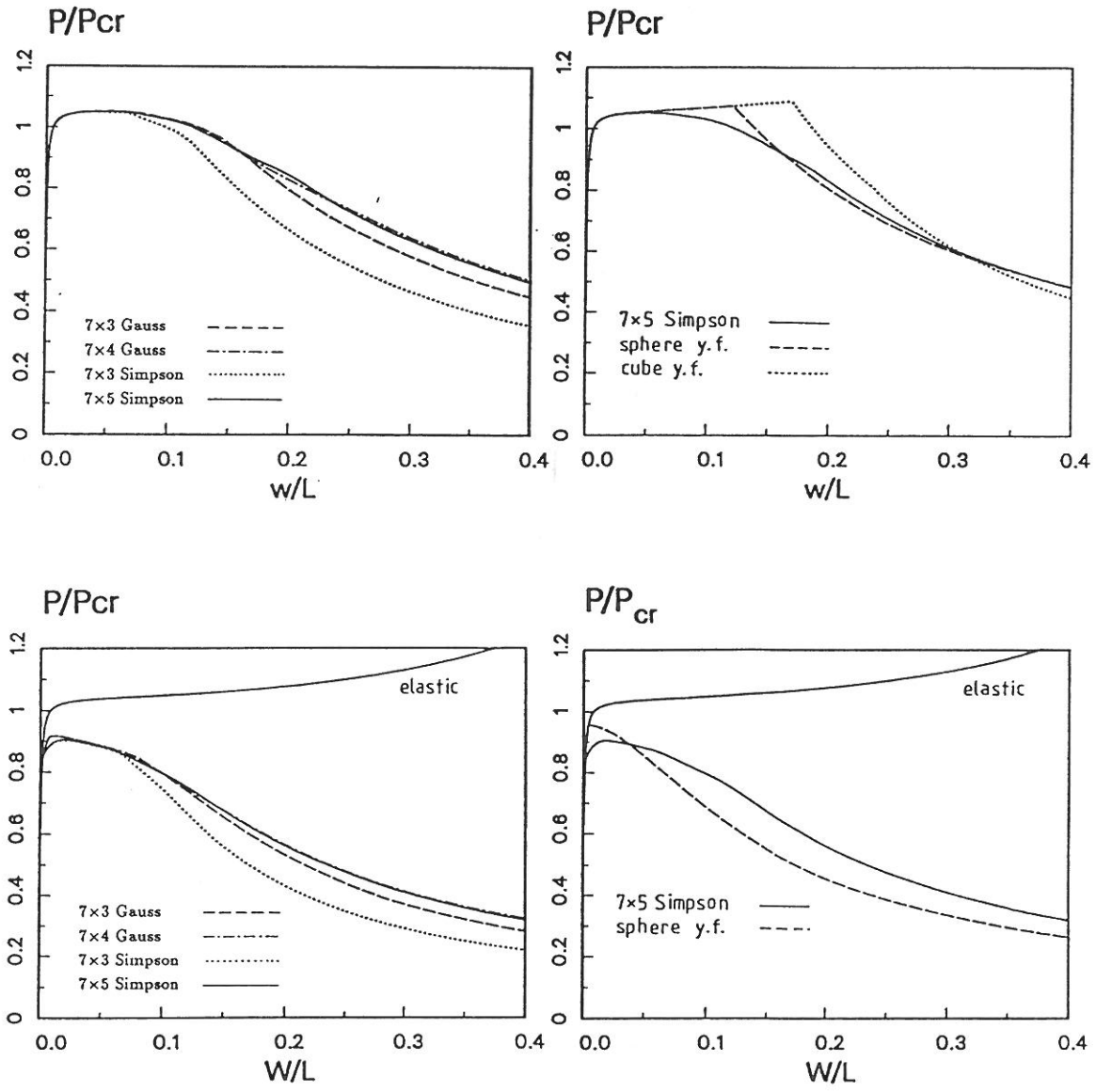

Figure 9.15 Lateral tip deflections vs. load of a cantilever beam when elasto-plastic material model is used. The material constants used are $E = 210$ GPa, $\nu = 0.3$, $E_t = 0$ and $\sigma_y = 250$ MPa in (a) and (b), $\sigma_y = 150$ MPa in (c) and (d).

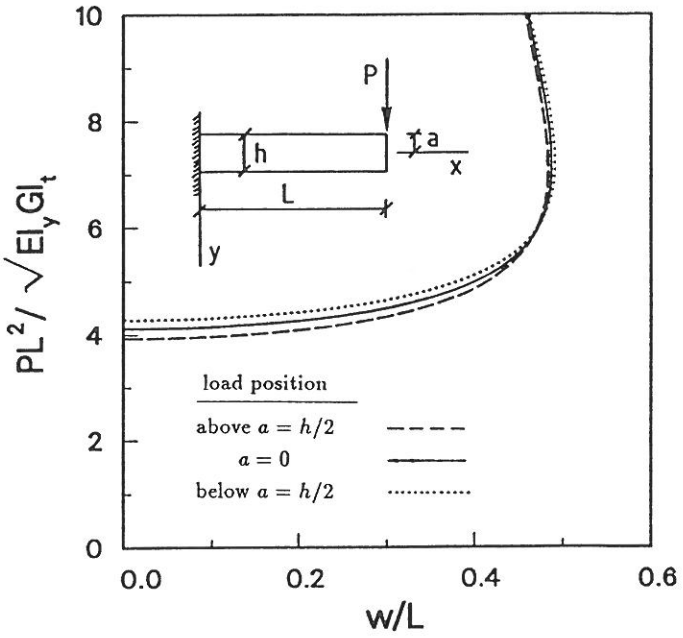

Figure 9.16 Lateral deflection vs. load of a cantilever beam.

Table 9.3 Critical load parameter λ_{cr} for a cantilever beam.
$P_{cr} = \lambda_{cr}\sqrt{EI_y GI_t}/L^2$

load position	Equation (9.4)	10 Tim. elem.
above $a = h/2$	3.846	3.913
$a = 0$	4.013	4.124
below $a = h/2$	4.180	4.294

beam is L=100 mm, height h=10 mm and width b=1 mm. The in plane tip displacement prior buckling is about 16-17 % of the height of the beam.

Lateral buckling analysis of a cantilever right-angle frame under end load is performed. This problem has also been analyzed by Argyris et al. (1979) and Simo et Vu-Quoc (1986). The geometric characteristics of the beam and the lateral displacement vs. load are shown in Figure 9.17. A constant perturbation load of 10^{-3} N has been used in computing the post buckling behaviour. The buckling load in the present calculation seems to be about 5 % lower than the values obtained by the references mentioned above.

9.7 Elastic lateral buckling analysis of a simply supported beam

The lateral buckling load of a simply supported beam in pure bending is calculated. The accuracy of the critical load obtained with different finite elements is studied.

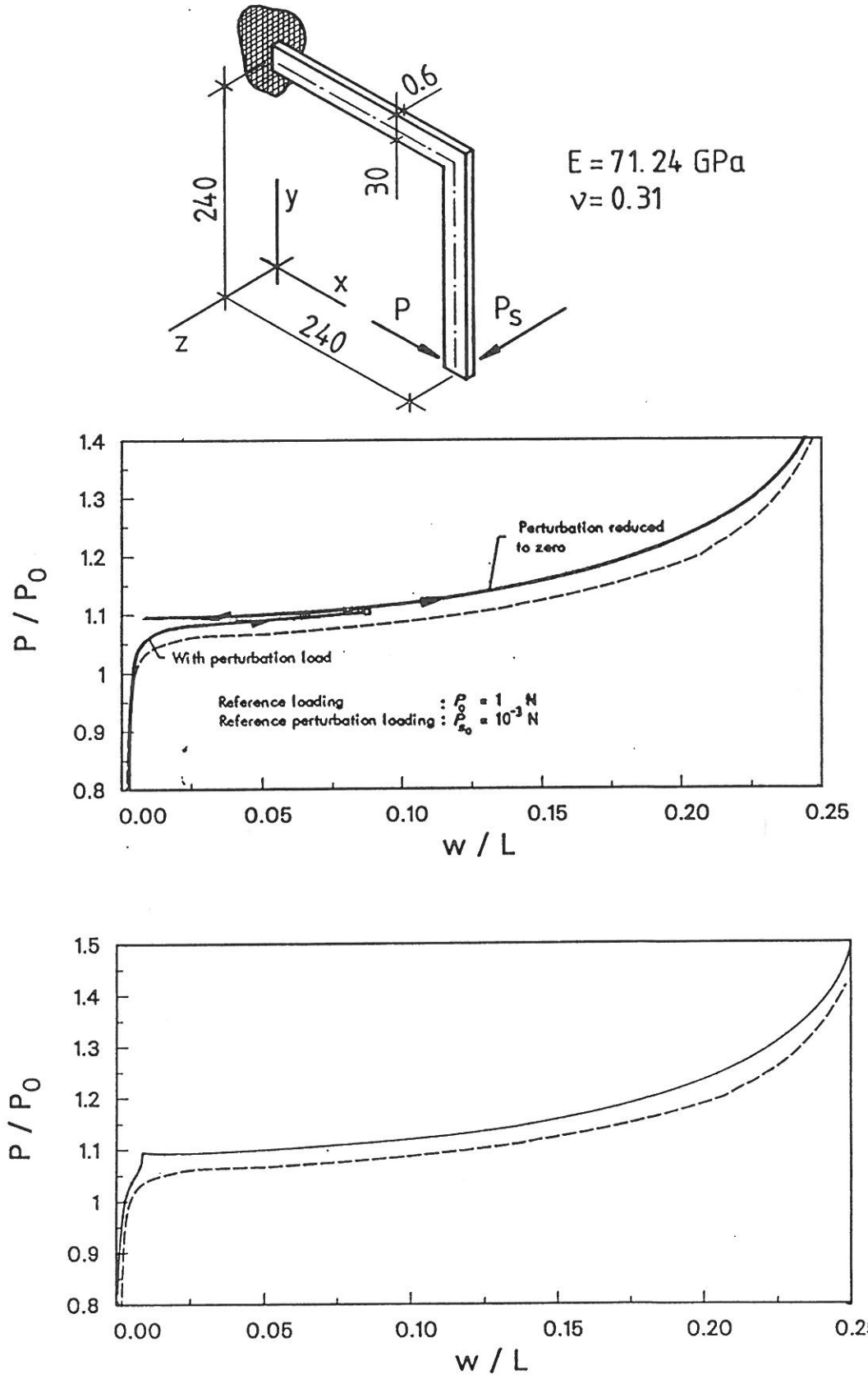

Figure 9.17 Lateral buckling of a cantilever right-angle frame. Result from the present analysis is shown by dashed line, comparison to the computations done by (a) Argyris et al. (1979) and (b) Simo et Vu-Quoc (1986).

The expression for the critical moment

$$M_{cr} = \frac{\pi}{L} \frac{\sqrt{EI_y GI_t}}{\sqrt{(1 - I_y/I_z)(1 - GI_t/EI_z)}} \tag{9.5}$$

is given by Trahair and Woolcock (1973) and by Van Erp (1989). This formula includes the effects of moderate pre-buckling deflections of the magnitude of beam height.

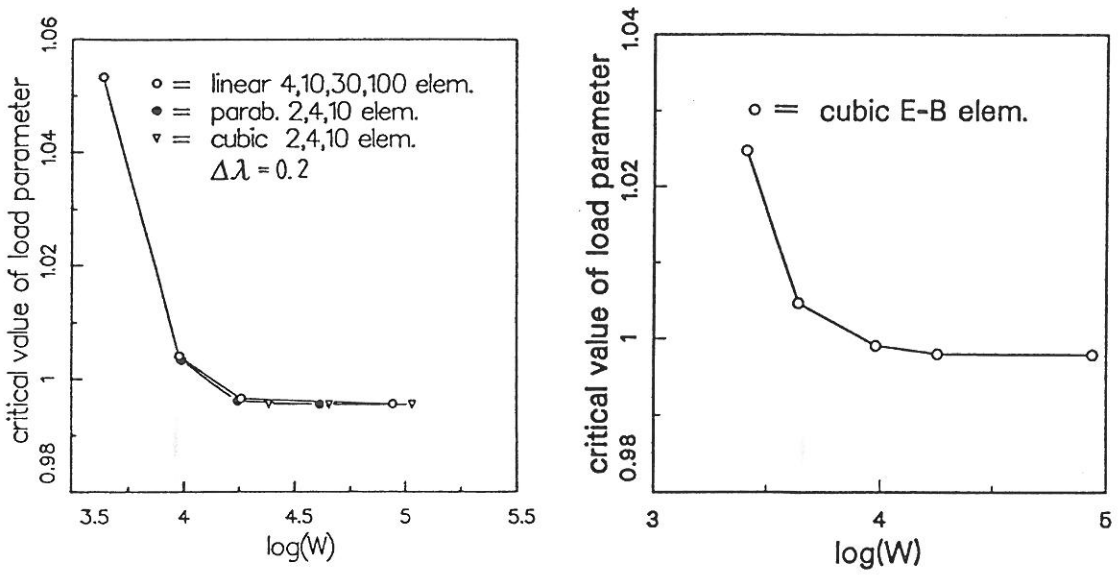

Figure 9.18 Convergence of the critical moment, a) Timoshenko- b) Euler-Bernoulli beam elements. Note the diffrent scale in the vertical axis.

The Timoshenko beam elements compared are a linear isoparametric one, a subparametric parabolic and a cubic element, which have two, three or four nodes, respectively. In the subparametric elements the geometry of an element is interpolated by linear shape functions. Figure 9.18a shows the convergence of the critical load as a function of computational work $W = nm_k^2$, where n is the number of degrees of freedom and m_k is the half bandwidth (including the diagonal term) of the stiffness matrix. The load parameter value 1 corresponds to the critical moment M_{cr}. The increment of load parameter used has been $\Delta\lambda = 0.2$. The critical moments obtained using different elements converge to smaller values than the value M_{cr} defined in Equation (9.5). This is due to the effect of shear deformations which are not allowed for in Equation (9.5).

Results from a convergence study using the Euler-Bernoulli beam element are shown in Figure 9.18b. Also in these calculations the critical moment converges to

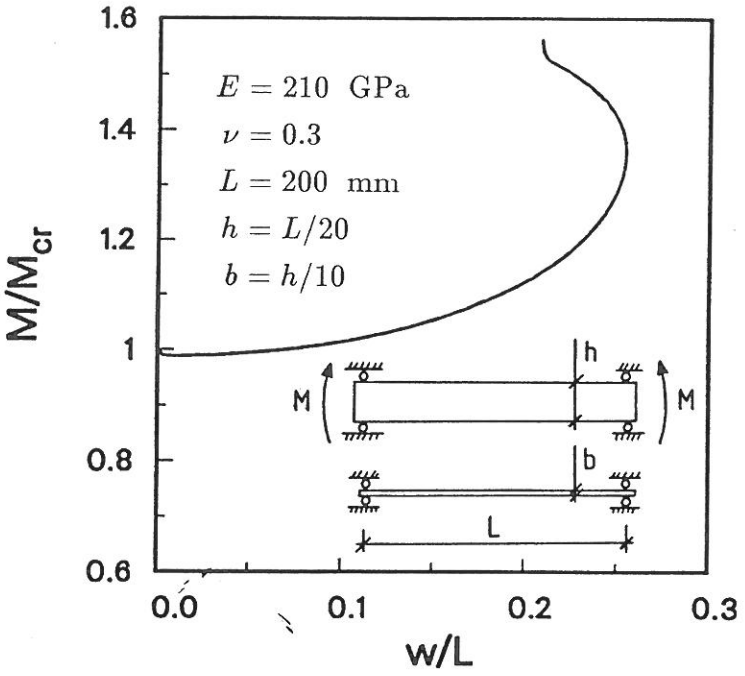

Figure 9.19 Lateral deflections of the midpoint of the beam vs. load from a large deflection post-buckling analysis of a simply supported beam in pure bending. Solid curve indicates the calculation when thirty equal Timoshenko beam elements is used. Dotted line indicates result from the calculation when the Euler-Bernoulli beam theory element is used (almost identical).

a smaller value (100 elements $\lambda_{cr} = 0.9979$) compared to the value obtained from Equation (9.5).

In addition, the post-buckling behaviour is determined. The computed equilibrium paths are shown in Figure 9.19, where the out of plane displacement of the midpoint of the beam are drawn.

9.8 Lateral buckling analysis of redundant beams

Masur and Milbrandt (1957) studied the post-buckling behaviour of elastic redundant beams both theoretically and experimentally. They have used theory of moderately large deflections which is analogous to the von Karman theory of plates, where the curvatures are approximated by linear expressions, but a second-order term in the axial strain is included. The behaviour of redundant and statically determinate beams in the post-buckling state is different due to the moment redistribution. Masur and Milbrandt found, that the redistribution of bending moments is accompanied by an increase in the external load magnitude, which approaches a limiting value as the lateral deformation increases.

Finite element analyses of simple redundant beams have been made. In the first example a doubly redundant beam is analysed. The ends are pinned in the

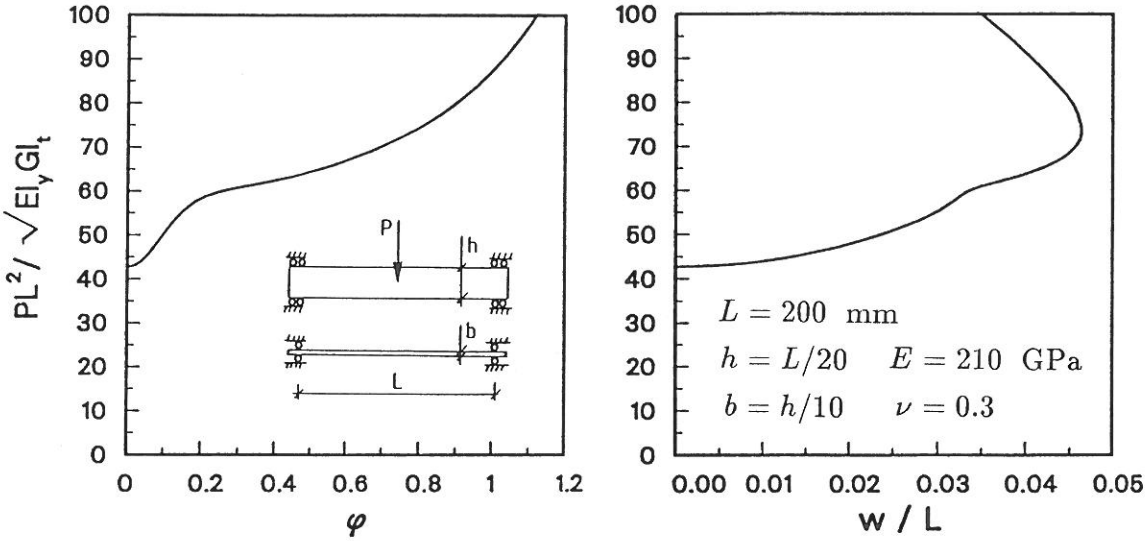

Figure 9.20 Lateral buckling analysis of a doubly redundant beam. The rotation about the axis of the beam (on the left hand side) and the lateral deflection at the midspan (on the right hand side) vs. load are shown.

lateral direction but fixed in the vertical plane. A concentrated load acts at the midspan. A finite element mesh with ten equal Timoshenko beam elements is used for a half of the beam. The buckling load obtained is 42.67 $\sqrt{EI_yGI_t}/L^2$, and the post-buckling behaviour is qualitatively in agreement with the results of Masur and Milbrandt. About 80 load steps are used in the computation of the deformation path, shown in Figure 9.20. The initial load step has the value 5 $\sqrt{EI_yGI_t}/L^2$.

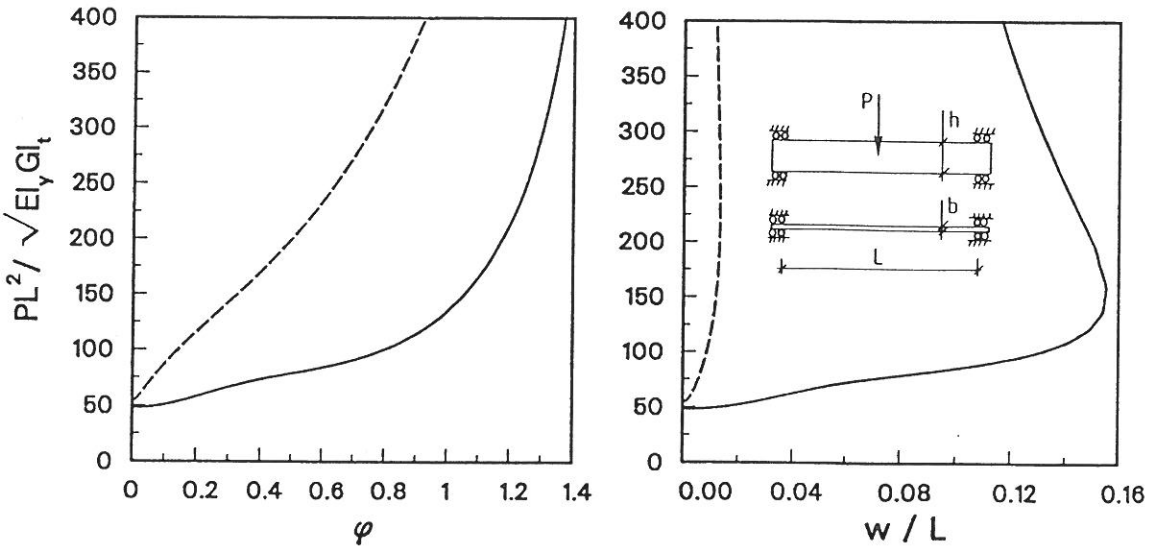

Figure 9.21 Lateral buckling analysis of a clamped beam. The rotation about the axis of the beam (on the left hand side) and the lateral deflection at the midpoint vs. load (on the right hand side) are shown. Dashed line indicates calculation of a beam with fully fixed ends.

Also a beam with clamped ends in both principal directions is analysed. Bifurcation occurs at the load value of 47.83 $\sqrt{EI_y GI_t}/L^2$, and the behaviour is similar compared to the one of the doubly redundant beam. Starting with load increment 10 $\sqrt{EI_y GI_t}/L^2$, 100 steps are required to follow the equilibrium path shown in Figure 9.21. An analysis of a beam with fully built in ends, i.e. with prevented axial displacement, is also performed. In the analysis the critical load obtained is 54.61 $\sqrt{EI_y GI_t}/L^2$. The corresponding load deflection curves are marked in Figure 9.21 by dashed lines.

9.9 Lateral buckling of a space truss

Lateral buckling of a roof truss with a span of 20 m is studied. The geometry and loading conditions are shown in Figure 9.22. The behaviour of the truss with two different types of lateral supports and boundary conditions have been compared. The lateral supports consist of slender beams the ends of which are free to move in the vertical direction but constrained in the $x-y$ plane. The slope of the buckling supports in the x-axis direction is also prevented (boundary conditions I). In the other set of boundary conditions the lateral supports are constrained only in y-axis direction (boundary conditions II). The first model has lateral supports only in the upper chord of the truss and the other (model 2) one lateral support at the midpoint of the lower chord. Linear Timoshenko beam elements are used to model the structure and the meshes consist of 245 and 255 elements, respectively.

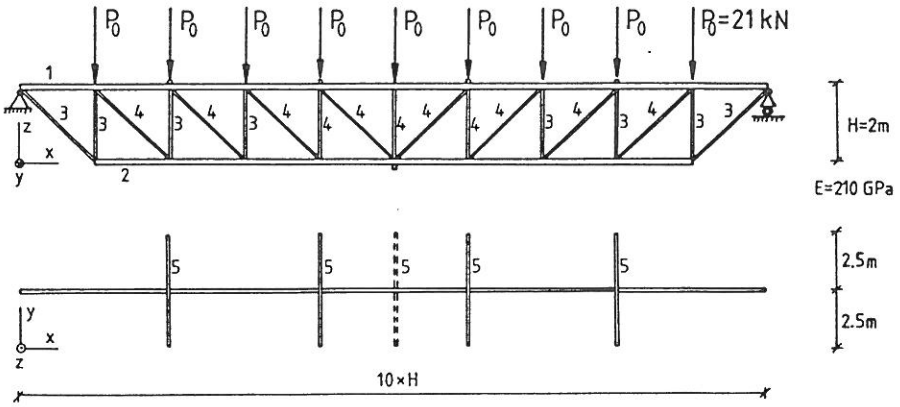

	1	2	3	4	5
$10^4 A$ / m^2	23.1	18.1	11.8	8.55	7.4
$10^6 I_t$ / m^4	8.12	4.42	1.56	0.73	0.07
$10^6 I_y$ / m^4	3.79	2.66	1.53	0.44	0.7
$10^6 I_z$ / m^4	7.07	2.66	0.69	0.44	0.28

Figure 9.22 Geometry and loading of a roof truss.

As expected, the lateral support in the lower chord has practically no influence to the behaviour of the truss. The buckling loads obtained are 3.44 P_0 (model 1), 3.45 P_0 (model 2) and the post-buckling behaviour is stable for both models. In analysing the second model, a load increment of very small size is needeed to get converged solution in the post-buckling regime, and the equilibrium path shown in Figure 9.23 is followed using about 80 load steps. In the case of boundary conditions II, the buckling load is 2.80 P_0 for both models. The initial load step is $0.5P_0$ and the solution diverges after 14 load steps at the load value of 3.23 P_0. In the first model, the buckling mode is dominated by the rigid body rotation of the truss, since the lateral bracing does not give good resistance for the rotation mode. However, in the post buckling region the deformations due to the upper chord buckling dominate. In Figure 9.23 the load-displacement curves and in Figure 9.24 the buckling modes for both model 1 and model 2 are shown. Deformed shapes in the post buckling regime are shown in Figure 9.25.

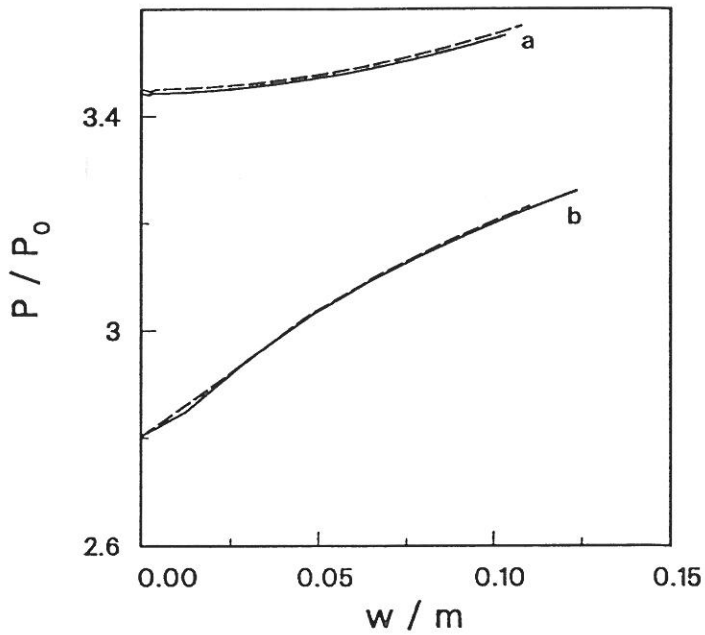

Figure 9.23 Lateral displacement at the midpoint of the upper chord. Results from the computations of model 1 are indicated by solid lines. Dashed lines correspond to model 2. (a) boundary conditions I, (b) boundary conditions II.

9.10 Elasto-plastic lateral buckling analysis of simply supported I-beams

Kitipornchai and Trahair (1975b) have made an experimental investigation of the inelastic flexural-torsional buckling of rolled steel I-beams. Their tests were carried out on full-scale simply supported 261×151 UB 43 beams with central concentrated

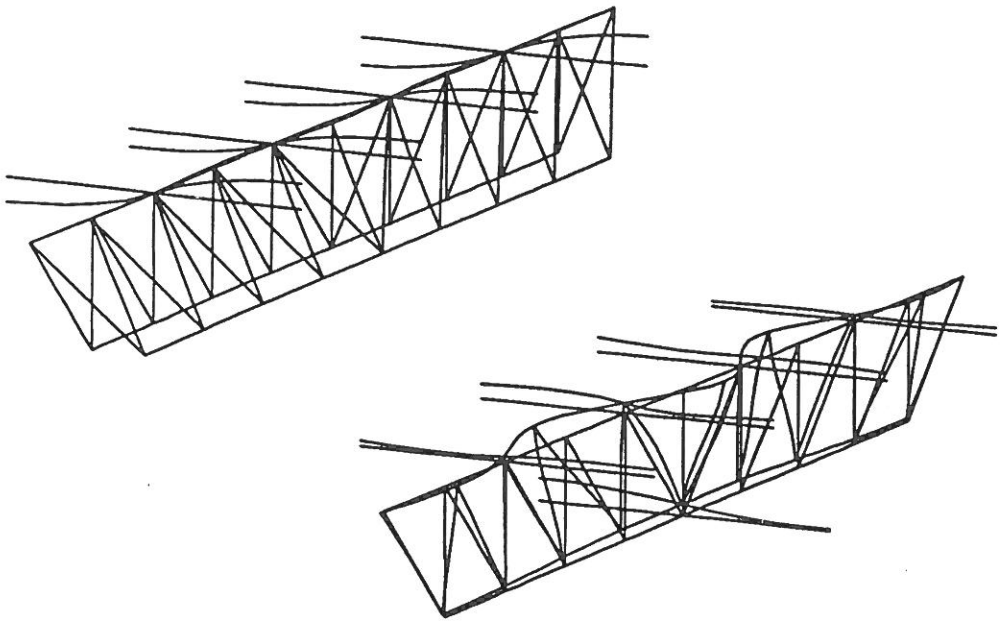

Figure 9.24 Buckling modes, (a) model 1, (b) model 2.

loads applied with a gravity load simulator. The 261×151 UB 43 section has a low ratio between the width and thickness of the flanges and so the beam's behaviour inhibits local buckling and allows lateral buckling to predominate. The end cross-sections of each beam were free to rotate about the major and minor axes and to warp. They tested six beams, four as-rolled and two annealed beams. The effect of residual stresses was not found to be significant which was also confirmed by the theoretical predictions made by Kitipornchai and Trahair (1975a) and by numerical computations in the present study. The reason is in high tensile residual stresses which inhibit the spread of plasticity in the compression flange, see Figure 9.28. The geometrical imperfections were found to be significant in decreasing the load carrying capasity compared to the predictions of the bifurcation loads of perfect structures.

Calculated test beams are chosen to be those which buckled in the inelastic range, i.e. beams S2-10, S3-12 and S4-8 (S = simply supported). The imperfection are included in the loading conditions so, that the point load was situated at a small distance from the middle plane of the beam. The cross-section of the beam 261×151 UB 43, the finite element discretizations used and the residual stress patterns are shown in Figure 9.26. Calculated load-deflection curves are shown in Figure 9.27, and the maximum loads obtained are tabulated in Table 9.4.

9.11 Elasto-plastic lateral buckling analysis of continuous I-beams

Poowannachaikul and Trahair (1975) have made an experimental investigation of the elastic and inelastic lateral buckling of unbraced two-span steel I-beams

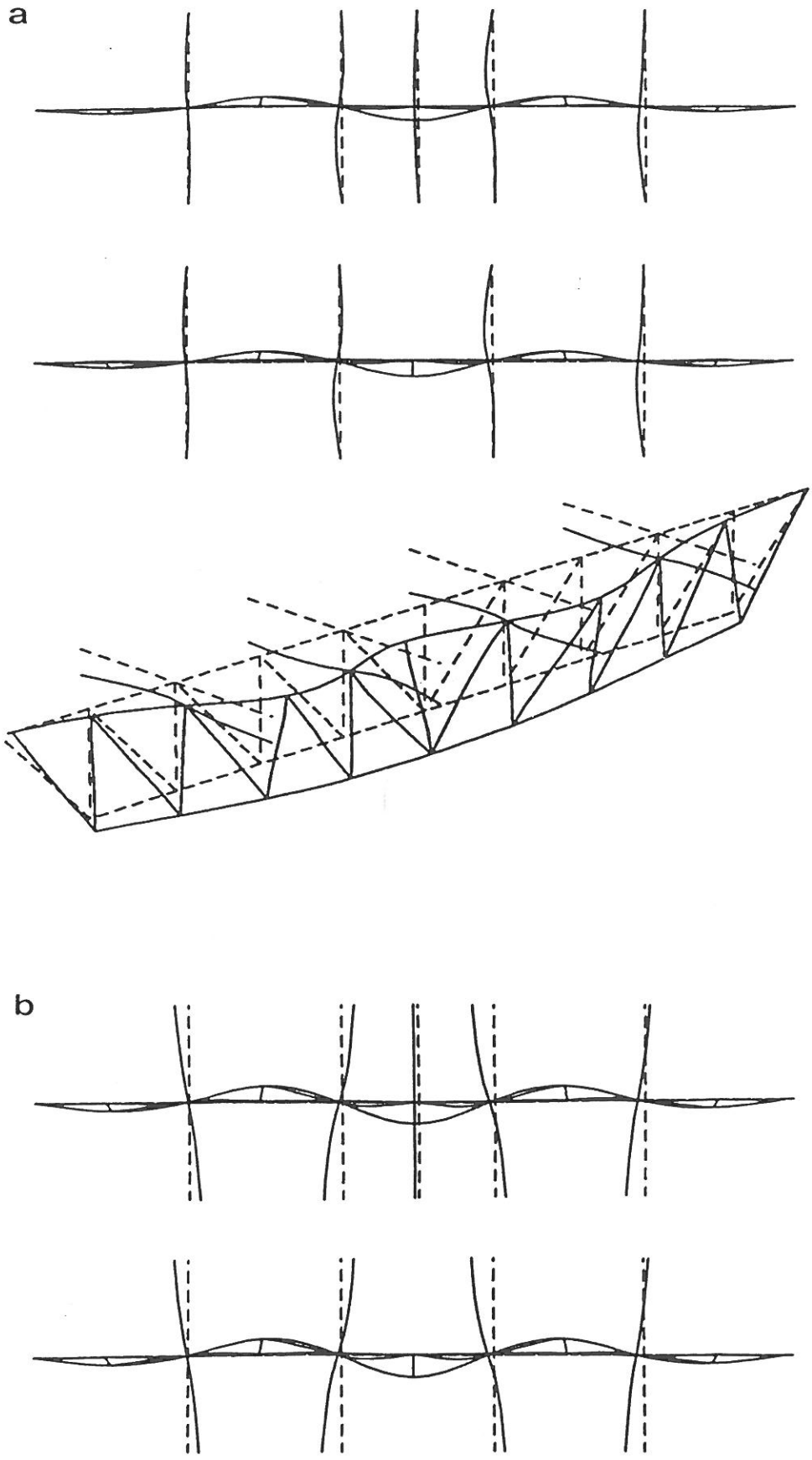

Figure 9.25 Deformed shape, magnified by a factor of 5, in the post buckling regime. (a) at the load value of 3.5 P_0, boundary conditions I. (b) at the load value 3.23 P_0, boundary conditions II.

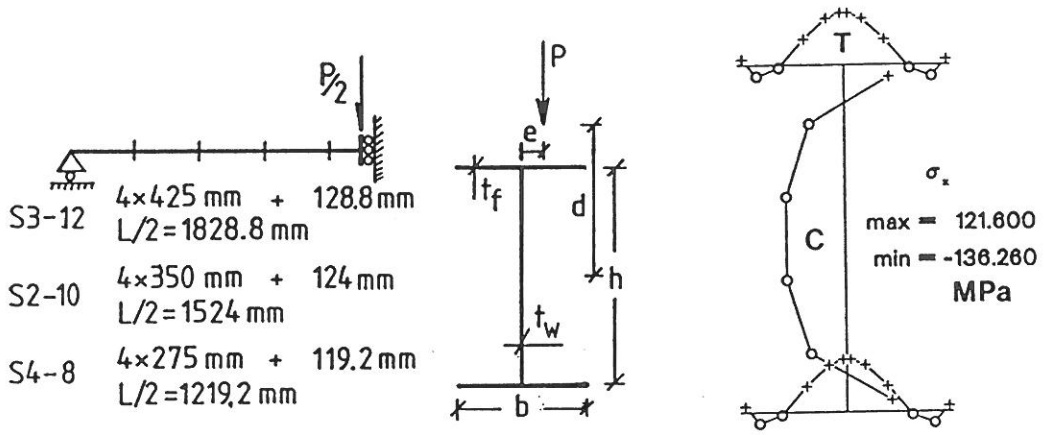

Figure 9.26 Finite element meshes used and the cross-section 261 × 151 UB 43 data: $h = 248.7$ mm, $b = 151.5$ mm, $t_w = 7.67$ mm, $t_f = 12.3$ mm and $d = 219$ mm. Residual stress distribution (quartic polynomials) are the same as by Kitipornchai and Trahair (1975b) (Fig. 7, pp. 1340). $E = 203$ GPa, $E_t = E/35$ (except one calculation for S4-8 beam with $E_t = 0$), $\sigma_Y = 320$ MPa, $\nu = 0.3$.

Table 9.4 Comparison of limit loads

	S3-12	S3-12-R	S2-10	S2-10-R	S4-8
experimental	145.1	140.2	185.1	194.0	235.0
FEM e=0.25 mm	147.9				281.3
FEM e=0.5 mm	144.4				277.8
FEM e=1 mm	139.6				271.4
FEM e=2 mm	134.1	134.9	184.5	185.4	260.4
FEM e=4 mm	126.1				244.1
FEM e=8 mm	114.7				222.3
FEM e=4 mm, $E_t = 0$					241.8

e means the excentrisity of the load position
all the tabulated values are in kN
R in the beam identification indicates the annealed beams,
i.e. there were no residual stresses in the computations

with concentrated loads at midspans. In this study four of the eight beam tests are simulated, i.e. the beams C2-8-12, C3-8-12A, C4-8-12A and C4-8-12B. These beams have the same geometry of the cross-section, material characteristics and residual stress distribution as the beams analysed in the previous chapter.

Theoretical buckling predictions have been presented by Yoshida et al. (1977)

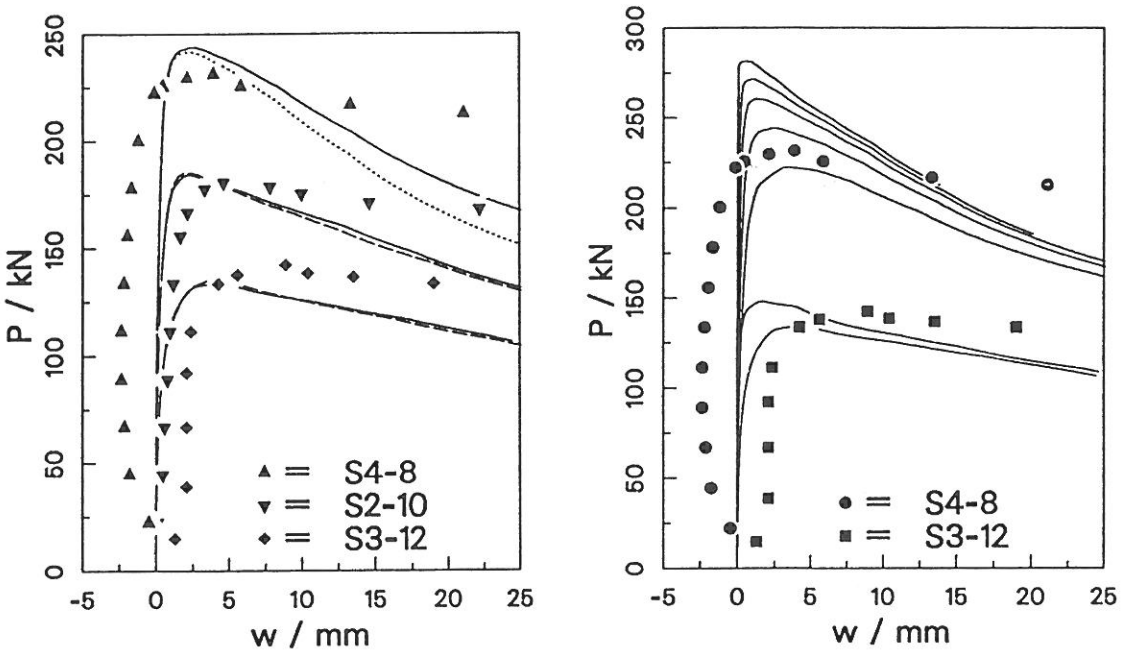

Figure 9.27 Lateral buckling analysis of simply supported beams. Dashed lines indicate calculations without residual stresses and the dotted line (beam S4-8) is the case with no strain hardening ($E_t = 0$, in all other calculations $E_t = E/35$) Calculations with residual stresses are marked with solid lines. Black markers which are not connected correspond to the experimental measurements. Imperfections in the FE calculations in the figure on the left hand side are: S4-8 $e = 4$ mm, S2-10 and S3-12 $e = 2$ mm; and in the figure on the right hand side: S4-8 $e = 0.25, 1, 2, 4, 8$ mm and S3-12 $e = 0.25$, 2 mm.

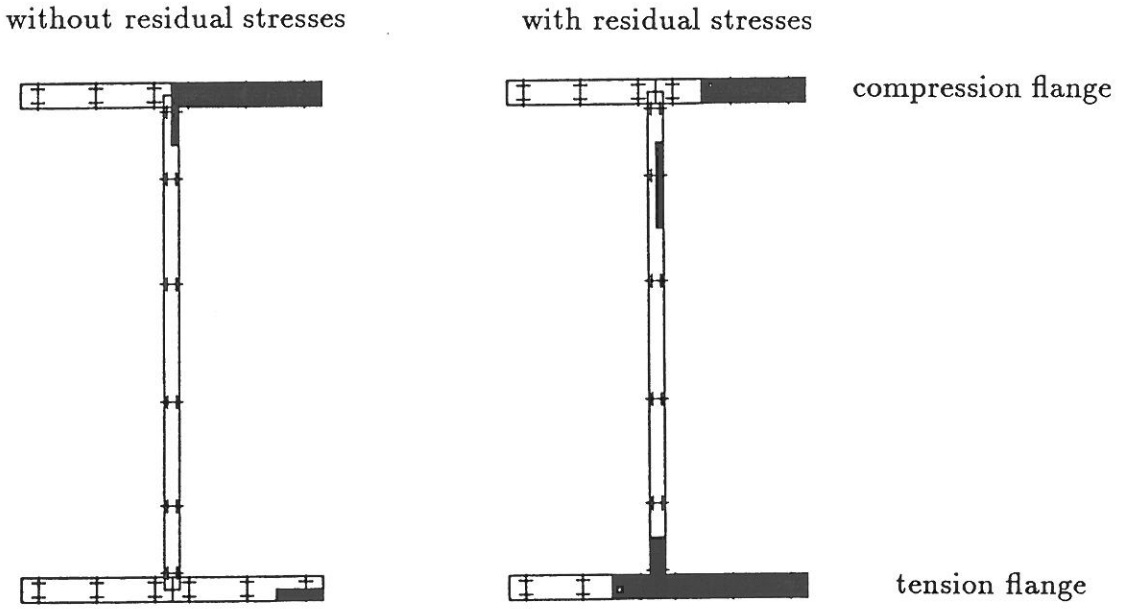

Figure 9.28 Plastic area of the cross-section at the integration point nearest the symmetry plane, beam S4-8 ($e = 4$ mm) at load level 240 kN.

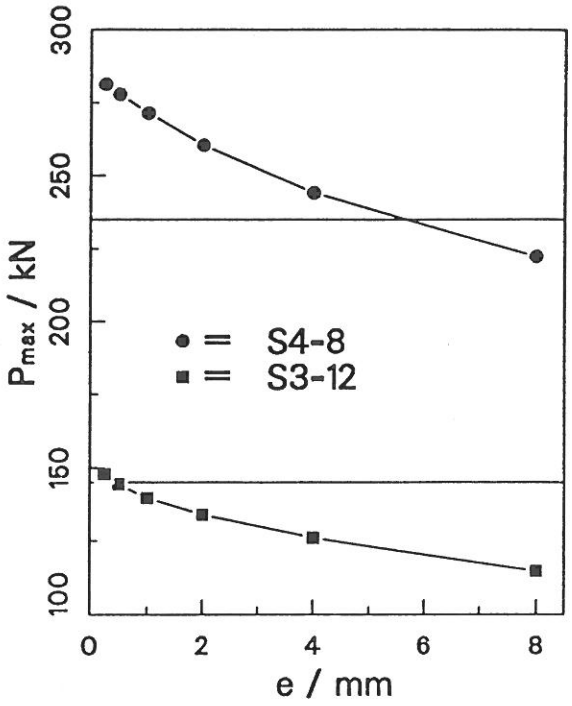

Figure 9.29 Imperfection sensitivity of simply supported elasto-plastic beams.

and Trahair (1983). The experimental results of the buckling load are much lower, for some beams over 20 %, compared to the theoretical buckling predictions. As mentioned by Trahair (1983) no satisfactory explanation have been advanced for those discrepancies.

Table 9.5 Summary of loadings.

load	beam			
	C2-8-12	C3-8-12	C4-8-12A	C4-8-12B
P_1	P	0	P	P
P_2	0	P	P	$2/5P$

In the present study a large deflection elasto-plastic finite element analysis of these two-span continuous beams have been made. The finite element mesh consist of 24 elements including two short elements (length $\approx$ 100 mm) around points A, B and at the midsupport. Computations have been performed with different imperfections in the loading conditions shown in Figure 9.30 and the calculated maximum loads are tabulated in Table 9.6. The imprefection sensitivity of the beams C2-8-12 and C4-8-12A are shown in Figure 9.29. In Figure 9.31 the lateral deflections of the midspans vs. load are shown. It can be seen from the imperfection sensitivity diagrams in Figures 9.29 and 9.32, that for beams S4-

8 and C2-8-12 the bifurcation load (zero imperfection) is much higher than the maximum load obtained from the experiments. For those beams considerable plastic deformations occur before the lateral buckling, so it is possible that the 'plastic buckling paradox', Hutchinson (1974), between flow- and deformation theory predictions takes place. It has been pointed out in many connections and by various researchers that the experimental plastic buckling observations fit quite well to the results of the deformation theory, whereas the flow theory yields much higher values for the buckling load. Calculations with deformation theory of plasticity have not been done in the present study.

Table 9.6 Comparison of limit loads

beam	experimental	present FEM analysis				
		$\alpha = 0.1°$	$\alpha = 0.5°$	$\alpha = 1°$	$\alpha = 2°$	$\alpha = 4°$
C2-8-12	259.9		323.2	304.2	278.5	238.1
C3-8-12	173.6		179.9	166.4	153.0	
C4-8-12A	197.6	204.6	182.7	168.8	153.6	
C4-8-12B	293.3		336.7	312.2	278.2	

α means the imperfection on the load direction
all the tabulated values are in kN

Table 9.7 Computed elastic bifurcation loads.

C2-8-12	C3-8-12	C4-8-12A	C4-8-12B
542.2	221.1	217.9	455.4

all the tabulated values are in kN

9.12 Post-buckling analysis of hybrid beams

In hybrid beams, the web is made of material which has considerably lower yield stress than that of the flanges. The effect of the weaker material of the web to the lateral plastic buckling behaviour is studied. A simply supported I-beam is analysed. The only difference to the analysis of the beams in chapter 9.10 is that the yield stress of the web is 80 %, 60 % or 40 % of the yield stress of the flanges. It can be concluded from the results, that the post-buckling behaviour of hybrid beams is similar to the ordinary one. The slope of the load-deflection curve in the

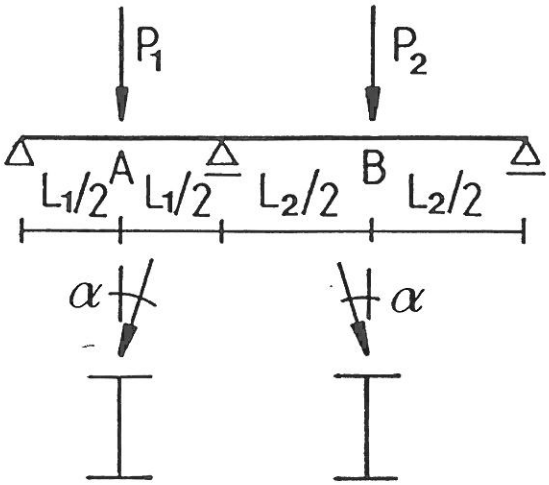

Figure 9.30 Continuous beam, geometry and loading.

post buckling regime seems to be almost unaffected from the yield stress variations of the web. The lateral deflection curves are shown in Figure 9.34.

9.13 Thermo-elasto-plastic analysis of steel frames

Applications of thermally loaded steel frames are chosen mainly to permit comparisons with the experimental data. Due to the lack of test results of three dimensional cases, only plane frames are analyzed. Two different models for the temperature dependency of material parameters are compared. First model is based on the European recommendations for the fire safety of steel structures (1983). For this model the temperature dependency of Young's modulus E and the yield stress σ_y are shown in Figure 9.35. Poisson's ratio ν and the tangent modulus E_t are assumed to be independent of temperature. In the second model, similar to the material model of Rubert and Schaumann (1985), a trilinear stress-strain curve is assumed. In that model the variation of Young's modulus, the lower yield stress σ_p and the upper yield stress σ_y are shown in Figure 9.6.

In all subsequent calculations of the present study a value of $12{\cdot}10^{-6}$ 1/°C for the thermal expansion is used. Some calculations for a more accurate description of the thermal expansion coefficient show neglible effect in comparison to the use of its constant value. The thermal expansion has variation from the value of $1.2{\cdot}10^{-5}$ 1/°C to $1.7{\cdot}10^{-5}$ 1/°C between the range of 20 - 600 °C according to the European recommendations for the fire safety of steel structures.

The only loading effect is due to temperature change. The temperature increment for the following step is adjusted by requiring the estimated norm of

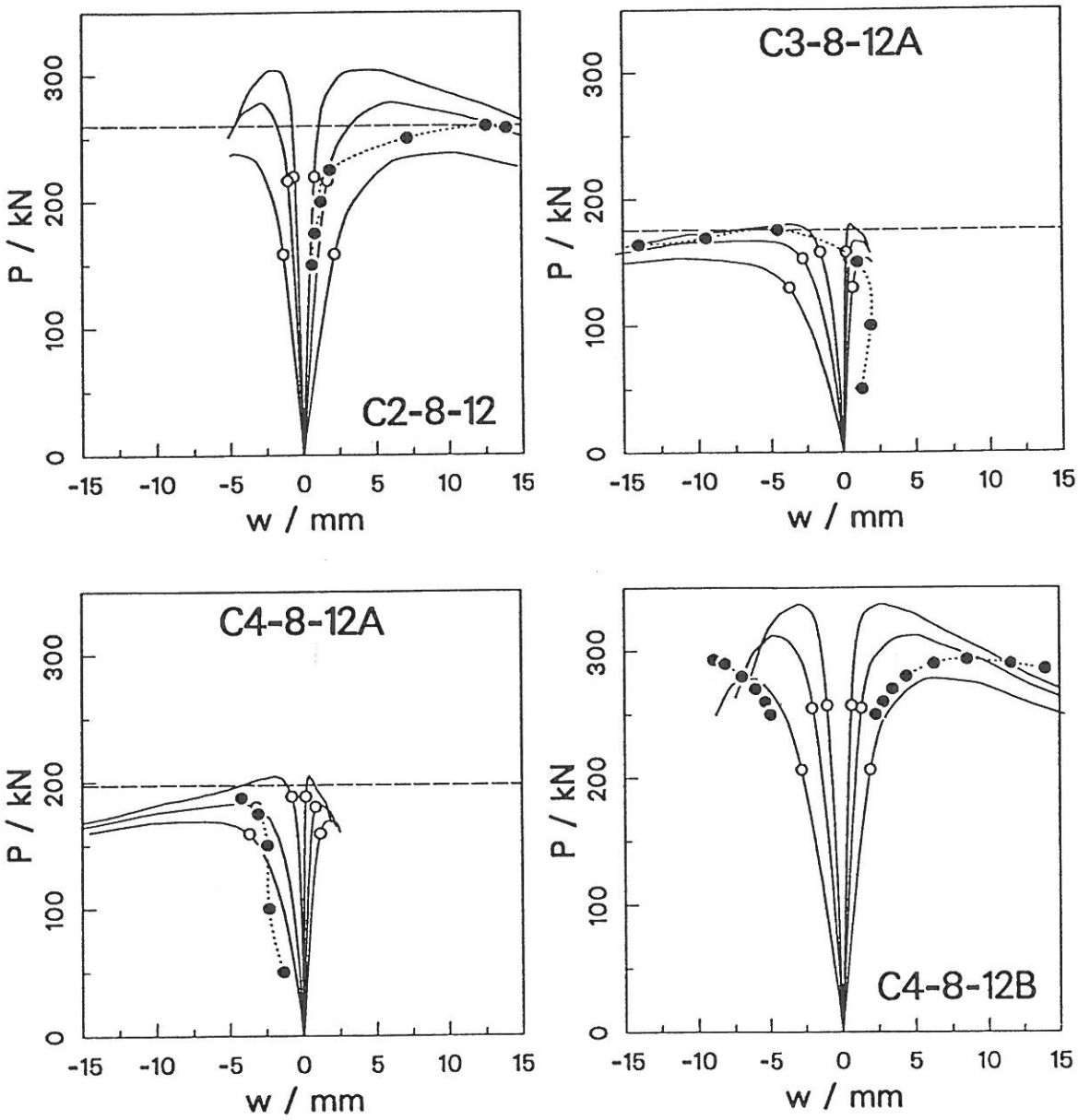

Figure 9.31 Lateral deflections at the midpoints of the spans. The circular shaded markers connected with dotted line are the experimental results. Solid curves indicate the calculated results with different values of imperfection. The blanked circle show the load level at which yield is noticed first. Imperfections in the FE computations: C2-8-12 ($P_1 = P, P_2 = 0$) $\alpha = 1°, 2°, 4°$; C3-8-12A ($P_1 = 0, P_2 = P$) and C4-8-12B ($P_1 = P, P_2 = 2/5P$) $\alpha = 0.5°, 1°, 2°$, C4-8-12A ($P_1 = P_2 = P$) $\alpha = 0.1°, 0.5°, 1°$. Deflections at point A are positive and at B negative, see Figure 9.30.

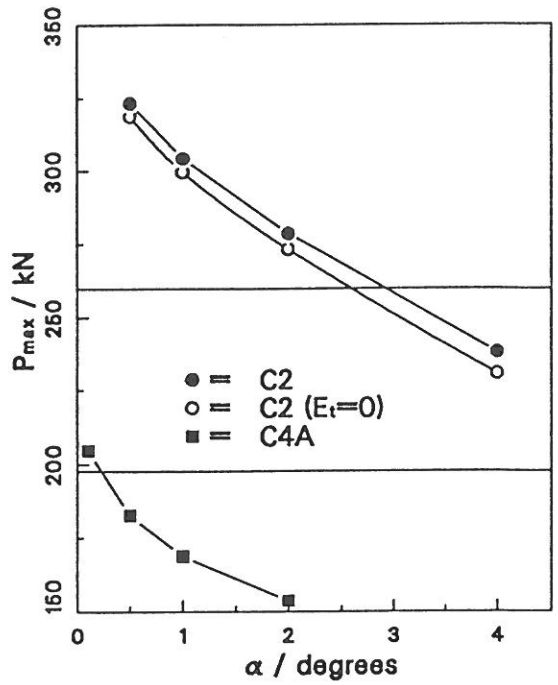

Figure 9.32 Imperfection sensitivity diagram.

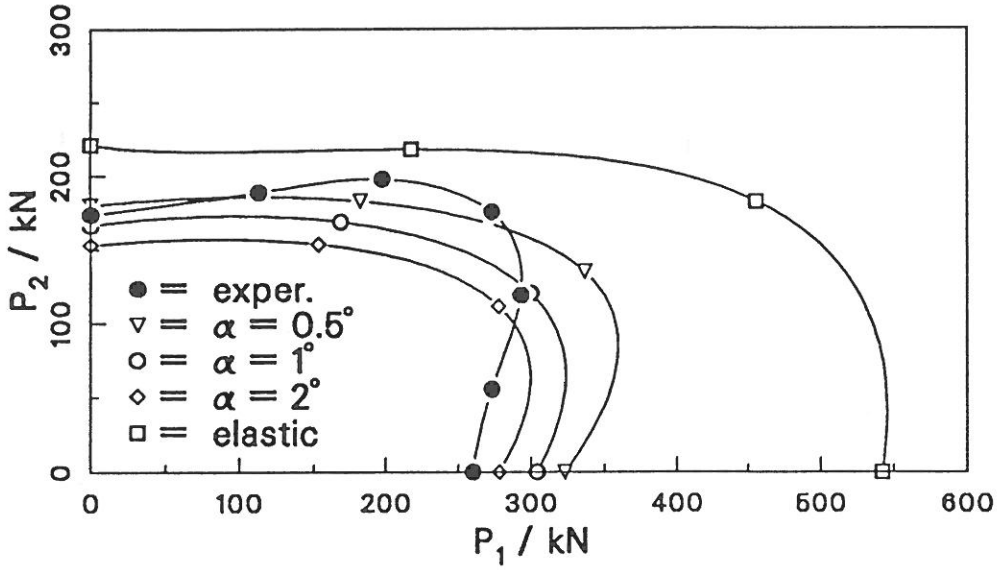

Figure 9.33 Interaction diagram for the continuous beams.

the displacement increment to be constant. Denoting

$$u_n = \|\Delta \mathbf{u}_n\|, \qquad v_n = \frac{u_n}{\Delta\theta}, \qquad a_n = \frac{v_n - v_{n-1}}{\Delta\theta},$$

where $\Delta\theta$ is the temperature increment, the requirement for the next step is

$$u_{n+1} = v_n \Delta\theta_{n+1} + \frac{1}{2} a_n (\Delta\theta_{n+1})^2 = u_n,$$

which yields

$$\Delta\theta_{n+1} = \frac{v_n}{a_n}\left(\sqrt{1 + \frac{2u_n a_n}{v_n^2}} - 1\right).$$

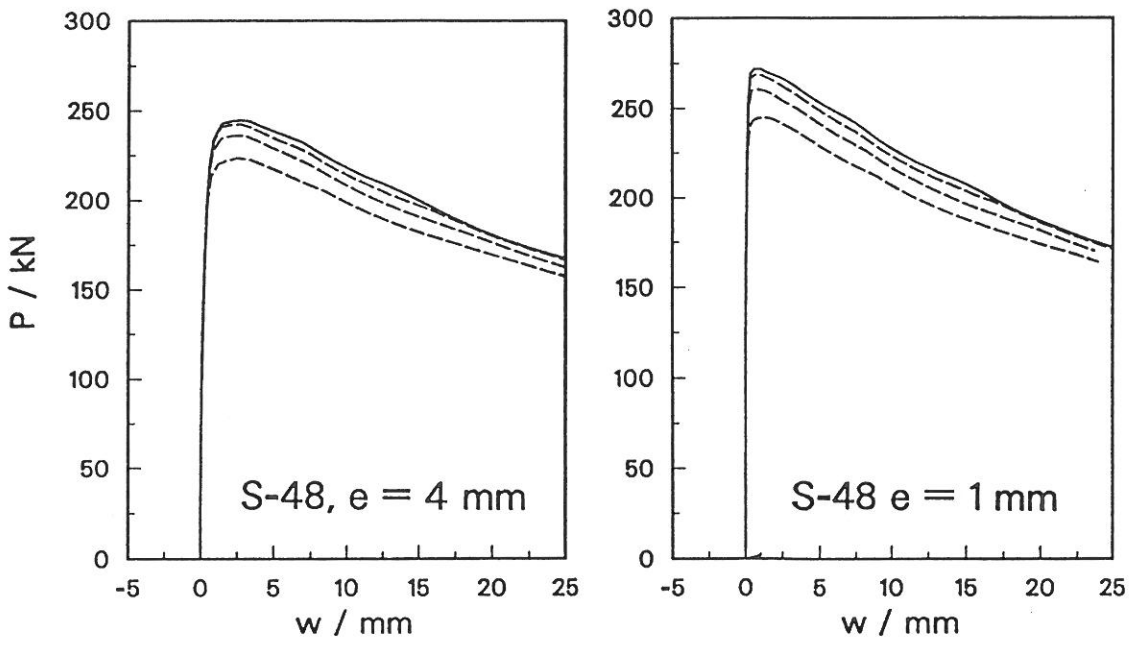

Figure 9.34 Post-buckling behaviour of hybrid beams, lateral deflection at the midspan vs. load. Dashed lines denote results from analyses of hybrid beams and solid line of an ordinary beam, respectively. The yield stress of the web is (a) 80 %, (b) 60 % and (c) 40 % of the yield stress of the flanges.

If $a_n = 0$ the equality $\Delta\theta_{n+1} = \Delta\theta_n$ holds. However, in numerical computations the temperature increment for the next step is determined from the approximate expression

$$\Delta\theta_{n+1} = \frac{u_n}{v_n}(1 - \frac{1}{2}\frac{u_n a_n}{v_n^2}). \tag{9.6}$$

Rubert and Schaumann (1985) have made experimental and computational analyses of simply supported IPE-80 beams with a concentrated load at the midspan. Four different load magnitudes are used, P = 24 kN, 23 kN, 16kN and 6 kN for beams WK1-4. Corresponding utilization factors are P/P_u = 0.85, 0.70, 0.50, 0.20, respectively. Present results of quasi static calculations are compared to the experimental results where the lowest value of the heating rate $\dot{T}$ = 2.67 K/min is used. According to the experimental results the effect of heating rate, which were between the values of 2.67 - 32 K/min in the experiments, is not significant to the behaviour of the beams WK1 and WK2. For beam WK4, which has the lowest load, the effect of heating rate results in 10 % difference in the critical temperature. A half of the beam is modelled with five linear elements using two short elements near the symmetry line. Five point and nine point Gaussian quadratures are used in the integration of the stiffness matrix and the internal force vector for flanges and web, respectively. The initial temperature increment used is 20 °C (as in all other examples in this chapter) and it was automatically reduced during the

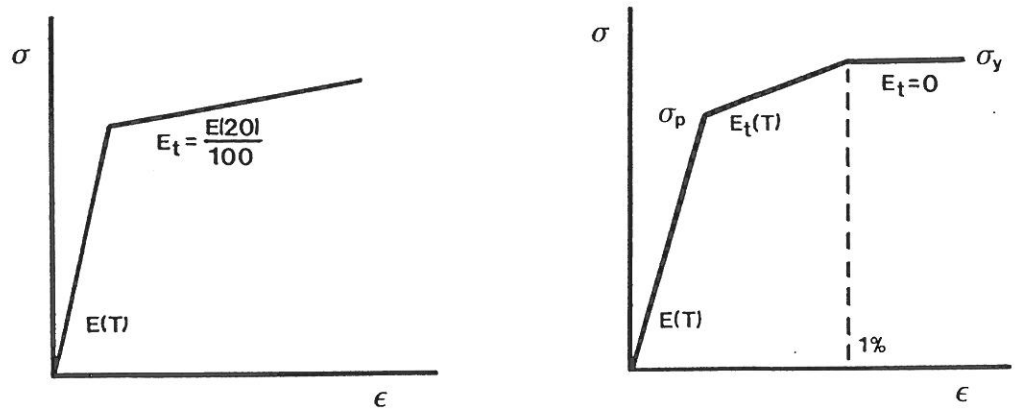

Figure 9.35 Uniaxial stress-strain relationship which is used in accordance with (a) ECCS model (model 1) and (b) the model developed by Rubert and Schaumann (model 2).

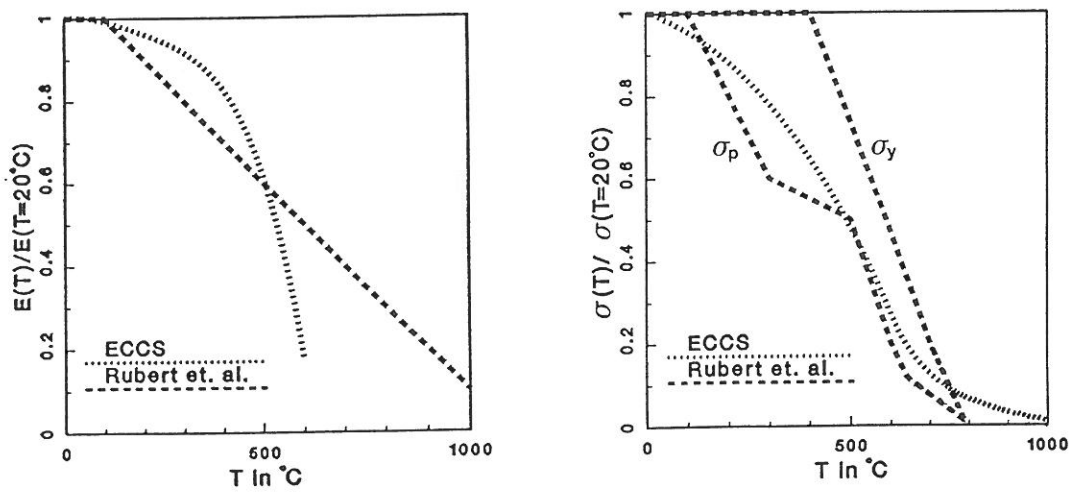

Figure 9.36 Modulus of elasticity and yield stress as a function of temperature.

heating process according to Equation (9.6).

The results of the computations where the material parameters of the second model are used, fits very well to the experimental results in this particular example. Especially, the infuence of the slow decrease interval of the lower yield stress between the temperatures 300-500 °C is clearly seen in the deflection-temperature curves for beams WK1 and WK2, see Figure 9.37. This slow increase interval of the dispacement has also been noticed in the calculations made by Rubert and Schaumann but it is not visible in the results obtained by Bock and Wernersson (1986) in their calculations using the ADINA program.

A two bay test frame ZSR1, Rubert and Schaumann (1985),is analysed. The problem definition and the calculated temperature-displacement curves are

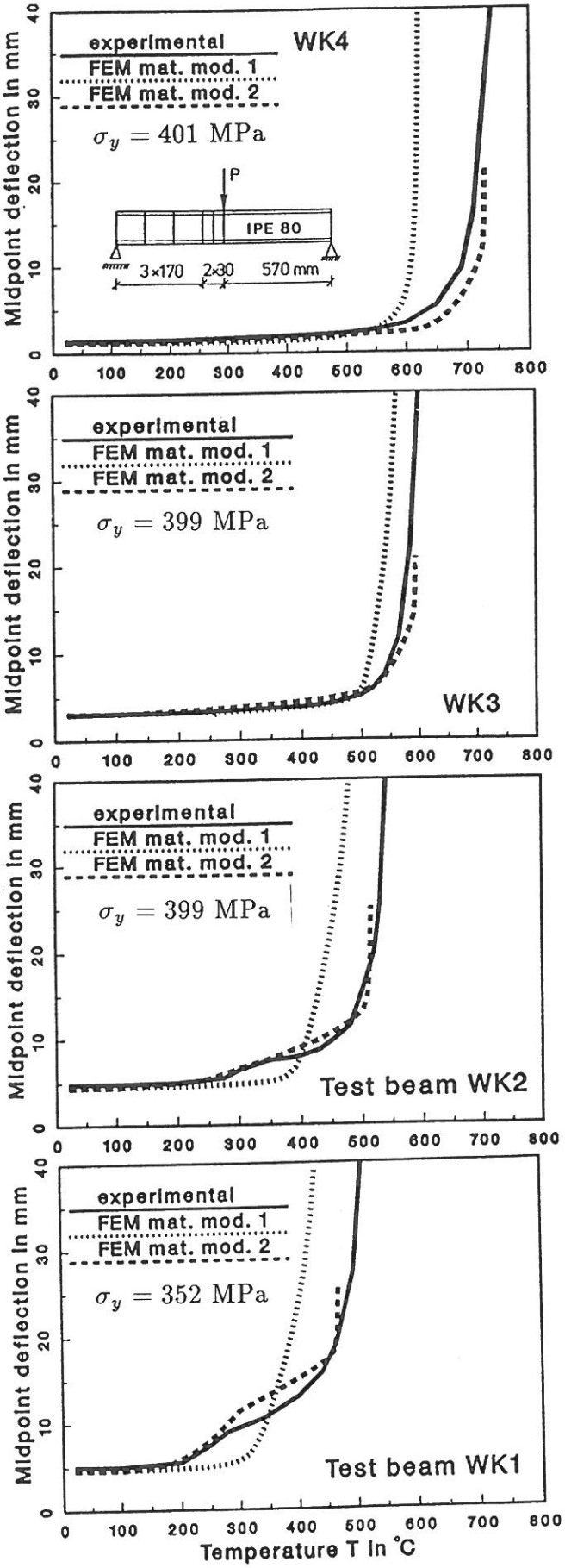

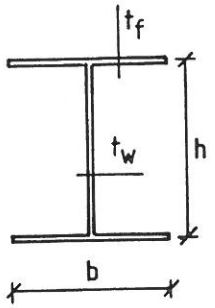

	h	b	t_f	t_w
IPE 80	74.8	46	5.2	3.8

Figure 9.37 Deflections of the midspan as a function of temperature for a simply supported beam.

shown in Figure 9.38. In this example the analyses yield almost the same critical temperature for both material models, although model 2 gives larger and model 1 correspondingly smaller displacements than the experimental measurements at the temperature range between 200-450 °C. The computed value for the collapse temperature is about 10 % lower than obtained from the experiments. The frame is modelled using 25 linear Timoshenko beam elements i.e. five elements of equal length per a member. In the integration of the stiffness matrix and the internal force vector, two point and five point Gaussian quadratures are used in the flanges and the web, respectively.

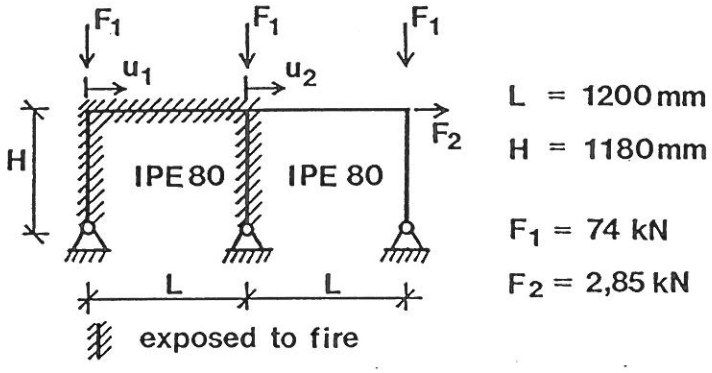

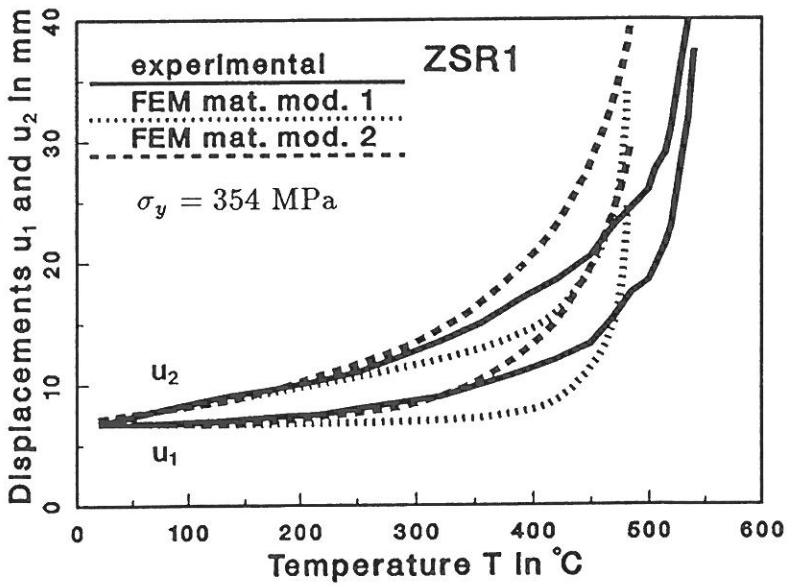

Figure 9.38 Two bay frame. Geometry and temperature-displacement curves.

An analysis of an ECCS calibrating frame, Vogel (1985), subjected to a local fire in the bottom bay on the right hand side, is performed, see Figure 9.39. In the omputations only the material model 1 (ECCS) are used. The finite element mesh consists of 162 linear Timoshenko beam elements and 153 nodal points. The

load intensities are one half of the values shown in Figure 9.39, i.e. the load factor $\gamma=1/2$.

The first yield occurred at the temperature 320 °C and the calculated temperature at collapse is 480 °C. Bending moment distributions and deflected shapes are shown in Figure 9.40. The start of yielding at the top of the column in the right hand side in the ground floor is greatly influenced by the bending moments due to the thermal expansion. When the temperature increases the bending moment capacity decreases rapidly in the two heated colums and the resistance of the structure to the horizontal loads is carried almost by the column on the left hand side. Finally the plastic deformations in the bottom column on the left hand side lead to the collapse in the sway mode, see Figure 9.40.

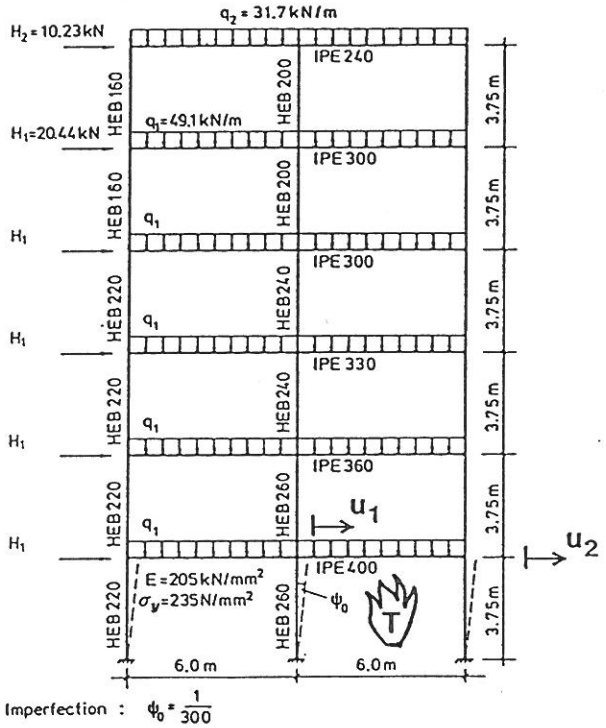

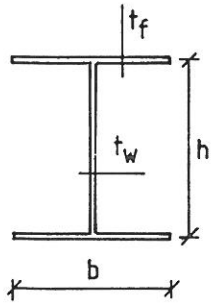

	h	b	t_f	t_w
HEB 160	147	160	13	8
HEB 200	185	200	15	9
HEB 220	204	220	16	9.5
HEB 240	223	240	17	10
HEB 260	242.5	260	17.5	10
IPE 240	230.4	120	9.6	6.2
IPE 300	289.3	150	10.7	7.1
IPE 330	318.5	160	11.5	7.5
IPE 360	347.3	170	12.7	8
IPE 400	386.5	180	13.5	8.6

Figure 9.39 Multistorey frame.

9.14 Dynamic plastic bifurcation of a pin-ended beam

The behaviour of a pin-ended beam subjected to uniform transverse loading applied as a short pulse is studied. The deflection history depends, in an extremely sensitive manner, on the interplay between momentum transfer, geometry changes and energy dissipation in plastic flow as pointed out by Symonds et al. (1986). Symonds and Yu (1985) give results of computations using ten different FE codes. An agreement to the prediction of the first peak deflection for all codes is obtained but the permanant displacements differ significantly. The unexpected result of

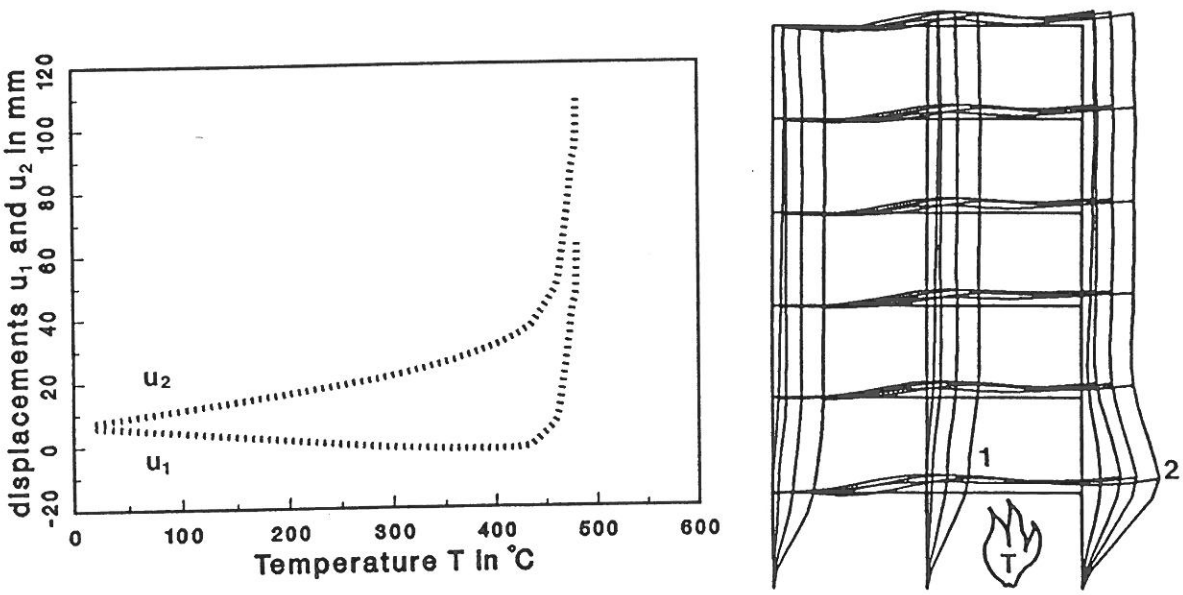

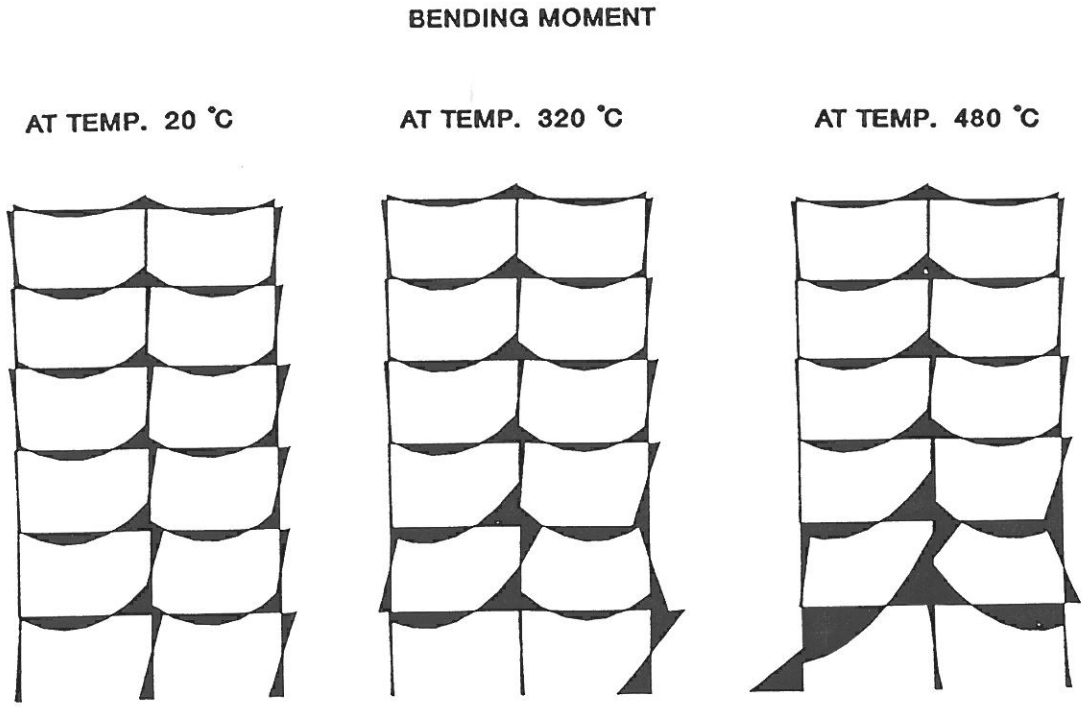

Figure 9.40 Horizontal deflections of points 1 and 2 and deformed shapes magnified by a factor of 30 at temperatures 320 (first yield) 460,470,480 °C. Bending moment distributions at the reference temperature 20 °C and at 320 and 480 °C (just before collapse).

those computations was the negative permanent displacement, implying that the final rest displacement is in the opposite direction to that of the load.

In the present analysis a half of the beam is modelled by ten linear Timoshenko beam elements. The central difference scheme with a diagonal mass matrix and the time step of 1.5 μs gives permanent deflection in the direction of the load. Also the trapezoidal rule with the time step of 25 μs time step and a consistent mass matrix yields qualitatively the same result, but the time-midpoint deflection curve starts to differ significantly after 1 ms. When the trapezoidal rule with a diagonal mass matrix and the time steps of 25 μs and 35 μs are used, negative permanent deflections occur. Those four completely different deflection histories are shown in Figure 9.41.

The determinant of the effective stiffness matrix is plotted in Figure 9.42. At the time, about 0.5 ms, the determinat is zero indicating nonuniquenes in the solution of the incremental equations of motion. That time period corresponds to the phase of plastic extension of the beam. So, small deviations in the elongation of the beam's axis can cause significantly different compressive stresses in the elastic recovery phase, which can in certain circumstances lead to the snap through instability.

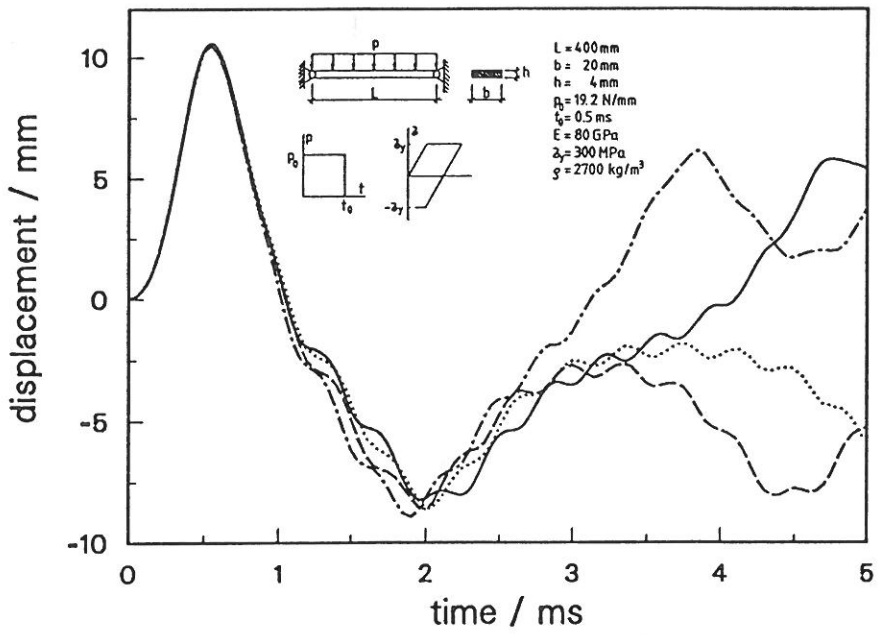

Figure 9.41 Response history of a pin-ended beam to pulse loading. Solid curve: the central difference method (CD), $\Delta t = 1.5$ μs; dashed line: the trapezoidal rule (TRAP), $\Delta t = 25$ μs; dotted line: TRAP, $\Delta t = 35$ μs and all these three computations with a diagonal mass matrix. The dash-dotted line indicates computation with the trapezoidal rule using a consistent mass matrix and the time step of 25 μs.

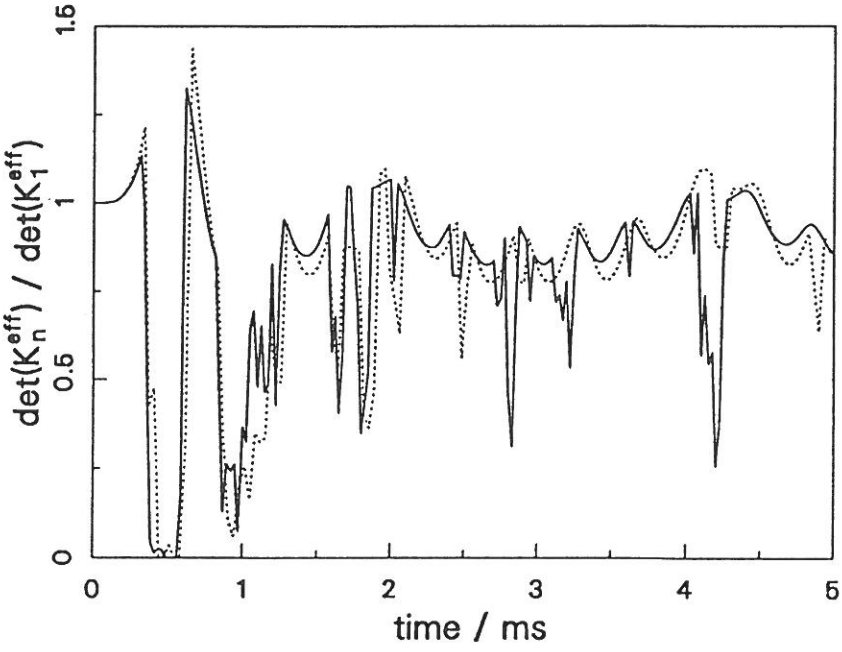

Figure 9.42 Normalized determinant of the effective stiffness matrix as a function of time in a problem of a pin-ended beam. Solid curve corresponds to the computation with the trapezoidal rule using the time step of 25 μs and the dotted line corresponds to the computation with the time step of 35 μs. In both cases a diagonal mass matrix have been used.

9.15 Dynamic analysis of an elasto-plastic cantilever beam

The responses of a cantilever I-section beam under both static and dynamic step loading are studied. The geometrical data and loading are given in Figure 9.43.

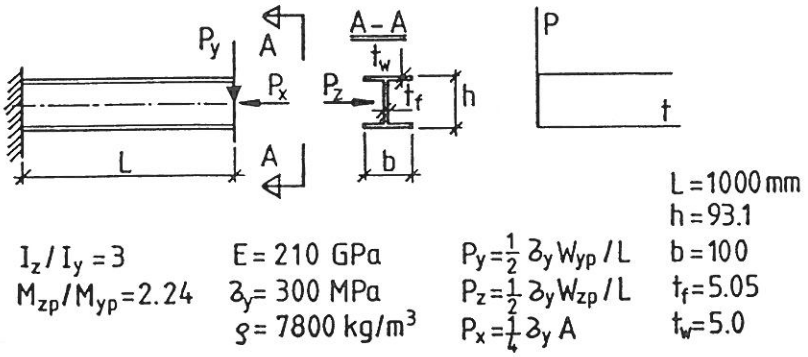

Figure 9.43 Geometry and loading of a cantilever beam.

The static responces are shown in Figure 9.44 when different representations to the yield function are used in the computation. Using the spherical yield surface expressed in terms of stress resultants, Equation (6.30), gives quite satisfactory results compared to the use of the layered model. In the computations with the yield surface, expressed in Equation (6.31), the plastic collapse occurred not until

the moment in the primary bending plane reaches the fully plastic moment, so overestimating the load carrying capasity about 35 %.

In Figure 9.45 the results from the analyses of the dynamic response of the cantilever beam under the step load are shown. Rao and Raghavan (1987) have also investigated the same problem. The type of modelling the plastic behaviour of the material has a great influence in the results. The use of approximate yield surfaces expressed in terms of stress resultants, give considerably smaller displacement values compared to the use of the layered model. The result is obvious, since the plastic deformations when the layered model is used start to develop earlier. As an extreme case, when the yield surface expressed in Equation (6.31) is used, no plastic deformations occur, see Figure 9.45. Warping has only a small effect on the behaviour of the beam when the layered model is used and neglible when the approximate expression to the yield surface are used. The results in Figure 9.45 differ from those obtained by Rao and Raghavan (curve 3 in Figure 3). One reason for that could be in the inaccurate integration over the cross-sectional area. Rao and Raghavan have used six integration points in the flanges and four in the web. In the present calculation both flanges and web are integrated using 12 points (2×6).

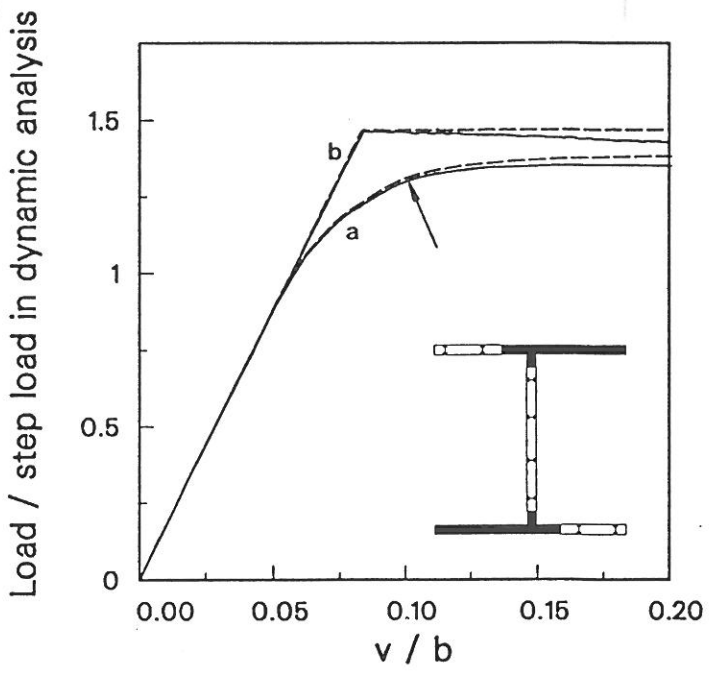

Figure 9.44 Static elasto-plastic response of a cantilever I-section beam, using (a) the layered model, (b) the approximate yield surface of spherical form, Equation (6.30). Solid lines correspond to the computations where the effect of warping is neglected and dashed lines where it is included.

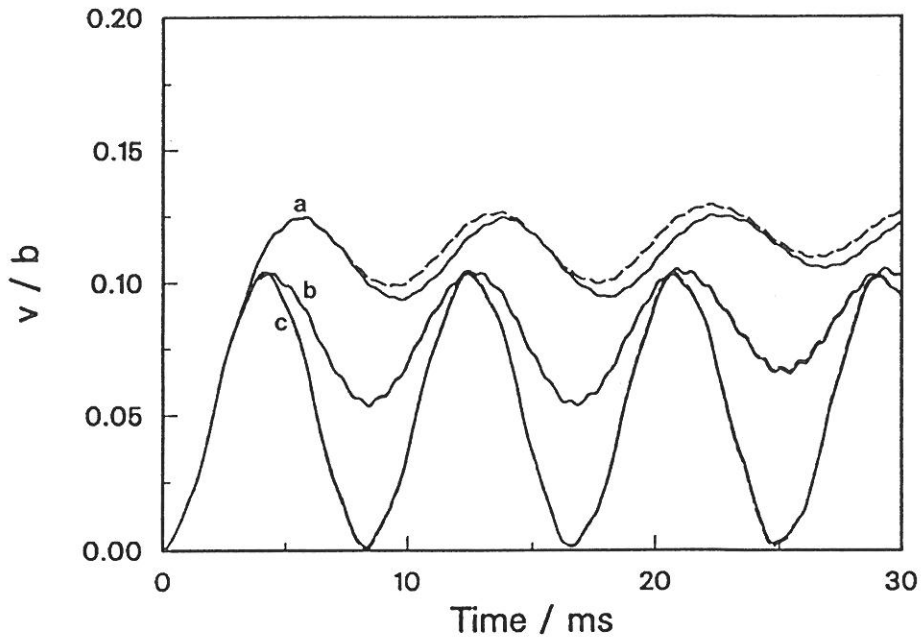

Figure 9.45 Dynamic elasto-plastic response of a cantilever I-section beam, using (a) the layered model, (b) the approximate yield surface, sphere, Equation (6.30) and (c) cube, Equation (6.31). Solid lines correspond to the computations where the effect of warping is neglected and dashed lines where it is included.

9.16 Dynamic elasto-plastic behaviour of a portal frame

A portal frame, clamped at its supports, with a mass fixed in the midspan of the horizontal beam, is subjected to an impact load perpendicular to the plane of the frame by a 0.22 lead bullet. Experimental results have been reported by Messmer (1987), and Messmer and Sayir (1988). The loading time have been between the range of 40 to 60 μs, and the measured shape of the load pulse is almost triangle, Figure 4 in Reference Messmer and Sayir (1988). However, the shape and the loading time variations (40-60 μs) have a little influence to the response of the frame. In the present calculations the rectangular pulse, shown in Figure 9.47 (duration 60 μs and impulse 0.72 Ns), is used. One half of the frame is modelled by using twenty equal elements. In Figure 9.47 the lateral displacements of the impacted point are shown when the linear Timoshenko beam element is used in the computation. Both elasto-plastic and visco-plastic material models are used in the analyses. When the layered models are used the 7×7 Gaussian quadrature is adopted. Two versions of the Perzyna's viscoplastic material is used. In the first one the viscoplastic part of the strain rate has the form

$$\dot{\varepsilon}_{ij}^{vp} = \sum_{\alpha=1}^{5} B_\alpha \langle \frac{\sigma_e}{\sigma_y} - 1 \rangle^\alpha \frac{\partial f}{\partial \sigma_{ij}}, \tag{9.7}$$

and in the second one

$$\dot{\varepsilon}_{ij}^{vp} = \gamma \langle \frac{\sigma_e}{\sigma_y} - 1 \rangle^p \frac{\partial f}{\partial \sigma_{ij}}, \tag{9.8}$$

where the parameters used are $\gamma = 40$ 1/s and p=5. In equations (9.7) and (9.8) the notations

$$f = \sigma_e = \sqrt{3J_2} = \sqrt{\frac{3}{2}\sigma'_{ij}\sigma'_{ij}},$$

$$\sigma'_{ij} = \sigma_{ij} - \frac{1}{3}\sigma_{kk}\delta_{ij}$$

are used. Perzyna has determined the material constants B_α from the experiments made by Clark and Duwez, Perzyna (1966). They are given in Table 9.7. The yield stress as a function of strain rate for both models (9.7) and (9.8) are shown in Figure 9.46.

Table 9.7 Material parameters B_α in Equation (9.7).

α	1	2	3	4	5
B_α (1/s)	337.53	-1470.56	3271.71	-3339.98	1280.06

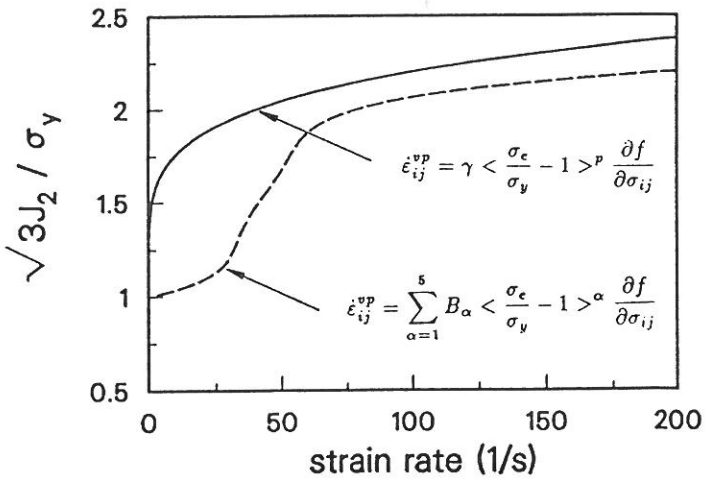

Figure 9.46 Yield stress as a function of strain rate.

Also computations with the element based on the Euler-Bernoulli beam theory are performed. Results of the computation using Euler-Bernoulli elements are shown in Figure 9.48. Obviously, the displacements are smaller when compared to the results obtained by using the Timoshenko beam theory.

It can be concluded that in this particular model the stress resultant representation of the yield surface gives results which are in good agreement with the computations of layered models. The permanent deflections of the mass point

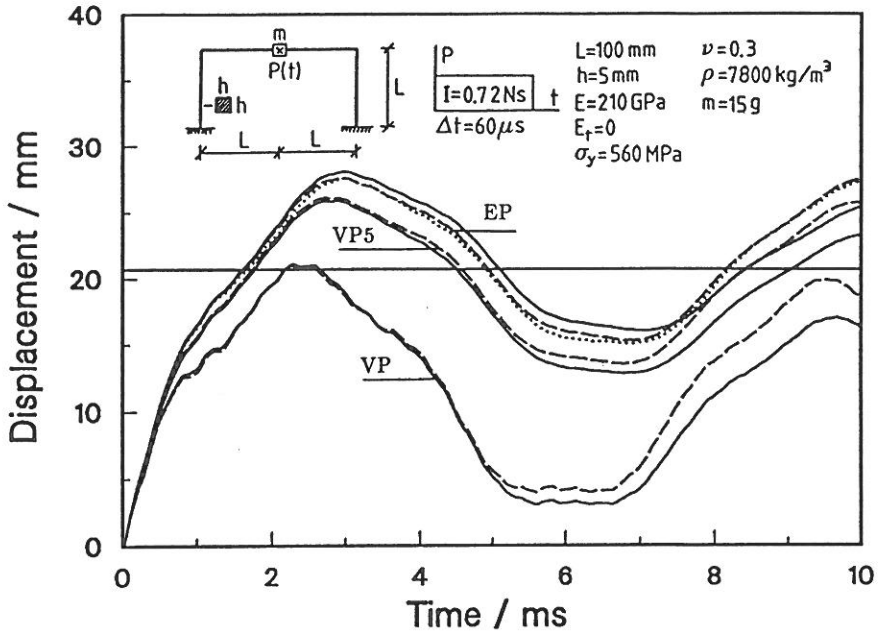

Figure 9.47 Displacement of the mass. Twenty equal linear Timoshenko beam elements. Solid lines correspond to the layered model computations with the 7×7 Gaussian quadrature. Dashed and dotted lines indicate computations where the sphere or the cube yield surface are used. The permanent experimental deflection was 20.7 mm. Notations; EP: elasto-plastic, VP: visco-plastic model (9.7), VP5: visco-plastic model (9.8).

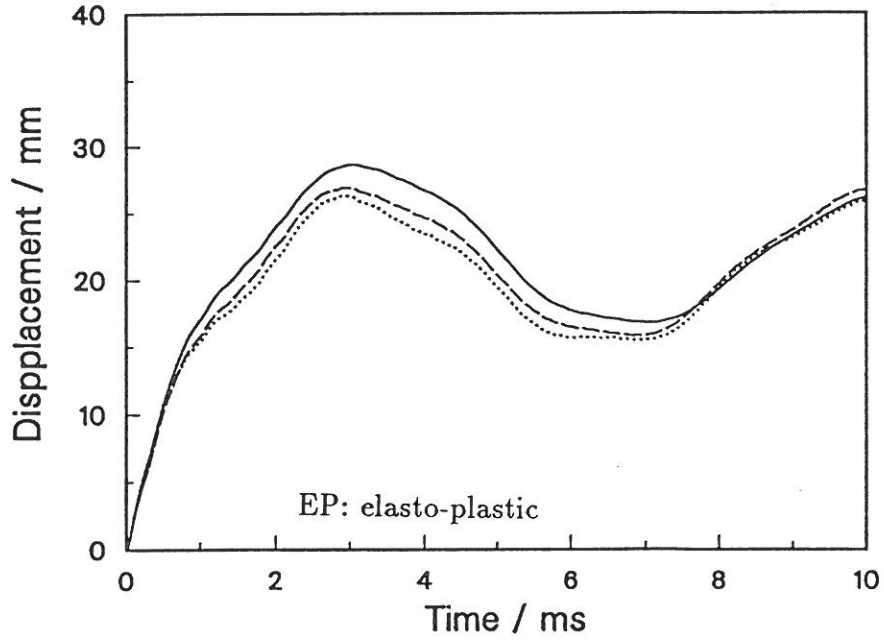

Figure 9.48 Displacement of the mass. Twenty equal cubic Euler-Bernoulli beam elements. The meaning of the different line types are the same as in Figure 9.47.

fit quite well to the experimental measurements, Messmer (1987), for the elasto-plastic material models. The viscoplastic model (9.8) gives considerably too small deflections, but the amplitude of the elastic vibration phase is in a satisfactory agreement with the experimental result (about 21 mm), while in the case of elasto-plastic models the amplitudes are too small (about 12 mm). Computed maximum and permanent deflections are tabulated in Table 9.8.

Table 9.8 Computed maximum and permanent deflections

element	material model	maximum defl.	permanent defl.
lin. Tim.	EP-L	28.1	22
lin. Tim.	EP-S	27.6	21
lin. Tim.	EP-C	27.6	21
lin. Tim.	VP-L	21.1	12
lin. Tim.	VP-S	21.0	12
lin. Tim.	VP5-L	25.8	19
lin. Tim.	VP5-S	26.1	20
cubic E-B	EP-L	28.7	23
cubic E-B	EP-S	26.9	21
cubic E-B	EP-C	26.3	21

all the tabulated values are in mm
EP = elasto plastic
VP = visco-plastic model (9.7)
VP5 = visco-plastic model (9.8)
L = layered model 7×7 Gaussian integration
S = yield surface (6.30)
C = yield surface (6.31)

In the computation with the yield surface (6.30) the first plastic hinge appears at the impacted point after the time of 29 μs and it disappears at the time of 120 μs for a while. The bending moment reach again the fully plastic moment at the time 160 μs for duration time of 60 μs. There are also plastic deformations in the horizontal beam between the struck and corner points in distance 50-80 mm from the struck point, see Figure 9.49. It is also confirmed in the experiments, Messmer (1987). At the time of 420 μs the plastic hinges in bending appear at the clampings for a time period of 90 μs and reappears again at the time of 840 μs. The frame swings out elastically after the time 3.59 ms when the plastic hinges

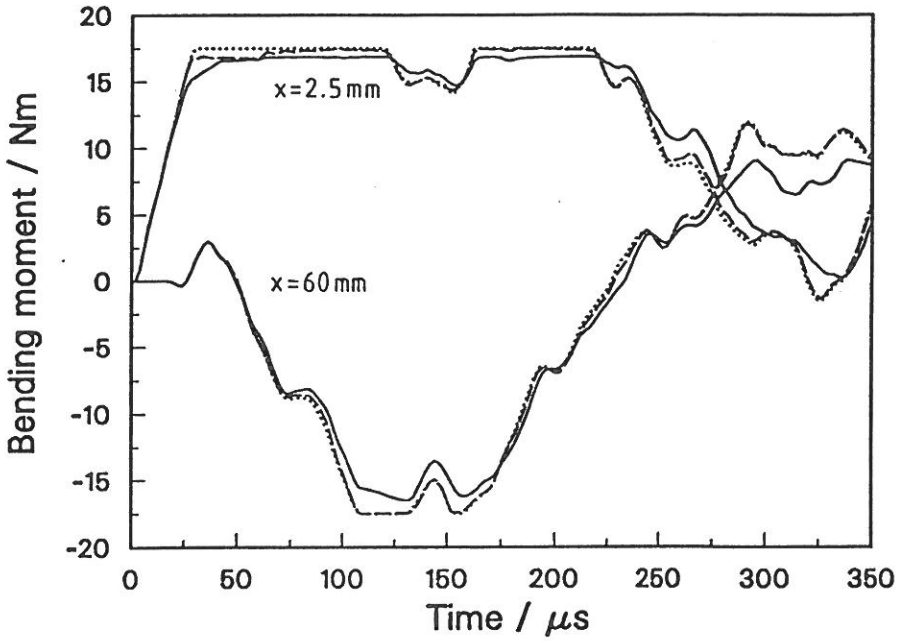

Figure 9.49 Bending moments in the horizontal beam, (a) 2.5 mm (b) 60 mm from the midspan. The meaning of the different line types are the same as in Figure 9.47.

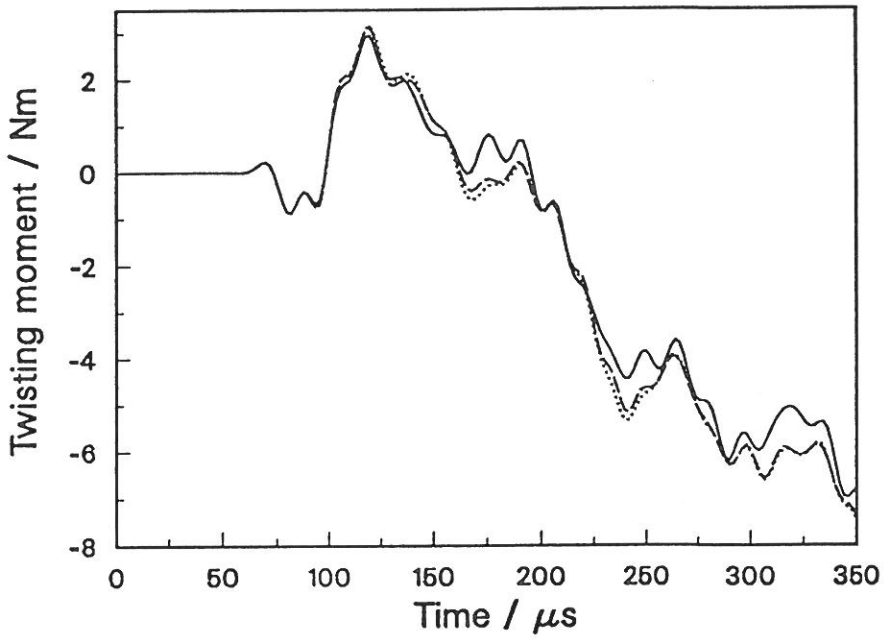

Figure 9.50 Twisting moment in the vertical beam at the point placed 20 mm from the clamping. The meaning of the different line types are the same as in Figure 9.47.

disappears at the clampings. There are also small periods of plastic deformation at the time 5.6 ms and between the period 6.4 to 6.8 ms. The computed bending moment histories, shown in Figure 9.49, and the twisting moment history, Figure 9.50, are in agreement with Messmer's theoretical calculations.

9.17 An I-beam impacted by a mass

A steel beam of wide flange W12×40 cross-section impacted by a mass at the center of the beam is considered. One a half of the beam is modelled with ten linear Timoshenko beam elements including one short element (length 25 mm) close the impacted point. The total length of the whole beam is 18.288 m. The loading is given by the initial velocity $v_y = 81.26984$ m/s at the impacted node. For the ratio Hm/G a value 1.1065 has been chosen (H = height of the beam, m = mass per unit length of the beam, G mass of the impacting particle). A similar beam has been analysed by Jones and Gomes de Oliveira (1979).

Also analyses of the case where the impact is not in the primary bending plane of the beam are performed. The initial velocity components are $v_y = 80.03517$ m/s and $v_z = 14.11236$ m/s, corresponding the inclination of 10 degrees from the primary bending plane. The calculations where the effect of warping is included result in about 5 % smaller deflections in the simply supported case, but the corresponding difference is smaller in the case of clamped boundaries.

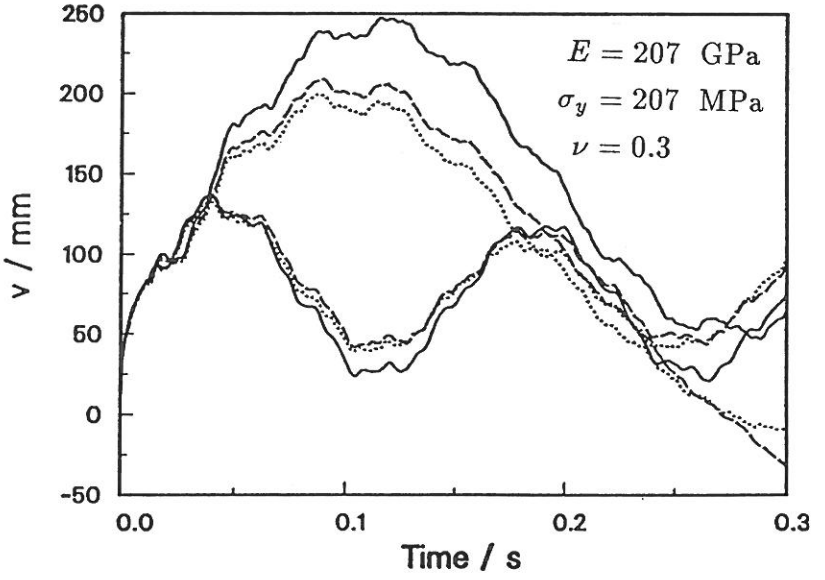

h	b
292.1	203.2
t_f	t_w
12.7	7.94

Figure 9.51 I-beam hit centrally by a mass. Deflection history of the midpoint. The three upper curves correspond to the analyses of a beam with simply supported boundaries and the three lowest to the case of a beam with clamped boundaries. Solid lines indicate the calculations where the impact is in the primary bending plane. Dotted lines (warping neglected) and dashed lines (warping included) correspond to the calculations where the impact has an inclination angle of 10 ° to the primary bending plane.

10 DISCUSSION AND CONCLUSIONS

The numerical methods for analysing the nonlinear behaviour of space frames with either solid or thin-walled open non-deformable cross-sections have been developed. An updated incremental Lagrangian approach is used in formulating the nonlinear equilibrium equations. The material models adopted are elasto-plastic, viscoplastic and temperature dependent elasto-plastic. The stiffness matrices and internal force vectors are derived for elements based on Timoshenko beam theory and on the classical Euler-Bernoulli theory of a thin beam. In numerical computations performed in this study, the elements developed, have worked well. However, minor discrepancies between some solutions found in literature have been noticed. These deviations are possibly due to the inaccurate modelling of the stucture under consideration in the references. Particularly, in the plastic range the linear Timoshenko beam element has proved it's effecience and reliability. In the case of beams with thin-walled open cross-section a theory which takes into account the average warping shear stresses has been developed. The conventional theory of torsion by Vlasov can be obtained from the presented theory using a simple constraint. The penalty finite element method is used in the constrained version of the element.

Special attention is paid to the determination of singular points and branching onto the secondary equilibrium path. Reliability is the primary consern in developing solution procedures of the nonlinear equilibrium equations. The orthogonal trajectory method, proposed by Fried, has been used in this study. It has proved to be a robust continuation algorithm.

Further developments should be focused to the modelling of the behaviour of joints, especially when a thin-walled beam element with the warping degree of freedom is in question. Also a curved isoparametric formulation is a natural extension to the presented method. However, the linear isoparametric element could be practically accurate enough in elasto-plastic cases if an adaptive mesh refinement strategy is used. The accuracy of the presented theory, which takes the average shear strains due to torsion into account, should be investigated in particularly in the plastic range.

The simple description of plastic material behaviour by means of yield functions expressed in terms of stress resultants is fascinating, due to it's simplicity and computational economy. However, the use of the yield functions described in this study can result in considerably erroneous solutions. For a remedy of that shortcoming an approximative Ramberg and Osgood type relationship to the generalized strain and the corresponding stress resultant should be developed.

REFERENCES

ASCIONE, L., GRIMALDI, A., 1983, On the stability and postbuckling behaviour of elastic beams, *Thin-Walled Structures,* **1**, pp. 325-351.

ARGYRIS, J.H., DUNNE, P.C., SCHARPF, D.W., 1978, On large displacement- small strain analysis of structures with rotational degrees of freedom, *Computer Methods in Applied Mechanics and Engineering*, **14**, pp. 401-451.

ARGYRIS, J.H., 1982, An excursion into large rotations, *Computer Methods in Applied Mechanics and Engineering*, **32**, pp. 85-155.

ARGYRIS, J.H., BALMER, H., DOLTSINIS, J.St., DUNNE, P.C., HAASE, M., KLEIBER, M., MALEJANNAKIS, G.A., MLEJNEK, H.-P., MÜLLER, M., SCHARPF, D.W., 1979, Finite element method - the natural approach, *Computer Methods in Applied Mechanics and Engineering*, **17/18**, pp. 1-106.

ARGYRIS, J.H., STRAUB, K., SYMEONIDIS, Sp., 1982, Static and dynamic stability of nonlinear elastic systems under nonconservative forces-natural approac, *Computer Methods in Applied Mechanics and Engineering*, **32**, pp. 59-83.

ATTARD, M.M., 1986a, Lateral buckling of the beams by the FEM, *Computers & Structures*, **23** pp. 217-231.

ATTARD, M.M., 1986b, Nonlinear theory of non-uniform torsion of thin-walled open beams, *Thin-Walled Structures*, **4** pp. 101-134.

ATTARD, M.M., 1987, Non-linear analysis of thin-walled open beams , *Computers & Structures*, **25** pp. 437-443.

BABUŠKA, I., SZABO, B., 1983, *Lecture Notes on Finite Element Analysis*, manuscript

BARSOUM, R.S., GALLAGHER, R.H., 1970, Finite element analysis of torsional and torsional-flexural stability problems, *International Journal for Numerical Methods in Engineering*, **2** pp. 335-352.

BATHE, K.J., BOLOURCHI, S., 1979, Large displacement analysis of three dimensional beam structures, *International Journal for Numerical Methods in Engineering*, **14** pp. 961-986.

BATHE, K.J., CHAUNDHARY, A., 1982, On the displacement formulation of torsion shafts with rectangular cross-sections, *International Journal for Numerical Methods in Engineering*, **18** pp. 1565-1568.

BATHE, K.J. DVORKIN, E.N., 1983, On the automatic solution of non-linear finite element equations, *Computers & Structures*, **17**, pp. 871-879.

BATHE, K.J., WIENER, P.M., 1983, On elastic-plastic analysis of I-beams, *Computers & Structures* **17**, pp. 711-718.

BATOZ, J.L., DHATT, G., 1979, Incremental displacement algorithms for nonlinear problems, *International Journal for Numerical Methods in Engineering*, **14**, 1262-1267.

BAŽANT, Z.P., EL NIMEIRI, M., 1973, Large deflection spatial buckling of thin-walled beams and frames, *Journal of Engineering Mechanics*, **99** pp. 1259-1281.

BELYTSCHKO, T., SCHWER, L., KLEIN, M.J., 1977, Large displacement, transient analysis of space frames, *International Journal for Numerical Methods in Engineering,*

11 pp. 65-84.

BERGAN, P.G., 1981, Solution by iteration in displacement and load spaces, in W. Wunderlich et al. (eds.), *Nonlinear Finite Element Analysis in Structural Mechanics*, pp. 553-571.

BESSELING, J.F., 1977, Derivatives of deformation parameters for bar elements and their use in buckling and postbuckling analysis, *Computer Methods in Applied Mechanics and Engineering*, **12**, pp. 97-124.

BOCK, H.M., WERNERSSON, H., 1986, Zur rechnerischen Analyse des Tragverhaltens brandbeanspruchter Stahlträger, *Stahlbau*, No 1, pp. 7-14.

DE BORST, 1987, Computation of post-bifurcation and post-failure behaviour of strain-softening solids, *Computers & Structures*, **25**, pp. 211-224.

CARDONA, A., GERADIN, M., 1988, A beam finite element non-linear theory with finite rotations, *International Journal for Numerical Methods in Engineering*, **26** pp. 2403-2438.

CHAISOMPHOB, T., KANOK-NUKULCHAI, W., NISHINO, F., 1988, An automatic arc lenght control algorithm for tracing equilibrium paths of nonlinear structures, *Structural Engineering / Earthquake Engineering*, **5** pp. 205-208.

CHAN, S.L., 1988, Geometric and material non-linear analysis of beam-columns and frames using the minimum residual displacement method, *International Journal for Numerical Methods in Engineering,* **26** pp. 2657-2699.

CHAN, T.F., 1984, Deflated decomposition of solutions of nearly singular systems, *SIAM Journal of Numerical Analysis*, **21**, pp. 738-754.

CHEN, H., BLANFORD, G.E., 1989, A C^0 finite element formulation for thin-walled beams, *International Journal for Numerical Methods in Engineering,* **28** pp. 2239-2255.

CHU, K-H., RAMPETSREITER, R.H., 1972, Large deflection buckling of space frames, *Journal of the Structural Division*, ASCE **98**, pp. 2701-2711.

CONNOR, J.Jr., LOGCHER, R.D., CHAN S.C., 1968, Nonlinear analysis of elastic framed structures, *Journal of the Structural Division*, ASCE **94** pp. 1525-1547.

CRISFIELD, M.A., 1979, A faster modified Newton-Raphson iteration, *Computer Methods in Applied Mechanics and Engineering*, **20**, pp. 267-278.

CRISFIELD, M.A., 1981, A fast incremental/iterative solution procedure that handles snap-through, *Computers & Structures*, **13**, pp. 55-62.

CRISFIELD, M.A., 1986, New solution procedures for linear and non-linear finite element analysis, in J. Whiteman (ed.), *The Mathematics of Finite Elements and Applications V*, Academic Press, London.

DAHLQUIST, G., BJÖRCK, Å, 1974, *Numerical Methods*, Prentice-Hall, Inc. Englewood Criffs, New Jersey.

DENNIS, J.E., MORE, J.J., 1977, Quasi-Newton methods, motivation and theory, *SIAM Review,* **19**, pp. 46-89.

DINNO, K.S., MERCHANT, W., 1965, A procedure for calculating the plastic collapse of I-section under bending and torsion, *Structural Engineer,* **43**, pp. 219-221.

DVORKIN, E.N., ONATE, E., OLIVER, J., 1988, On the non-linear formulation for curved Timoshenko beam elements considering large displacement/rotation increments, *International Journal for Numerical Methods in Engineering*, **26** pp. 1597-1613.

EPSTEIN, M., MURRAY, D.,W., 1976, Three dimensional large deformation analysis of thin-walled beams, *International Journal of Solids and Structures*, **12** pp. 867-876.

ERIKSSON, A., 1987, Using eigenvector projections to improve convergence in non-linear finite element equilibrium equations, *International Journal for Numerical Methods in Engineering*, **24**, pp. 497-512.

ERIKSSON, A., 1988, On some path-related measures for non-linear structural F.E. problems, *International Journal for Numerical Methods in Engineering*, **26**, pp. 1791-1803.

ERIKSSON, A., 1989, On linear constraints for Newton-Raphson corrections and critical point searches in structural F.E. problems, *International Journal for Numerical Methods in Engineering*, **28**, pp. 1317-1334.

ERIKSSON, A., 1990, On the numerical treatment of the stability properties of elastic equilibrium solutions, *Publication TRITA-BRO-9001*, Department of Structural Engineering, The Royal Institute of Technology, Stockholm, Sweden.

VAN ERP, G.M., 1989, Advanced buckling analyses of beams with arbitrary cross sections, Ph. D. thesis, Technical University of Eindhoven.

VAN ERP, G.M., MENKEN, C.M., VELDPAUS, F.E., 1988, The non-linear flexural-torsional behaviour of straight slender elastic beams with arbitrary cross section, *Thin-Walled Structures*, **6**, pp. 385-404.

European Recommendations for the Fire Safety of Steel Structures, ECCS-Technical Committee 3, Elsevier, 1983.

FARARD, M., BEAULIEU, D., DHATT, G., 1987, Buckling of thin-walled members by finite elements, *Computers & Structures*, **25**, pp. 183-190.

FORDE, B.W.R., STIEMER, S.F., 1987, Improved arc length orthogonality methods for nonlinear finite element analysis, *Computers & Structures*, **27**, pp. 625-630.

FRIBERG, P.O., 1985, Beam element matrices derived from Vlasov's theory of open thin-walled elastic beams, *International Journal for Numerical Methods in Engineering,* **21**, pp. 1205-1228.

FRIBERG, O., 1988a, Computation of Euler parameters from multipoint data, *Journal of Mechanisms, Transmission and Automation in Design*, **110**, pp. 116-121.

FRIBERG, O., 1988b, A set of parameters for finite rotations and translations, *Computer Methods in Applied Mechanics and Engineering*, **66**, pp. 163-171.

FRIED, I., 1984, Orthogonal trajectory accession to the equilibrium curve, *Computer Methods in Applied Mechanics and Engineering*, **47** pp. 283-297.

HASEGAWA, A., LIYANAGE, K.,K., NISHINO, F., 1987a, A non-iterative nonlinear analysis scheme of frames with thin-walled elastic members, *Structural Engineering / Earthquake Engineering*, **4** pp. 19-29.

HASEGAWA, A., LIYANAGE, K.,K., NODA, M., NISHINO, F., 1987b, An inelastic

finite displacement formulation of thin-walled members, *Structural Engineering / Earthquake Engineering*, **4** pp. 269-276.

HASELGROVE, C.B., 1961, The solution of non-linear equations and of differential equations with two point boundary conditions, *Computer Journal*, **4**, pp. 255-259.

HIBBIT, H.D., 1979, Some follower forces and load stiffness, *International Journal for Numerical Methods in Engineering*, **14**, pp. 937-941.

HILL, R., 1959, Some basic principles in the mechanics of solids without a natural time, *Journal of Mechanics and Physics of Solids*, **7**, pp. 209-225.

HUTCHINSON, J.W., 1974, Plastic buckling, *Advances in Applied Mechanics*, **14**, pp. 67-144.

JONES, N, GOMES DE OLIVEIRA, J., 1979, The influence of rotatory inertia and transverse shear on the dynamic plastic behaviour of beams, *Journal of Applied Mechanics*, **46**, pp. 303-310.

JOHNSON, D., 1988, A cellular analogy for the elastic-plastic Saint-Venant torsion problem, *International Journal of Solids and Structures*, **24**, pp. 321-329.

KHESHGI, H.S., SCRIVEN, L.E., 1985, Variable penalty method for finite element analysis of incompressible flow, *International Journal for Numerical Methods in Fluids*, **5**, pp. 785-803.

KITIPORNCHAI, S., TRAHAIR, N.,S., 1975a, Buckling of inelastic I-beams under moment gradient, *Journal of the Structural Division*, ASCE **101** pp. 991-1004.

KITIPORNCHAI, S., TRAHAIR, N.,S., 1975b, Inelastic buckling of simply supported steel I-beams, *Journal of the Structural Division*, ASCE **101** pp. 1333-1347.

KOJIĆ, M., BATHE, K.J., 1987a, Thermo-elasto-plastic and creep analysis of shell structures, *Computers & Structures*, **26**, pp. 135-143.

KOJIĆ, M., BATHE, K.J., 1987b, The 'effective-stress-function' algorithm for thermo-elasto-plasticity and creep, *International Journal for Numerical Methods in Engineering*, **24**, pp. 1509-1532.

KOUHIA, R., 1986, Iterations of Newtonian type in non-linear structural analysis (in Finnish), *Journal of Structural Mechanics (Rakenteiden Mekaniikka)*, **19**, No 4 pp. 15-51.

KOUHIA, R., MIKKOLA, M., 1989, Tracing the equilibrium path beyond simple critical points, *International Journal for Numerical Methods in Engineering*, **28**, pp. 2923-2941.

KRAHULA, J.L., (1967), Analysis of bent and twisted bars using the finite element method, *AIAA Journal*, **5**, pp. 1194-1197.

KRAJCINOVIC, D., 1969, A consistent discrete elements technique for thinwalled assemblages, *International Journal of Solids and Structures*, **5**, pp. 639-662.

LEHMANN, TH., 1988, On thermodynamically-consistent constitutive laws in plasticity and viscoplasticity, *Arch. Mech.*, **40**, pp. 415-431.

LEE, H.,P., HARRIS, P.,J., HSU, C-T.,T., 1984, A nonlinear finite element computer program for thin-walled members, *Thin-Walled Structures*, **2** pp. 355-376.

LOVE, A.E.H., 1944, *The Mathematical Theory of Elasticity*, Dover Publ. Inc., New York.

MALVERN, L.E., 1969, *Introduction to the Mechanics of a Continuous Medium*, Prentice-Hall Inc., Englewood Cliffs, New Jersey.

MASUR, E.F., MILBRANDT, K.P., 1957, Collapse strength of redundant beams after lateral buckling, *Journal of Applied Mechanics*, **24**, pp. 283-288.

MATTHIES, H., STRANG, G., 1979, The solution of nonlinear finite element equations, *International Journal for Numerical Methods in Engineering*, **14**, pp. 1613-1626.

MESSMER, S., 1987, Dynamic elastic-plastic behaviour of a frame including coupled bending and torsion, *Transactions of the 9th International Conference on Structural Mechanics in Reactor Technology.*

MESSMER, S., SAYIR, M., 1988, Dynamic elastic-plastic behaviour of a frame, *Engineering Computation*, **5**, pp. 231-240.

MØLLMANN, H., 1981, Thin-walled elastic beams with finite displacements, *Report R142, Technical University of Denmark, Department of Structural Engineering.*

MEEK, J.L., LOGANATHAN, S., 1989, Geometrically non-linear behaviour of space frame structures, *Computers & Structures*, **31**, pp. 35-45.

MEEK, J.L., TAN, H.,S, 1984, Geometrically nonlinear analysis of space frames by an incremental iterative technique, *Computer Methods in Applied Mechanics and Engineering*, **47** pp. 261-282.

MIKKOLA, M, TUOMALA, M, 1989, Mechanics of impact energy absorption, *Report 104, Helsinki University of Technology, Department of Structural Engineering.*

MOTTERSHEAD, J.E., 1988a, Warping torsion in thin-walled open section beams using the semiloof beam element, *International Journal for Numerical Methods in Engineering*, **26**, pp. 231-243.

MOTTERSHEAD, J.E., 1988b, Geometric stiffness of thin-walled open section beams using a semiloof beam formulation, *International Journal for Numerical Methods in Engineering*, **26**, pp. 2267-2278.

NEE, K.M., HALDAR, A., 1988, Elastoplastic nonlinear post-buckling analysis of partially restrained space-structures, *Computer Methods in Applied Mechanics and Engineering*, **71** pp. 69-97.

ORTEGA, J.M., RHEINBOLDT, W.C., 1970, *Iterative Solution of Nonlinear Equation in Several Variables*, Acadenic Press, New York.

PAPADRAKAKIS M., 1981, Post-buckling analysis of spatial structures by vector iteration method, *Computers & Structures* **14**, pp. 393-402.

PEDERSEN, C., 1982a, Stability properties and non-linear behaviour of thin-walled elastic beams of open cross-section, Part 1: Basic analysis, *Report R149, Technical University of Denmark, Department of Structural Engineering.*

PEDERSEN, C., 1982b, Stability properties and non-linear behaviour of thin-walled elastic beams of open cross-section, Part 2: Numerical Examples, *Report R150, Technical University of Denmark, Department of Structural Engineering.*

PERZYNA, P., 1966, Fundamental problems in viscoplasticity, *Advances in Applied Mechanics*, **9**, pp. 243-377.

POOWANNACHAIKUL, T., TRAHAIR, N.,S., 1976, Inelastic buckling of continuous steel beams, *Civil Engineering Transactions, Institution of Engineers, Australia*, CE **8**, pp. 134-139.

RAJASEKARAN, S., MURRAY, D.W., 1973, Finite element solution of inelastic beam equations, *Journal of Engineering Mechanics*, **99** pp. 1025-1041.

RAMM, E., 1980, Strategies for tracing the nonlinear responce near limit points, in K.J. Bathe et al. (eds.), *Europe-U.S. Workshop on Nonlinear Finite Element Analysis of Structural Mechanics*, Ruhr Universität Bochum, Germany, Springer-Werlag, Berlin, pp. 63-89.

RAO, S.S., RAGHAVAN, K.S., 1987, Finite-element dynamic inelastic analysis of beams and plates under combined loading, *Computers & Structures*, **25**, pp. 355-364.

RAY, S.K., UTKU, S., 1989, A numerical model for the thermo- elasto-plastic behaviour of material, *International Journal for Numerical Methods in Engineering*, **28** pp. 1103-1114.

REMSETH, S.N., 1979, Nonlinear static and dynamic analysis of framed structures, *Computers & Structures*, **10**, pp. 879-897.

RENTON, J.D., 1962, Stability of space frames by computer analysis, *Journal of Structural Division*, **88** ST4, pp. 81-103.

RHEINBOLDT, W.C., 1977, Numerical continuation methods for finite element applications, in K.J. Bathe et al. (eds.), *Formulations and Computational Algorithms in FE analysis, Proc. U.S.-Germany Symposium*, pp. 599-631.

RHEINBOLDT, W.C., 1978, Numerical methods for a class of finite dimensional bifurcation problems, *SIAM, Journal of Numerical Analysis*, **15**, pp. 1-11.

RHEINBOLDT, W.C., 1986, *Numerical Analysis of Parametrized Nonlinear Equations*, Wiley, New York.

RHEINBOLDT, W.C., 1988, On the computation of multi-dimensional manifolds of parametrized equations, *Numerische Mathematik*, **53**, pp.165-181.

RIFF, R, SIMITSES, G.J., 1988, Thermo-elasto-viscoplastic analysis of problems in extension and shear, *Computers & Structures*, **29**, pp. 293-300.

RIKS, E., 1972, The application of Newton's method to the problem of elastic stability, *Journal of Applied Mechanics*, **39**, pp. 1060-1065.

RIKS, E., 1974, The incremental solution of some basic problems of elastic stability, *Report NLR TR 74005 U*, National Aerospace Laboratory NLR, The Netherlands.

RIKS, E., 1979, An incremental approach to the solution of snapping and buckling problems, *International Journal of Solids and Structures*, **15**, pp. 529-551.

RIKS, E., 1984, Some computational aspects of the stability analysis of nonlinear structures, *Computer Methods in Applied Mechanics and Engineering*, **57** pp. 219-259.

RUBERT, A., SCHAUMANN, P., (1985), Tragverhalten stählerner Rahmensysteme bei Brandbeanspruchung, *Stahlbau*, **54**, pp. 280-287.

SALONEN, E-M., 1976, An iterative penalty function method in structural analysis, *International Journal for Numerical Methods in Engineering*, **10**, pp. 413-421.

SANDHU, J.S., STEVENS, K.A., DAVIES, G.A.O., 1990, A 3-D, co-rotational, curved and twisted beam element, *Computers & Structures*, **35**, pp. 69-79.

SCHWEIZERHOF, K., RAMM, E., 1984, Displacement dependent pressure loads in nonlinear finite element analysis, *Computers & Structures*, **18**, pp. 1099-1114.

SCHWEIZERHOF, K.H., WRIGGERS, P., 1986, Consistent linearization for path following methods in nonlinear FE analysis, *Computer Methods in Applied Mechanics and Engineering*, **59**, pp. 261-279.

SIMO, J.C., 1985, A finite strain beam formulation. The three dimensional dynamic problem, Part I, *Computer Methods in Applied Mechanics and Engineering*, **49** pp. 55-70.

SIMO, J.C., VU-QUOC, L., 1986, A three dimensional finite strain rod model, Part II: Computational aspects, *Computer Methods in Applied Mechanics and Engineering*, **58** pp. 79-115.

SIMO, J.C., KENNEDY, J.G., GOVINDJEE, S., 1988, Non-smooth multisurface plasticity and viscoplasticity. Loading/unloading conditions and numerical algorithms, *International Journal for Numerical Methods in Engineering*, **26**, pp. 2161-2185.

SEKULOVIĆ, M., 1986, Geometrically nonlinear analysis of thin-walled members, Proceedings *'Steel Structures: Recent Research Advances and Their Applications to Design'*, Elsevier Applied Science Publishers Ltd. pp. 219-243.

SHI, G., ATLURI, S.N., 1988, Elasto-plastic large deformation analysis of space-frames: A plastic-hinge and stress based explicit derivation of tangent stiffnesses, *International Journal for Numerical Methods in Engineering*, **26**, pp. 589-615.

SMITH, J.O., SIDEBOTTOM, O.M., 1965, Inelastic Behaviour of Load-Carrying Members, Wiley, New York.

SURANA, K.S., SOREM, R.,M., 1989, Geometrically non-linear formulation for three dimensional curved beam elements with large rotations, *International Journal for Numerical Methods in Engineering*, **28**, pp. 43-73.

SYMONDS, P.S., YU, T.X., 1985, Counterintuitive behaviour in a problem of elastic-plastic beam dynamics, *Journal of Applied Mechanics*, **107**, pp. 517-522.

SYMONDS, P.S., MCNAMARA, J.F., GENNA, F., 1986, Vibrations and permanent displacements of a pin-ended beam deformed plastically by short pulse excitation, *International Journal of Impact Engineering*, **4**, pp. 73-82.

TEZCAN, S.S., MAHAPATRA, B.C., 1969, Tangent stiffness matrix for space frame members, *Journal of the Structural Division*, ASCE, **95**, pp. 1257-1270.

THOMPSON, J.M.T., HUNT, G.W., 1973, *A General Theory of Elastic Stability*, Wiley, London.

TIMOSHENKO, S.P., GERE, J.M., 1961, *Theory of Elastic Stability*, McGraw-Hill, New York.

TRAHAIR, N.S., WOOLCOCK, S.T., 1973, Effects of major axis curvature on I-beam stability, *Journal of the Engineering Mechanics Division*, **99**, pp. 85-98.

TRAHAIR, N.S., 1983, Inelastic lateral buckling of beams, in *Beams and Beam Columns, Stability and Strenght*, Ed. R. Narayanan, Applied Science publishers Ltd. pp. 35-69.

TUOMALA, M, KOUHIA, R, 1986, Adaptive finite element analysis of geometrically nonlinear elasto-plastic structures, *Report 10, Tampere University of Technology, Department of Civil Engineering, Structural Mechanics.*

VIRTANEN, H., MIKKOLA, M., 1985, Geometrically nonlinear analysis of space frames (in Finnish), *Journal of Structural Mechanics (Rakenteiden Mekaniikka)*, **18**, No 3 pp. 82-97.

VLASOV, V.Z., (1963), *Thin-Walled elastic beams*, Israel Program for Scientific Translations.

VOGEL, U., 1985, Calibrating frames, *Stahlbau*, **54**, pp. 295-301.

WATSON, L.T., HOLZER, M., 1983, Quadratic convergence of Crisfield's method, *Computers & Structures*, **17**, pp. 69-72.

WEMPNER, G.A., 1971, Discrete approximations related to the nonlinear theories of solids, *International Journal of Solids and Structures*, **7**, pp. 1581-1599.

WOOLCOCK, S.T., TRAHAIR, N.S., 1974, Post-buckling behaviour of determinate beams, *Journal of the Engineering Mechanics Division,* **100**, pp. 151-171.

WUNDERLICH, W., OBRECHT, H., SCHRÖDTER, V., 1986, Nonlinear analysis and elastic-plastic load-carrying behaviour of thin-walled spatial beams with warping constraints, *International Journal for Numerical Methods in Engineering,* **22** pp. 671-695.

YANG, Y-B., CHERN, S-M., FAN, H-T., 1989, Yield surfaces for I-sections with bimoments, *Journal of Structural Engineering*, **115**, pp. 3044-3058.

YOSHIDA, H., 1977, Buckling curves for welded beams, *Preliminary Report, 2nd International Colloquium on Stability of Steel Structures,* ECCS-IABSE, Liege, pp. 191-196.

ZIEGLER, H., 1968, *Principles of Structural Stability*, Blaisdell Publishing Company.

APPENDIX 1

Differential equations for shear deformable torsion bar

The differential equations in terms of the displacement quantities ϕ and ϑ can be obtained from the equilibrium conditions

$$\begin{cases} -(M_\omega + M_{xf})_{,x} = m_x, \\ B_{,x} = M_\omega, \end{cases} \tag{A1.1}$$

where m_x is the distributed torque along the axis of the bar. Bimoment B, warping torsion M_ω and St. Venant's torque M_{xf} are defined by the equations

$$\begin{aligned} B &= -EI_\omega \vartheta_{,x}, \\ M_\omega &= GI_s(\phi_{,x} - \vartheta), \\ M_{xf} &= GI_t \phi_{,x}, \end{aligned} \tag{A1.2}$$

where I_ω is the warping rigidity, I_s the warping shear rigidity and I_t the St. Venant torsional rigidity. Substituting Equations (A1.2) into the system (A1.1) gives

$$\begin{cases} -GI_t\phi_{,xx} - GI_s(\phi_{,xx} - \vartheta_{,x}) = m_x, \\ -EI_\omega\vartheta_{,xx} - GI_s(\phi_{,x} - \vartheta) = 0. \end{cases} \tag{A1.3}$$

Eliminating $\phi_{,xx}$ from the upper equation, yields a third order ordinary differential equation in ϑ

$$EI_\omega(1 + \frac{I_t}{I_s})\vartheta_{,xxx} - GI_s\vartheta_{,x} = m_x. \tag{A1.4}$$

As an example, a clamped beam with a concentrated torque M_o at the midspan is analysed. The resulting angle of twist ϕ and bimoment B have the following expressions

$$\begin{aligned} \phi(x) &= \frac{M_o}{2GI_t}\left\{(\frac{L}{\tilde{k}})\frac{1}{1 + I_t/I_s}\left[\frac{\cosh\tilde{k} - 1}{\sinh\tilde{k}}(\cosh\frac{\tilde{k}x}{L} - 1) - \sinh\frac{\tilde{k}x}{L}\right] + x\right\}, \\ B(x) &= M_o(\frac{L}{\tilde{k}})\frac{1}{1 + I_t/I_s}(\sinh\frac{\tilde{k}x}{L} + \frac{1 - \cosh\tilde{k}}{\sinh\tilde{k}}\cosh\frac{\tilde{k}x}{L}), \end{aligned} \tag{A1.5}$$

where

$$\tilde{k} = \sqrt{\frac{GI_t}{EI_\omega(1 + I_t/I_s)}}L, \tag{A1.6}$$

and L is the length of the beam. The corresponding solutions according to the Vlasov's theory are

$$\begin{aligned} \phi(x) &= \frac{M_o}{2GI_t}\left\{(\frac{L}{k})\left[\frac{\cosh k - 1}{\sinh k}(\cosh\frac{kx}{L} - 1) - \sinh\frac{kx}{L}\right] + x\right\}, \\ B(x) &= M_o(\frac{L}{k})(\sinh\frac{kx}{L} + \frac{1 - \cosh k}{\sinh k}\cosh\frac{kx}{L}), \end{aligned} \tag{A1.7}$$

in which

$$k = \sqrt{\frac{GI_t}{EI_\omega}}L. \tag{A1.8}$$

APPENDIX 2

Grading functions

A grading function $\Gamma(x)$ establishes one to one correspondence between the uniform meshes characterized by the number of elements N and the graded meshes generated by the grading function, Babuška and Szabo (1983). It is a continuous increasing function on an interval $I = (a, b)$, defined such that

$$\begin{aligned} &\Gamma(a) = 0, \quad \Gamma(b) = 1, \\ &\Gamma(x_j) = \frac{1}{N} j, \qquad j = 0, 1, ..., N. \end{aligned} \tag{A2.1}$$

Typical grading functions are, defined in unit interval $I = (0, 1)$:

$$\Gamma(x) = x^{\beta}, \tag{A2.2}$$

$$\Gamma(x) = \left[\frac{1}{|\log(\frac{1}{x})|} \right]^{\frac{1}{\beta}}, \tag{A2.3}$$

which are called polynomial and logarithmic grading functions,respectively and in which β is a parameter. Grading the element lengths in a geometric proportion q, yields the following equation for nodal point coordinates

$$x_j = \frac{1 - q}{1 - q^N} q^{j-1}, \qquad j = 0, 1, ..., N. \tag{A2.4}$$

For example, in Section 9.1 the nodal points are graded according to the polynomial grading function (A2.2) where the parameter $\beta = 3$, yielding the following coordinates for a five noded mesh (finer mesh at the left clamped end)

$$\frac{x_j}{L} = 0.0, \quad 0.0914, \quad 0.2063, \quad 0.37, \quad 1.0.$$

With $\beta = 1.4$ Equation (A2.2) gives

$$\frac{x_j}{L} = 0.0, \quad 0.186, \quad 0.391, \quad 0.629, \quad 1.0.$$